

**Titre:** Piezoelectric Fibers for Sensing and Energy Generation  
Title:

**Auteur:** Xin Lu  
Author:

**Date:** 2018

**Type:** Mémoire ou thèse / Dissertation or Thesis

**Référence:** Lu, X. (2018). Piezoelectric Fibers for Sensing and Energy Generation [Thèse de doctorat, École Polytechnique de Montréal]. PolyPublie.  
Citation: <https://publications.polymtl.ca/3671/>

 **Document en libre accès dans PolyPublie**  
Open Access document in PolyPublie

**URL de PolyPublie:** <https://publications.polymtl.ca/3671/>  
PolyPublie URL:

**Directeurs de recherche:** Maksim A. Skorobogatiy  
Advisors:

**Programme:** Génie métallurgique  
Program:



UNIVERSITÉ DE MONTRÉAL

PIEZOELECTRIC FIBERS FOR SENSING AND ENERGY GENERATION

XIN LU

DÉPARTEMENT DE GÉNIE PHYSIQUE  
ÉCOLE POLYTECHNIQUE DE MONTRÉAL

THÈSE PRÉSENTÉE EN VUE DE L'OBTENTION  
DU DIPLÔME DE PHILOSOPHIAE DOCTOR  
(GÉNIE MÉTALLURGIQUE)

SEPTEMBRE 2018



UNIVERSITÉ DE MONTRÉAL

ÉCOLE POLYTECHNIQUE DE MONTRÉAL

Cette thèse intitulée :

PIEZOELECTRIC FIBERS FOR SENSING AND ENERGY GENERATION

présentée par : LU Xin

en vue de l'obtention du diplôme de : Philosophiae Doctor

a été dûment acceptée par le jury d'examen constitué de :

Mme SANTATO Clara, Doctorat, présidente

M. SKOROBOGATIY Maksim A., Ph. D., membre et directeur de recherche

M. TERRIAULT Daniel, Ph. D., membre

M. VENGALLATORE Srikar, Ph. D., membre externe



## DEDICATION

*I would like to dedicate this thesis to my parents for their love and support*



## ACKNOWLEDGEMENTS

I would like to express my deepest and heartfelt gratitude to my supervisor and research director, Prof. Maksim Skorobogatiy, for his guidance and support during my Ph.D. study, especially when I struggled in the predicaments. Prof. Skorobogatiy's help allowed me to pursue successfully my scientific dream, become more mature, and enrich my curiosity.

I would like to thank all my friends and colleagues in Engineering Physics, Ecole Polytechnique de Montreal, Hang Qu, Tian Ma, Jingwen Li, Hichem Guerboukha, Katirvel Nallapan, Yang Cao and others. I would like to thank them for the helpful discussions, constructive interactions and mutual support in the past four years. I also would like to thank the technicians in our group, Francis Boutet and Yves Leblanc, for their plenty of technical assistance.

Finally, I wish to thank my parents for their unconditional support during my doctoral study. They have always been understanding and patient, and I could always address to them for the encouragement and support when I needed it.



## RÉSUMÉ

Au cours de la dernière décennie, la recherche et le développement de générateurs fibrés a reçu une attention significative en raison de la popularité grandissante des appareils électroniques que l'on peut porter, tels que les écrans sur vêtements, les dispositifs de réalité virtuelle, les senseurs médicaux/cliniques portables et les montres intelligentes. Parmi les générateurs fibrés, les fibres piézoélectriques qui opèrent en se basant sur l'effet piézoélectrique sont spécialement attrayantes, parce qu'elles peuvent convertir les vibrations mécaniques de la vie quotidienne (causées par exemple par la marche, les courants d'air ou les battements cardiaques) en signaux électriques. Pour augmenter le potentiel des technologies portables, des textiles piézoélectriques pour alimenter les dispositifs électroniques ont été fabriqués en intégrant les fibres piézoélectriques dans des fibres commerciales utilisant les techniques de fabrication conventionnelles.

Les fibres piézoélectriques peuvent aussi avoir des applications techniques dans les domaines de l'information et des communications, dans l'automatisation industrielle, dans le diagnostic médical, dans le control du trafic et dans le secteur de la défense. Par exemple, ces fibres pourraient être implantées dans les avions et les véhicules pour surveiller l'intégrité de la structure mécanique, ainsi qu'alimenter les systèmes électroniques embarqués tels que les réseaux de senseurs sans-fil (WSN) à faible puissance. D'autres applications incluent les détecteurs acoustiques de haute-sensibilité pour la détection des ondes sonores, les actuateurs de micro-positionnement pour les microscopes à force atomique (AFM), les microscopes à effet tunnel (STM), les miroirs laser d'alignement et les dispositifs médicaux implantables (IMD).

Encouragés par le marché sans cesse grandissant des appareils électroniques portatifs, des efforts substantiels ont été investis dans la fabrication de fibres piézoélectriques. Aujourd'hui, la plupart des fibres piézoélectriques existantes sont fabriquées soit en faisant croître des nanostructures piézoélectriques dans un filament conducteur ou en extrudant des polymères piézoélectriques avec des polymères conducteurs par trempe sur roue (*melt-spinning*). La performance et les applications de ces fibres piézoélectriques sont limitées par leur géométries simpliste, leur grandes taille, leur faible fiabilité mécanique, leur coût élevé et leur faible réponse piézoélectrique.

Cette thèse a pour objectif de démontrer des fibres piézoélectriques micro et nanostructurées pouvant répondre à ces limitations. Dans notre approche, des fibres



piézoélectriques de plusieurs kilomètres de dimensions sous-millimétriques sont thermiquement étirées à partir de préformes macroscopiques. Les fibres piézoélectriques sont constituées d'un cœur creux mou de polycarbonate entouré d'une gaine de multicouches spiralées fait de couches alternatives de nanocomposites piézoélectriques (polyvinylidène augmenté avec BTO, PZT ou CNT) et de polymères conducteurs (polyéthylène rempli de carbone). Les deux couches de polymères conductrices jouent le rôle d'électrodes et forment des connecteurs électriques spatialement séparés pour faciliter la connexion. La structure multicouche de taille micro/nanométrique augmente l'efficacité de polarité grâce à la courte distance entre les électrodes conductrices entourant les couches piézoélectriques composites. Additionnellement, la structure en spirale augmente grandement la région active du composite piézoélectrique, en permettant la génération de voltage plus grande, résultant en des efficacités de génération de puissances de 10 à 100 fois plus importantes que les câbles piézoélectriques conventionnels.

Par la suite, nous avons réalisé une étude comparative des fibres piézoélectriques en utilisant trois combinaisons de matériaux (PVDF-BTO, PVDF-PZT et PVDF-CNT). La fibre microstructurée BTO/PVDF (longueur de 10 cm, concentration de BTO : 20 wt%) a pu générer un voltage en circuit-ouvert de 1.4 V et un courant de court-circuit de 0.8 nA, quand une des terminaisons de la fibre a été déplacée de 10 mm dans la direction transversale. Les voltages et courants correspondants étaient de ~6 V and ~4 nA pour la fibre de PZT-PVDF (20 wt% PZT) et de ~3V et ~1.2 nA pour la fibre de CNT-PVDF (0.4 wt%).

Comme exemples d'applications pratiques des fibres piézoélectriques proposées, nous présentons des textiles générateurs d'énergie utilisant des fibres BTO-PVDF, et nous caractérisons leurs performances dans le contexte de microgénérateurs que l'on peut porter. Nous présentons aussi la détection du son en utilisant des fibres CNT-PVDF avec des voltages piézoélectriques générés par des ondes sonores proportionnelles à la racine carrée de la puissance acoustique.

Additionnellement, nous avons assemblé des générateurs piézoélectriques planaires en sandwichant un nanocomposite piézoélectrique entre deux films de polymères conducteurs (C-LDPE). Les générateurs ainsi formés ont un voltage en circuit ouvert jusqu'à 8 V et un courant de court-circuit jusqu'à 40 nA avec une région active de plusieurs dizaines de cm<sup>2</sup>. La durabilité de ce générateur a été confirmée en répétant continuellement des mesures d'étirage pendant trois jours.



Le générateur a bien retenu ses caractéristiques de voltage et de courant piézoélectriques durant tout le test qui comprenant 26000 cycles d'étirage.



## ABSTRACT

In the past decade, the R&D (research and development) of fiber generators has received significant attention due to the growing popularity of wearable mobile electronic systems such as on-garment displays, virtual-reality devices, wearable medical/clinic sensors and smart watches. Among all of these fiber generators, piezoelectric fibers that operate based on piezoelectric effect are especially attractive, because they could convert mechanical vibrations accessible in our daily life (i.e. walking, air flow and heart beating) into electrical signals. To make further improvements to the wearable applications, piezoelectric textiles that power on-body electronics have been fabricated by integrating piezoelectric fibers into commercial fabrics using traditional textile fabrication techniques.

Piezoelectric fibers can also find technical applications in the fields of information and communication, industrial automation, medical diagnostics, automation and traffic control, and in the defense industries. For instance, piezoelectric fibers could be implanted on the airplanes and vehicles, for the purpose of structural integrity monitoring, as well as powering the on-board electronic systems such as wireless sensor networks (WSNs) with low-power consumption. Other common examples include ultrasensitive sound detectors for stand-off sound detection, micro-positioning actuators for atomic force microscopes (AFM), scanning tunneling microscopes (STM), and laser mirror alignment; as well as power sources for implanted medical devices (IMDs).

Driven by the ever-growing market, extensive effort has been put into the fabrication of piezoelectric fibers. Currently, most of the existing piezoelectric fibers are fabricated either by growing piezoelectric nanostructures along a conductive filament or by extruding piezoelectric polymers together with a conductive polymer by melt-spinning. The performance and applications of these piezoelectric fibers are limited by their simple fiber geometries, large fiber size, poor mechanical reliability, high-cost, and low piezoelectric response.

This thesis aims to demonstrate micro- and nanostructured piezoelectric fibers that address these limitations. In our approach, kilometer-long piezoelectric fibers of sub-millimeter diameters are thermally drawn from a macroscopic preform. The piezoelectric fibers feature a soft hollow polycarbonate core surrounded with a spiral multilayer cladding consisting of alternating layers of piezoelectric electrospun nanocomposites (polyvinylidene enhanced with BTO, PZT or CNT) and



conductive polymer (carbon filled polyethylene). The conductive polymer layers serve as two electrodes and form two spatially offset electric connectors on the fiber surface designed for the ease of connectorization. The micron/nano-size multilayer structure enhances in-fiber poling efficiency, thanks to the small distance between the conducting electrodes surrounding the piezoelectric composite layers. Additionally, the spiral structure greatly increases the active area of the piezoelectric composite, thus promoting higher voltage generation and resulting in 10-100 higher power generation efficiency over the existing piezoelectric cables.

Afterwards, we performed a comparative study of the piezoelectric fibers using three material combinations (PVDF-BTO, PVDF-PZT and PVDF-CNT). A BTO/PVDF microstructured fiber (10 cm long; BTO concentration: 20 wt%) could generate an open-circuit voltage of 1.4 V and a short-circuit current of 0.8 nA, when the moving end of the generator was displaced transversely by 10 mm. The corresponding voltage and current were  $\sim 6$  V and  $\sim 4$  nA for a PZT-PVDF (20 wt% PZT) fiber generator, and  $\sim 3$  V and  $\sim 1.2$  nA for a CNT-PVDF (0.4 wt% CNT) fiber generator.

As examples of practical applications of the proposed piezoelectric fibers, we present energy harvesting textiles using BTO-PVDF fibers, and characterized their performance in the context of wearable and automotive microgenerators. We also present detection of sound using CNT-PVDF fiber that feature piezoelectric voltage generated by sound wave to be proportional to the square root of the acoustic power.

Additionally, we have assembled piezoelectric planar generators by sandwiching a piezoelectric nanocomposite between two conductive polymer films (C-LDPE). Such planar generators can generate open-circuit voltages of up to 8 V and short-circuit voltage of up to 40 nA with an active area of several tens of  $\text{cm}^2$ . The durability of this generator was confirmed by continuously repeating the bend-release measurements for 3 days. The generator retained well its piezoelectric voltage and current throughout the whole test that comprised  $\sim 26000$  bend/release cycles.



## TABLE OF CONTENTS

DEDICATION .....	III
ACKNOWLEDGEMENTS .....	IV
RÉSUMÉ.....	V
ABSTRACT .....	VIII
TABLE OF CONTENTS .....	X
LIST OF TABLES .....	XIV
LIST OF FIGURES.....	XV
LIST OF SYMBOLS AND ABBREVIATIONS.....	XXIII
CHAPTER 1 INTRODUCTION.....	1
CHAPTER 2 LITERATURE REVIEW .....	5
2.1 The working principles of the piezoelectric generators .....	5
2.2 The wearable piezoelectric generators .....	7
2.2.1 Wearable piezoelectric generators based on piezoelectric polymers .....	7
2.2.2 Wearable piezoelectric generators based on piezoelectric ceramics.....	13
2.3 The motivation and objectives .....	22
2.3.1 The motivation .....	22
2.3.2 The objectives .....	23
CHAPTER 3 METHODOLOGY .....	25
3.1 Fabrication.....	25
3.1.1 Preparation of piezoelectric nanocomposites using electrospinning.....	25
3.1.2 Fabrication of the piezoelectric planar generators .....	28
3.1.3 Fabrication of the micro-/nanostructured piezoelectric fibers <i>via</i> fiber drawing technique .....	28



3.1.4	Fabrication of piezoelectric fiber generators.....	31
3.1.5	Fabrication of the piezoelectric textiles .....	32
3.2	Characterization .....	32
3.2.1	Material characterization.....	32
3.2.2	Electrical characterization .....	34
CHAPTER 4 ARTICLE 1: PIEZOELECTRIC MICRO- AND NANOSTRUCTURED FIBERS FABRICATED FROM THERMOPLASTIC NANOCOMPOSITES USING A FIBER DRAWING TECHNIQUE: COMPARATIVE STUDY AND POTENTIAL APPLICATIONS 37		
4.1	Introduction .....	38
4.2	Results and discussion.....	42
4.2.1	Fabrication of the piezoelectric micro-/nanostructured fibers .....	42
4.2.2	Characterization of piezoelectric micro-/nanostructured fibers .....	44
4.3	Examples of practical applications of piezoelectric fibers.....	51
4.3.1	Stand-off distributed sound detection .....	51
4.3.2	Textile-based piezoelectric generators woven using BTO-PVDF fibers .....	54
4.4	Conclusion.....	57
4.5	Experimental section .....	58
4.5.1	Solution preparation .....	58
4.5.2	Electrospinning of BTO-PVDF, PZT-PVDF and CNT-PVDF solutions .....	59
4.5.3	Preparation of the piezoelectric fiber preforms and fiber drawing .....	59
4.5.4	Electrical measurements.....	60
4.6	Supporting information .....	60
CHAPTER 5 ARTICLE 2: PIEZOELECTRIC MICROSTRUCTURED FIBERS VIA DRAWING OF MULTIMATERIAL PREFORMS ..... 64		
5.1	Introduction .....	64



5.2	Results .....	68
5.2.1	Fabrication and characterization of the laminated piezoelectric generators .....	68
5.2.2	Electro-mechanical model of the planar piezoelectric generator .....	71
5.2.3	Fabrication of the piezoelectric fibers via drawing of the multimaterial preforms....	74
5.2.4	Characterization of the piezoelectric microstructured fibers .....	75
5.3	Examples of the potential applications of the piezoelectric fiber generators.....	79
5.4	Conclusion.....	80
5.5	Methods.....	82
5.5.1	Materials.....	82
5.5.2	Preparation of polymer solutions .....	82
5.5.3	Electrospinning.....	83
5.5.4	Preforms and fibers fabrication .....	83
5.6	Supplementary Figures and Notes.....	83
CHAPTER 6	GENERAL DISCUSSION.....	93
6.1	The material selection in the piezoelectric fibers.....	93
6.1.1	The piezoelectric material selection .....	93
6.1.2	The conductive material selection.....	95
6.2	The relationship between fiber performance and structural parameters .....	96
6.3	Electrical poling for the fiber performance .....	97
6.4	Switching-polarity tests of the piezoelectric generators .....	99
6.5	The piezoelectric stability of the fibers with respect to temperature .....	100
6.6	The potential applications of the piezoelectric fiber inside the blood vessels .....	101
CHAPTER 7	CONCLUSION AND PERSPECTIVES .....	102
7.1	Summary of accomplishments .....	102



7.2	Future work .....	103
7.3	Conclusion.....	104
BIBLIOGRAPHY .....		106



## LIST OF TABLES

Table 2.1: The comparison between the different types of wearable piezoelectric generators based on piezoelectric polymers.....	12
Table 2.2: The comparison between the different types of wearable piezoelectric generators based on piezoelectric ceramics .....	21
Table 6.1. The Curie temperature of the piezoelectric materials .....	101



# LIST OF FIGURES

Figure 2.1: Design and working principles of the piezoelectric generators. (a), Schematic illustration of the application of the stress onto a poled piezoelectric generator (e.g. the BaTiO<sub>3</sub> generator). In the initial state (after electrical poling), the electric dipoles maintain the permanent polarization. When mechanical stress is applied onto the piezoelectric generator, the polarization density of the piezoelectric film is changed and the electrons are forced to flow from one electrode to the other, thus generating a piezoelectric potential. (b), The equivalent electric circuit in the measurement. The piezoelectric generator is considered as a capacitor, while  $R_L$  is the resistance of the load in the electric circuit. ....7

Figure 2.2: Schematic description of the  $\alpha$  (TGTG'),  $\beta$  (TTTT) and  $\gamma$  (TTTGTTTG') phase of PVDF. Reprinted from Ref [67]. ....8

Figure 2.3: Summary of the piezoelectric polymer fibers. (a), Schematic of the direct-write, and electrical poling PVDF fibers *via* NFES. Reprinted from Ref [83]. (b), Schematic of the fabrication of the piezoelectric PVDF micro- and nanoribbons using iterative size reduction technique. Reprinted from Ref [93]. (c), Cross-section of the PVDF fiber that uses carbon-black (CB)/polypropylene (PP) as the core. Reprinted from Ref [63]. (d), Schematic of the fabrication of the piezoelectric microstructured PVDF fiber using fiber drawing technique. Reprinted from Ref [66]. ....11

Figure 2.4: (a), Change of unit cell of a BaTiO<sub>3</sub> crystal during spontaneous polarization. (b), Reaction of a poled piezoelectric element to applied stimuli. Reprinted from Ref [117]. ....15

Figure 2.5: Wearable BaTiO<sub>3</sub> generators. (a), Schematics of the fabrication process of the BaTiO<sub>3</sub>-graphitic carbons nanocomposite generator. Reprinted from Ref [120]. (b, c), SEM images of the cross-section of the piezoelectric generator based on BaTiO<sub>3</sub>/PVDF micropillar arrays. c), A magnified top view of the SEM image of MWCNT layer. Reprinted from Ref [121]. ....16

Figure 2.6: Wearable PZT generators. (a, b, c), Transfer printing of PZT nanoribbons onto flexible substrates. (a), A high-quality crystalline PZT was firstly deposited on an MgO host substrate, which was subsequently etched, and then PZT nanoribbons were transferred onto flexible plastic substrate using a PDMS stamp. (b), Optical micrograph of PZT ribbons on MgO substrate before transfer, and PZT ribbons on PDMS after transfer printing. (c), Photograph



of a flexible PZT generator. Reprinted from Ref [76, 130]. (d), Schematic diagram of the process for fabricating a PZT textile using electrospinning. Reprinted from Ref [129].	18
Figure 2.7: (a), The wurtzite structure model of ZnO. (b), Schematic diagrams showing the piezoelectric effect in a tetrahedrally coordinated cation–anion unit. Reprinted from Ref [133].	19
Figure 2.8: Wearable ZnO generator. (a), 3D Schematic diagram depicting the structure of a hybrid-fiber nanogenerator. (b), Image of the experimental setup. (c), Open-circuit output voltage and short-circuit output current density of a fiber device under a strain of $\sim 0.1\%$ . Reprinted from Ref [51].	20
Figure 3.1 : The probe-type ultrasonicator (Fisher Scientific Inc.)	26
Figure 3.2: (a) Photo of the electrospinning setup. (b), Schematic of the electrospinning. Reprinted from Ref [139].	28
Figure 3.3: The design of piezoelectric planar generators	28
Figure 3.4: Assembly of the fiber preform.	30
Figure 3.5: The fiber drawing process. (a), image of the fiber drawing tower. (b), image of the fiber preform cross-section. The blue scale bar is of $\sim 1$ cm. (c), image of the clamp tractor. (d), schematic of the fiber cross-section. The preform is fabricated by co-rolling electrospun polyvinylidene fluoride (PVDF) mat and C-LDPE film around a polycarbonate tube (PC tube).	30
Figure 3.6 : (a) Schematic diagram and (b) Image of the piezoelectric fiber generator.	31
Figure 3.7: (a), The loom and a fabricated textile integrated with piezoelectric fibers. The scale bar is $\sim 6$ cm. (b), The piezoelectric textile generators. The scale bar is $\sim 5$ cm. (c), The image of the piezoelectric fiber. The scale bar is $\sim 1$ cm. (d) Schematic of the electrodes connection (connected in series) at one fiber end.	32
Figure 3.8: The experimental setup for the electrical characterization in (a) bent state and (b) released state.	35
Figure 4.1: (a) Schematic of a fiber drawing process. (b) Schematic of the multilayer structure in the preform and in the drawn fiber. (c) Photo of a preform cross-section. (d) Photo of a cross	



section of the piezoelectric fiber with a diameter of  $\sim 900 \mu\text{m}$  (drawn using 2 kV voltage on the preform electrodes). Inset: the magnified view of a multilayer structure. (e) A spool of a piezoelectric fiber. (f) SEM images of the CNT/PVDF electrospun mats at different magnifications. (g) Photo of a cross section of the piezoelectric fiber with a diameter of  $\sim 300 \mu\text{m}$  (drawn using 5 kV voltage on the preform electrodes). Inset: the magnified view of a multilayer structure. (h) A piezoelectric fiber wrapped on a pencil. ....43

Figure 4.2: (a) Schematic and a photo (b) of a BTO-PVDF fiber test cell. (c) Fiber in the bent and released states. ....44

Figure 4.3: Schematics of the charge separation mechanism in the drawn fibers. (a) All dipoles are oriented in the direction of the local electric fields during electric poling (no bending). When mechanical strain is applied along the device by bending, the polarization density is changed and the electrons are forced to flow from one electrode to the other, thus generating voltage differential. (b) A schematic of a piezoelectric fiber in the bent state. The piezoelectric fiber was attached to a plane PS substrate and covered with Kapton tape in order to induce a uniform strain during bending. (c) The open-circuit voltage and short-circuit current of the piezoelectric fiber during the bend and release actions. The insert image shows the equivalent circuit of the piezoelectric fiber connected to a voltmeter or a current meter. The piezoelectric fiber is modeled as a capacitor  $C_f$ , the voltmeter is modeled as a resistor  $R_v$  and the fiber resistance is  $R_f$ . The black line represents the measured output signals during the bend and release state. The red squares represent the modeled results during the bent and released state. ....46

Figure 4.4: (a) Open-circuit voltage generated by a 10 cm long BTO-PVDF fiber with the BTO concentration of 5, 10, 15, 20, and 25 wt% subjected to a 1-cm displacement. (b-c) Comparison of the piezoelectric voltages generated by the poled BTO-PVDF fiber generator and the unpoled one. (d) and (e) show the open-circuit output voltage and short-circuit current generated by a 10 cm-long BTO-PVDF fiber generator (20 wt% BTO in the BTO-PVDF composite) when its moving end is displaced by 5, 10, 15, and 20 mm. (f-g) A durability test for the 10 cm long BTO-PVDF fiber (20 wt% BTO in BTO-PVDF composite) by continuously repeating 1 cm amplitude bend-release movements for 3 days. The open-circuit



voltage and short-circuit current generated in a 1000 s period at the beginning of the first day (f) and at the end of the third day (g) are shown. ....49

Figure 4.5: (a) and (b) show the open-circuit voltage and the short-circuit current generated by a 10 cm-long PZT-PVDF fiber generator (20 wt% PZT in the PZT-PVDF composite), when its moving end is displaced by 10 mm. ....50

Figure 4.6 : (a) Photo of a CNT/PVDF fiber generator. (b) Open-circuit voltage of a 10-cm long CNT-PVDF fiber generators with CNT concentrations of 0.1, 0.2, 0.4 and 0.6 wt% under 10 mm displacement. (c) and (d) show the open-circuit voltage and short-circuit current of a 10-cm long CNT-PVDF fiber (CNT concentration: 0.4 wt%), when the moving end of the fiber was displaced by 5, 10, 15, 20 mm. ....51

Figure 4.7 : (a) Schematics of the experimental setup. (b) The sound wave (Red) and the output voltage from the CNT/PVDF fiber actuated by the sound wave. ....52

Figure 4.8 : (a) The output voltage generated by the CNT/PVDF fiber at the frequencies of the actuating sound wave of 1 Hz, 2 Hz and 4 Hz for SPL of  $\sim 20$  dB. (b) The square of the output voltage of the piezoelectric fiber vs. frequency of the sound wave. In the experiment, we measured 20 pulses, and the value of the mean voltage was calculated by averaging the peak value of the measured pulses. The error bar is calculated by the standard deviation (SD) of the peak value of measured pulses. ....52

Figure 4.9: (a) Schematic and a photo (b) of experimental setup of the underwater ultrasound detection using a CNT-PVDF fiber. (c) Piezoelectric voltages generated by the fiber, when the source acoustic powers were 2 W, 4 W and 6 W. (d) The square of the piezoelectric voltage generated by the generator has a linear relationship with the acoustic power. In the experiment, we measured 20 pulses, and the value of the mean voltage was calculated by averaging the peak value of the measured pulses. The error bar is calculated by the standard deviation (SD) of the peak value of measured pulses. ....54

Figure 4.10: (a) Dobby loom was used to weave piezoelectric fibers into a cotton textile. During weaving, cotton yarns are used as a warp (longitudinal threads forming the textile base). Piezoelectric fibers are introduced during weaving as a weft by passing them through the warp cotton yarns. (b) A cotton-based textile containing 4 piezoelectric fibers woven using a Dobby



loom. (c) Electrical properties of the piezoelectric textile in a  $90^\circ$  folding-release action of the elbow. (d) Open-circuit voltages and short-circuit currents generated by the piezoelectric textile during repeated fold-release motion of the elbow. (e) Open-circuit voltage of the piezoelectric textile in a fold-release elbow action. ....55

Figure 4.11: (a) Photo of the experimental setup for the in-car test. The piezoelectric fiber textile (b) (consisting of fifteen 20 cm-long piezoelectric fibers connected in parallel) was utilized as an automotive microgenerator pad to charge a  $10\ \mu\text{F}$  capacitor *via* a bridge rectifier circuit shown in (c). (d) Voltage of the capacitor charged by a piezoelectric textile during driving and stationary state of the vehicle. ....56

Figure 5.1: Fabrication of the piezoelectric microstructured fibers *via* drawing of the multimaterial preforms. (a) Schematic of the fabrication process of a piezoelectric fiber. (b) Schematic of the multilayer structure in the fiber preform and in the microstructured fiber. (c) Photo of a preform cross section. (d) Photo of a cross section of the piezoelectric microstructured fiber. Insert: the magnified view of a multilayer structure. (e) Photo of a piezoelectric microstructured fiber. ....68

Figure 5.2: Design and performance of the laminated piezoelectric generators. (a) Schematic of a laminated BTO-PVDF generator that uses an electrospun piezoelectric mat. (b) SEM images of a BTO-PVDF mat at different magnifications. Insert: a magnified image of the BTO-PVDF nanocomposite. (c-d) Testing the laminated piezoelectric generator in its bent and released state. ....69

Figure 5.3: Performance of the laminated piezoelectric generators. (a) and (b) show the generated output voltage of the laminated planar generator under bending cycle at different bending displacements (5, 10, 15, and 20 mm). (c) and (d) show the output voltages and currents generated by a BTO-PVDF generator (20 wt.% BTO in the BTO-PVDF composite) when subjected to a 10 mm bending displacement. ....70

Figure 5.4: Electrical properties of the laminated piezoelectric generators under bending. (a), Schematic of charge separation in the piezoelectric mat under bending. (b), Equivalent electric circuit of the generator with a resistance load  $R_L$ . (c, d), The measured output voltages (c) and currents (d) generated by a laminated generator (BTO concentration: 20 wt%) under different displacements ( $\Delta l$ ) compared to the calculated ones (red lines) using Eq. (6). (e, f), The



relationship between the output voltage (current) and piezoelectric mat width  $w$  (e), and piezoelectric mat thickness  $dp$  (f). .....74

Figure 5.5: Design and working principles of the fiber-based piezoelectric generators. (a), Schematic of a BTO-PVDF fiber-based generator. (b), Setup for testing of microstructured fiber generator. (c), Measured voltage response of the piezoelectric fiber under cycling bending at 0.1 Hz. The top and bottom insets show photographs of the fiber during bending and release, respectively. (d), When mechanical strain is applied along the fiber by bending, the polarization density of the BTO-PVDF layer is changed and the electrons are forced to flow from one electrode to the other, thus generating voltage differential. (e, f), The open-circuit voltage (e) and the short-circuit current (f) of the piezoelectric fiber during the bend and release actions. Relaxation of the short circuit current and open circuit voltage on time can be described as single exponential decays with two distinct time constants (red curve fits). .....77

Figure 5.6: Performance of the piezoelectric microstructured fibers. (a) and (b) show the generated output voltage of the fiber-based generator under bending cycle at different bending displacements (5, 10, 15, and 20 mm). (c) and (d) show the output voltages and currents generated by a 10 cm-long PZT-PVDF fiber generator (20 wt.% PZT in the PZT-PVDF composite) when subjected to a 10 mm bending displacement. ....79

Figure 5.7: Potential applications of the piezoelectric fiber generators. (a, b), A cotton-based textile containing piezoelectric fibers woven using a Dobby loom. (c), Electrical properties of the piezoelectric textile actuated by the human hand tapping. (d), Open-circuit voltages of the piezoelectric textile in a hand tapping-releasing actions. (e), Open-circuit voltages and short-circuit currents generated by the piezoelectric textile during repeated hand tap-release motions. (f, g), Piezoelectric fibers implanted on the airplane wing (f) and the airplane body (g). (h), Open-circuit voltages generated by the piezoelectric fibers during rotation of the airplane propeller. (i), Open-circuit voltages generated by the vibrations induced by the airplane motor operation with the motor speeds set at zero, 1/4, 1/2, 3/4 of its maximum speed.....81

Figure 5.8 : Open-circuit voltage generated by the laminated BTO-PVDF generators with the BTO concentration of 5, 10, 15, 20, and 25 wt%. 10 mm-displacement was used in all tests. ....83



Figure 5.9: Comparison of the open-circuit voltage generated by the poled laminated BTO-PVDF (20 wt% BTO) generator to that of the unpoled one.....	84
Figure 5.10 : A durability test was carried out for the laminated BTO-PVDF generator (20 wt% BTO) by continuously repeating the bend-release test for 3 days. In each bend-release motion, the moving end of the generator was displaced by 10 mm. The open-circuit voltage and short-circuit current generated in a 1000 s period at the beginning of in the first day and at the end of the third day are shown. Overall, 25920 bend/release cycles were performed during 3 days. ....	84
Figure 5.11 : Open-circuit voltage generated by BTO-PVDF microstructured fiber with the BTO concentration of 5, 10, 15, 20, and 25 wt%.....	85
Figure 5.12 : Comparison of the open-circuit voltages generated by the poled BTO-PVDF microstructured fiber and the unpoled one.....	86
Figure 5.13 : A durability test was carried out for the BTO-PVDF microstructured fiber (20 wt% BTO in BTO-PVDF composite) by continuously repeating the bend-release test for 3 days. The open-circuit voltage and short-circuit current generated in a 1000 s period at the beginning of the first day and at the end of the third day are shown. ....	87
Figure 5.14 : FTIR spectra of BTO-PVDF electrospun mats at different BTO concentrations ....	88
Figure 5.15: The XRD patterns of the PVDF mats featuring different BTO concentrations .....	89
Figure 5.16: Strain calculation in the laminated piezoelectric generators under bending. ....	91
Figure 5.17: Schematic diagram of mechanics model for the planar piezoelectric generators under bending .....	92
Figure 6.1: Photos of the drawn fiber (when the BTO concertation is higher than 30%).....	94
Figure 6.2: Processes commonly employed to obtain piezoelectric PVDF films. ....	97
Figure 6.3 : (a), The fiber preform was placed into the furnace of the draw tower. (b), The preform electrode was connected to the copper wire.....	98
Figure 6.4 : (a), The measured output voltage and current signals of the planar device with 20 wt% BTO/PVDF in the forward connection during the periodic bending and unbending motions. (b), The output voltage and current signals generated in the reverse connection. ....	99



Figure 6.5 : (a), The measured output voltage and current signals of the piezoelectric fiber of 20 wt% BTO/PVDF in the forward connection during the periodic bending and unbending motions. (b), The output voltage and current signals generated in the reverse connection. 100



## LIST OF SYMBOLS AND ABBREVIATIONS

$C_f$	Fiber capacitance
$d_e$	Thickness of the electrode layer
$d_p$	Thickness of the piezoelectric mat
$d_{31}$	The piezoelectric coefficient
$I^{sc}(t)$	Short-circuit current
$l$	The length of a planar generator
$R_e$	Single electrode resistance
$R_f$	The resistance of in-fiber electrodes
$R_L$	Resistance of the load
$V^{oc}(t)$	Open-circuit voltage
$w$	Width of a planar generator
$Y_p$	Young's modulus of the piezoelectric material
$Z_f$	The fiber impedance
$\tau_0$	Time constant
$\tau_{co}$	Time constant for open-circuit voltage equilibration
$\tau_{sc}$	Time constant for short-circuit current equilibration
$\varepsilon$	The strain
$\epsilon_p$	The complex effective dielectric constant of BTO suspension in the PVDF matrix
$\epsilon_{BTO}$	The complex dielectric constants of the pure bulk BTO
$\epsilon_{PVDF}$	The complex dielectric constants of the pure bulk PVDF
$\Delta l$	The stage displacement
$\Delta Q$	Surface charges induced on the electrode
BTO	Barium titanate



CB	Carbon black
CNT	Carbon nanotubes
C-LDPE	Carbon filled low density polyethylene
DMF	Dimethylformamide
FT-IR	Fourier-transform infrared spectroscopy
LDPE	Low density polyethylene
LED	Light emitting diode
ICPs	Intrinsically conductive polymers
IMDs	Implantable medical devices
MWCNT	Multiwalled- carbon nanotubes
NFES	Near Field Electrospinning
NPs	Nanoparticles
NWs	Nanowires
PC	Polycarbonate
PE	Polyethylene
PP	Polypropylene
PS	Polystyrene
PVDF	Polyvinylidene fluoride
PZT	Lead zirconate titanate
SD	Standard deviation
SEM	Scanning electron microscopy
SPL	Sound pressure level
VR	Virtual-reality
XRD	X-ray diffraction



## **CHAPTER 1      INTRODUCTION**

In the past decades, the invention of electronic devices [1, 2], the internet, wireless communication [3, 4], etc., have completely changed the world and deeply affected our daily life. The rapid advancements in nanotechnology [5, 6] and micro-/nanofabrication techniques [7-10], enabled the miniaturization of electronic devices, making them portable and convenient. Moreover, tremendous effort was spent to integrate electronic devices into various kinds of textiles, garments, fabrics, thus making them wearable. The first commercialized wearable electronics, Apparel ICD+, were released in 2000 by Industrial Clothing Design Plus [11]. The commercialization of these products triggered a slew of investigations into various wearable electronics, including on-garment displays [11], virtual-reality (VR) devices [12, 13], wearable medical/clinic sensors and monitors [14-16], and smart accessories [17-19], some of which have already been successfully commercialized, such as VR headsets, Google glasses, and Apple watches.

While mobile technologies have advanced rapidly over the past 20 years, the development of power sources has lagged considerably [20]. Now most of existing portable electronics are powered by commercial batteries, mostly rechargeable lithium-ion batteries (LIB) [21]. These batteries are generally heavy, rigid, and require outlets for recharging, which somehow impedes the development and miniaturization of wearable electronics. An alternative approach is to harvest energy from the ambient environment [22]. Solar and thermal energies may be the most common and accessible sources of energy that one can harvest from environmental surroundings; however, utilization of these types of energy is generally limited by the environment of the users. In contrast, harvesting electricity from mechanical movements is more reliable, since mechanical energy is a resource that is largely abundant in our daily life with various energy scales and types such as walking [23], mechanical vibrations [24-26], flowing air and water [27, 28], eye blinking [29, 30] and muscle stretching [31].

In 1880, researchers discovered that piezoelectric materials that operated based on the ‘piezoelectric effect’ [32-34] could convert a sufficient part of mechanical energy into electricity. Since then, extensive effort has been put into this field and a variety of piezoelectric materials have been investigated, including natural quartz crystals [35, 36], mechanically flexible piezoelectric polymers [37], exotic and efficient ceramics [38], and other complex composites. Based on these piezoelectric materials, a range of energy harvesting and conversion devices have been proposed,



such as the bulk structures that can be used to dampen vibrations [39], piezoelectric nanowire-based generators for energy harvesting [40, 41], as well as micro-scale actuators fabricated *via* MEMS process [42-44].

Among all types of piezoelectric generators, perhaps the most promising ones are the piezoelectric fiber-based generators [45-49]. Technically, the advancement of nanotechnology has made it feasible to integrate piezoelectric structures on the surface or the inside of the individual fiber [50-52], which typically has a size from several to tens of microns. These fibers have high energy conversion efficiency, and are capable of harvesting power from small movements [51]. Mechanically, they can be folded, bent, twisted, or stretched while maintaining their electrical properties [53]. Due to their excellent mechanical robustness and flexibility, these fibers could be directly integrated into large-area textiles and fabrics using conventional weaving looms or knitting machines. The as-fabricated ‘piezoelectric garments’ could power on-body electronic systems such as wireless communication networks [54], implantable medical devices (IMDs) [55], and on-garment displays [11], to name a few.

Apart from their wearable applications, the piezoelectric fibers are particularly suitable for the applications in the areas of remote sensing, military industries [56] as well as automotive and aerospace industries [57]. For instance, the piezoelectric fibers could be used as the ultrasensitive sensor for the stand-off sound detection, which opens various possibilities in sensing and defense applications [58]. Moreover, their unique fiber-form-factor allows piezoelectric fibers to be placed/hidden into areas that are not easily accessible such as deep-water, forests, and deep-snow [52]. In a moving vehicle or airplane, piezoelectric fibers harvesting energy from a rotating propeller or other mechanical vibrations could power wireless devices implanted on the surface of the vehicle or airplane [59, 60].

In principle, by engineering the fiber structure and optimizing the fabrication conditions, the piezoelectric functionalities mentioned above could be achieved using a single fiber. Such fibers could be naturally integrated into cotton yarns or textiles, using cost-effective textile production processes. However, there are currently only a few reports regarding to such piezoelectric fibers, due to technical complexity of integration of various sub-components with different functionalities into a textile fiber [61]. In recent reports, most of the existing piezoelectric fibers are fabricated either by growing piezoelectric nanostructures along a conductive filament or by extruding



piezoelectric polymers together with a conductive polymer by melt-spinning [62-65]. The performance and applications of the existing piezoelectric fibers are limited by their simple fiber geometries, large diameter, poor mechanical reliability and relatively low piezoelectric response.

Multimaterial preform-to-fiber drawing methods [66], on the other hand, present unique opportunities for drawing flexible piezoelectric fibers of extended lengths. Most importantly, these methods allow for the fabrication of piezoelectric fibers with complex architectures that integrate a variety of sub-components with different functionalities [67, 68]. In this thesis, we report micro- and nanostructured piezoelectric fibers fabricated *via* heating and drawings of multimaterial preforms. The fibers feature a hollow polycarbonate (PC) core surrounded by a spiral multilayer cladding consisting of alternating piezoelectric PVDF-based nanocomposite layers and conductive layers (carbon-filled low-density polyethylene).

To achieve a successful fiber drawing process, we need to follow several general guidelines. The key challenge of fiber drawing is to maintain the geometry of the fiber while reducing its cross-sectional dimensions. Throughout our many experiments, the multimaterial preforms tended to break-up into filaments during the drawing process. This is because the drawing process decreases the feature size and viscosity, thus naturally causing flow instabilities and finally, facilitating fiber breakage. To achieve a stable drawing, the materials used must be carefully selected, ensuring that they are thermally and mechanically compatible. The materials used for this process must meet the following requirements [66, 67]:

First, at least one of the fiber materials should be amorphous, so that it can withstand the mechanical stress in the fiber drawing process.

In addition, all the materials should flow into a viscous state when heated above the softening temperature.

Also, all the materials used should exhibit good adhesion/wetting in their viscous and solid states without cracking, even when subjected to the rapid heating/cooling rate.

Finally, to obtain fibers with high piezoelectric properties, at least one of the fiber materials should have a high piezoelectric coefficient.

The rest of this thesis is organized as follows:



Chapter 2 begins with a literature review of wearable piezoelectric generators. The wearable power generators made of piezoelectric polymers, ceramics or composites are reviewed with their advantages and limitations discussed.

Chapter 3 provides the methodology in the R&D of piezoelectric micro-/nanostructured fibers, which includes the preparation of the piezoelectric nanocomposites *via* electrospinning, assembly of the planar piezoelectric generators, fabrication of the piezoelectric fibers *via* preform heating and drawing, fabrication of piezoelectric textiles/fabrics *via* loom-weaving, as well as characterization of the corresponding piezoelectric fibers and textiles.

Chapter 4 is based on my paper “Piezoelectric Micro- and Nanostructured Fibers Fabricated from Thermoplastic Nanocomposites Using a Fiber Drawing Technique: Comparative Study and Potential Applications” published in ACS Nano (2017). This paper conducts a comparative study of the piezoelectric micro- and nanostructured fibers using the material combinations including BTO-PVDF, PZT-PVDF and CNT-PVDF.

Chapter 5 is based on my paper “Piezoelectric Microstructured Fibers *via* Drawing of Multimaterial Preforms” published in Scientific Reports (2017). This paper demonstrates the fabrication and characterization of the piezoelectric generators using BTO-polyvinylidene and carbon-loaded-polyethylene in stripe forms as well as in fiber forms.

To conclude, I present a general discussion of results achieved so far and elaborate future research perspectives.



## CHAPTER 2 LITERATURE REVIEW

The electronic products of the future generation place a great demand for the R&D of novel energy harvesting devices that are wearable [40]. To date, significant effort has been put into the R&D of piezoelectric fiber-based generators as they are soft, flexible and comfortable to wearers. In principle, such piezoelectric fibers can be such designed that they feature both a very high energy conversion efficiency, close to that of piezoelectric ceramics, and a very high mechanical flexibility, close to that of piezoelectric polymers. Hence, it is of great importance to study the fiber-based power generators that are able to convert a significant part of the kinetic energy from ambient environment or human movements.

In this Chapter, we begin with a brief introduction of the working principles of the piezoelectric generators. Then, we review the wearable piezoelectric generators according to the different types of the piezoelectric materials. Finally, the motivation and objectives of my doctoral project will be presented.

### 2.1 The working principles of the piezoelectric generators

When the mechanical force is applied to the piezoelectric generators, electrical pulses of voltage (current) could be generated. To explain this phenomenon, we need to study the working principles and the effective electric model of the piezoelectric generators. As shown in Fig. 2.1, the piezoelectric generator could be considered as a capacitor that consists of electric dipoles dispersing in the matrix of the dielectric material [37, 69]. After electrical poling, the electric dipoles in the piezoelectric material could be aligned in the same direction. Even after the electric field is removed, the permanent polarization remains in the piezoelectric material. The electric field of the dipoles will induce the surface charge  $-Q$  at the top electrode and the  $+Q$  at the bottom electrode. When the mechanical stress is applied to the piezoelectric generator, the polarization density of the piezoelectric material will change, which will induce the change of the surface charge ( $\mp Q$ ) at the top and bottom electrode. In response to that, the electrons in the external circuit will force to move from one electrode to the other electrode, generating a piezoelectric potential.

The equivalent electric circuit in the measurement could be illustrated as Fig. 2.1b. In the case of a planar piezoelectric film of length  $l$ , width  $w$ , thickness  $d_p$ , and dielectric constant  $\epsilon_p$ , the



generator capacitance is  $C = \frac{\epsilon_p \epsilon_0 l w}{d_p}$ . And  $R_L$  is the resistance of the load in the electric circuit. The resistance of the electrode resistance that covers the piezoelectric film is  $R_e = \rho \frac{l}{w d_e}$ , where  $d_e$  is the electrode thickness and  $\rho$  is the bulk resistivity of the electrode material. Using standard analysis of this RC electric circuits, we can write the equations that govern time dynamics of the capacitor discharges:

$$\frac{q}{C} + \dot{q} R_L = 0 \quad (1)$$

$$q|_{t=0} = \Delta Q \quad (2)$$

We consider the resistance of the voltmeter  $R_V = \infty$  and the resistance of the currentmeter  $R_c = 0$ . Thus, for the open-circuit voltage measurement, we consider  $R_L \sim R_V$ ; for the short circuit current measurement, we consider  $R_L \sim R_e$ . Finally, we can find simple solutions that satisfy both (1) and initial conditions (2) in the following expressions for the open circuit voltage  $V^{oc}(t)$  and the short circuit current  $I^{sc}(t)$  :

$$\begin{aligned} \text{Open-circuit voltage:} \quad V^{oc}(t) &= \frac{\Delta Q}{C} e^{-\frac{t}{CR_V}} \\ V_{max}^{oc} &= V^{oc}(0) = \frac{\Delta Q}{C} \end{aligned} \quad (3)$$

$$\begin{aligned} \text{Short-circuit current:} \quad I^{sc}(t) &= \frac{\Delta Q}{CR_e} e^{-\frac{t}{CR_e}} \\ I_{max}^{sc} &= I^{sc}(0) = \frac{\Delta Q}{CR_e} \end{aligned} \quad (4)$$

According to the literature [70], fixed charges  $\Delta Q$  induced on the surface of a piezoelectric film of length  $l$  can be calculated as:

$$\Delta Q = d Y_p \epsilon w \cdot l \quad (5)$$

where  $d$  is the piezoelectric coefficient of a piezoelectric film,  $Y_p$  is the Young's modulus of the piezoelectric material,  $w$  is the width of the piezoelectric mat, and  $\epsilon$  is the applied strain. Thus, we can then conclude that the peak open circuit voltage and open circuit currents is proportional to the applied strain and piezoelectric film thickness:

$$|V_{max}^{oc}| = \epsilon \frac{d Y_p w l}{C} = \epsilon d_p \frac{d Y_p}{\epsilon_p \epsilon_0}$$



$$|I_{max}^{sc}| = \varepsilon \frac{w \cdot d_p d_e}{l} \frac{dY_p}{\rho \epsilon_p \epsilon_0} \quad (6)$$

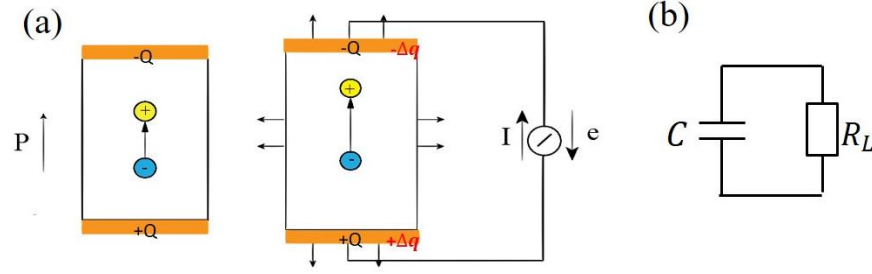


Figure 2.1: Design and working principles of the piezoelectric generators. (a), Schematic illustration of the application of the stress onto a poled piezoelectric generator (e.g. the BaTiO<sub>3</sub> generator). In the initial state (after electrical poling), the electric dipoles maintain the permanent polarization. When mechanical stress is applied onto the piezoelectric generator, the polarization density of the piezoelectric film is changed and the electrons are forced to flow from one electrode to the other, thus generating a piezoelectric potential. (b), The equivalent electric circuit in the measurement. The piezoelectric generator is considered as a capacitor, while  $R_L$  is the resistance of the load in the electric circuit.

## 2.2 The wearable piezoelectric generators

One of the most important concerns for the R&D of wearable piezoelectric generators is the choice of the piezoelectric materials utilized and the possibility to preserve their piezoelectric performance [61], while maintaining their durability, safety, and stability when integrated into flexible systems. In this regard, the following review of wearable piezoelectric generators including flexible planar and fiber devices, will be given based on the different types of piezoelectric materials.

### 2.2.1 Wearable piezoelectric generators based on piezoelectric polymers

The piezoelectric polymers are attractive due to their ease of production, high chemical resistance, superior flexibility, and excellent mechanical robustness [37]. One of the most widely used piezoelectric polymers is poly(vinylidene fluoride) [37] [71], which is also known as PVDF. Depending on the different stereochemical structures, the PVDF polymer has the most common three forms [37], namely  $\alpha$  (TGTG'),  $\beta$  (TTTT),  $\gamma$  (TTTGTTTG') phase respectively (Fig. 2.2).



Commercial PVDF generally has the  $\alpha$  phase, which may be obtained by the melt-extrusion or the film-casting [37]. In the  $\alpha$  phase, the electric dipoles are antiparallel along the chain axes, thus cancelling each other. Therefore,  $\alpha$  phase is a non-polar phase. The  $\beta$  phase is most highly polar phase, whose unit cell of the lattice consists two chains in the TTTT conformation. And the electric dipoles in the  $\beta$  phase are normal to the chain axes. The  $\beta$  phase PVDF could be obtained by stretching the  $\alpha$  phase PVDF together with electrical poling. In the  $\gamma$  phase, the polymer chains are in the TTTGTTTG' conformation, and thus,  $\gamma$  phase has lower polarity when compared with  $\beta$  phase. Consequently, the  $\beta$  phase PVDF is the most desirable phase for generating piezoelectricity [69]. To date, the considerable amount of work has been carried out, aimed at the production of high  $\beta$ -phase PVDF and their integration into wearable structures for energy harvesting. The first report of wearable PVDF piezoelectric generators was proposed by Kyminsis *et al.*[72], in which 8 layers of 28  $\mu\text{m}$  thick PVDF films were stacked in a sneaker. In the fabrication process, the polar  $\beta$ -phase was achieved *via* stretching the PVDF films, followed by an electrical poling. One of the major shortcomings of such generators is the low output power, due to their small active area and low fraction of polar  $\beta$  phase. To address this issue, PVDF nanofibers were produced and then integrated into various wearable generators. PVDF nanofibers are generally more attractive towards bulk PVDF as they have higher energy conversion efficiencies, due to their large surface areas. Recently, a wide range of techniques have been developed to fabricate high performance PVDF nanofibers.

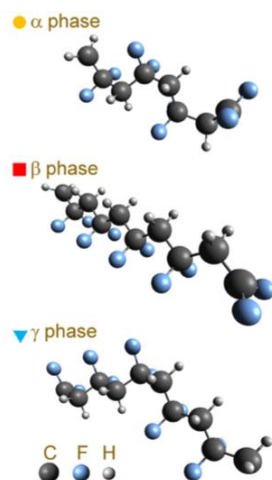


Figure 2.2: Schematic description of the  $\alpha$  (TGTG'),  $\beta$  (TTTT) and  $\gamma$  (TTTGTTTG') phase of PVDF. (a),  $\alpha$  phase. (b),  $\beta$  phase. Reprinted from Ref [67].



Electrospinning [55] is an efficient technique for the production of ultrafine, high  $\beta$  phase PVDF nanofibers. In a typical electrospinning process, a polymer solution is first pumped into a syringe needle that is connected to a high voltage (typically 10-30 kV) power supply. The polymer solution charged by high voltage is then ejected from the needle, and formed a liquid jet. As the solvent evaporates, polymer micro- or nanofibers are produced and collected by a fiber collector. The distance between the needle and the collector is typically in the range of 5-15 cm [73, 74]. And the ordered  $\beta$  phase is induced by the combination of mechanical stretching and electrical poling during electrospinning process [73]. To date, various wearable piezoelectric generators have been fabricated based on electrospun PVDF nanofibers. For example, Zeng *et al.*[75] demonstrated an all-fiber piezoelectric generator that was fabricated by sandwiching a fabric of electrospun PVDF- $\text{NaNbO}_3$  nanofibers between two fabric electrodes. This generator with an area of  $2.5 \times 2.5 \text{ cm}^2$  was able to produce an open-circuit voltage up to 3.4 V during a cyclic compression test (frequency: 1 Hz) with a maximum pressure of 0.2 MPa. Moreover, this generator retained its excellent performance even after 1,000,000 compression–recovery cycles.

It is worth noting that the alignment of nanofibers considerably influences their piezoelectric performance [55, 76]. An electrospun mat with all the nanofibers oriented neatly along their own dipole direction shows significantly improved energy generation efficiency. Also note that a good alignment of electrospun nanofibers can be achieved by the near-field electrospinning process (NFES) [77]. In a NFES, the distance between the collector and the needle is set in the range of millimeter scale, and the applied voltage is thus reduced to  $\sim 1 \text{ kV}$ . Using this technique, various piezoelectric generators based on aligned PVDF nanofibers have been proposed [78-82]. For instance, Fuh *et al.*[83] reported the fabrication of a wearable piezoelectric generator consisting of 20, 000 rows of well-aligned PVDF nanofibers (Fig. 2.3a). This piezoelectric generator ( $3.5 \times 1 \text{ cm}^2$ ) is able to create an open-circuit of 0.8 V with finger folding-releasing actions. Recently, the same group reported a 3-dimensional (3D) piezoelectric device by vertically stacking the electrospun PVDF nanoarrays [84]. Owing to the novel structure, this device could generate open-circuit voltages and short-circuit currents up to  $\sim 1.2 \text{ V}$  and 60 nA respectively. Note that in the fabrication of the piezoelectric generators mentioned above, the electrospun nanofibers are usually physically deposited or assembled on the top of flexible substrates. Thus, these generators typically suffer from poor stability due to the weak binding force between piezoelectric nanofibers and



substrates. Besides, some generators need to attach metal electrodes which limits their applications and lifetime.

Other spinning techniques such as wet-spinning [85] or melting-spinning [86] were also investigated for the fabrication of piezoelectric polymer fibers. As an example, Lund *et al.* fabricate melt-spun PVDF fibers (Fig. 2.3c) that adopt carbon-black filled polyethylene (CB-PE) as the electrodes [63, 87-89]. Typically, the polymer fibers fabricated by spinning techniques feature a core-sheath structure, in which a conductive filament serves as the core, and a piezoelectric polymer layer constitutes the sheath [90]. Besides, the as-spun fibers generally require an additional conductive coating as an external electrode. Such fibers may have reliability issues due to surface abrasion and repeated mechanical deformations.

Apart from traditional spinning techniques, fiber drawing [67, 91] is another efficient technique that can be used to produce piezoelectric polymer fibers. In this method, kilometer-long functional fibers are thermally drawn from a geometrically complex multimaterial fiber preform with a length of tens of centimeters [92]. In the fiber drawing process, firstly a fiber preform is assembled using a variety of materials such as polymers, metals, glass or other functional components and sub-components. Then, the preform is placed in a vertical furnace tower and heated above the transition temperature. Upon heating, extended lengths of fiber with controlled diameter are thermally drawn from the softened preforms. The resultant fiber generally maintains the preform structure but with a much smaller cross-section dimension, which is not achievable through the use of the traditional spinning technique. Kanik *et al.* [93] fabricated piezoelectric PVDF micro- and nanoribbons using an iterative size reduction technique based on thermal fiber drawing (Fig. 2.3b). In order to obtain spontaneously polar  $\gamma$  phase PVDF, the fiber needs to redraw several times. At this point, the fabrication process would be tedious and time-consuming.

In addition to PVDF, other piezoelectric polymers have been investigated for the application in wearable generators. For example, P(VDF-trifluoroethylene) [P(VDF-TrFE)] [94-96] is known for its higher piezoelectric constant than that of PVDF due to the highly ordered crystalline structure by aligning CF<sub>2</sub> dipoles in preferable directions. Various piezoelectric devices based on P(VDF-TrFE) have been fabricated using a range of techniques including electrospinning, melt-spinning, and fiber drawing [66, 97-99]. Egusa *et al.* [66] demonstrated a polycarbonate fiber containing P(VDF-TrFE) as the piezoelectric element and indium filaments as the electrodes (Fig.



2.3d). To fabricate this fiber, a multilayered shell comprising conductive polycarbonate and P(VDF-TrFE) was assembled with indium filaments within a poly(carbonate) cladding to produce a fiber preform that was subsequently drawn by a polymer-fiber drawing tower. The as-drawn fiber was reported to generate an audible sound between 7 kHz and 15 kHz with a driving voltage of 5 V. However, P(VDF-TrFE) copolymers are much more expensive than PVDF.

Table 2.1 summarizes the different types of wearable piezoelectric generators based on piezoelectric polymers. Generally speaking, the piezoelectric polymer generators usually have a long-time lifespan due to the mechanical robustness of the piezoelectric polymer. However, such generators typically suffer from the following shortcomings: First of all, most of the existing piezoelectric generators need to attach metal electrodes which limits their applications and lifetime. The metal electrodes under repeated mechanical deformations generally result in fatigue and fracture. Second, in the most of the existing piezoelectric generators, the piezoelectric fibers/mats are usually physically embedded or deposited onto flexible substrates. These generators suffer from poor stability due to the weak binding force between piezoelectric polymers and substrates. Finally, the output power of some polymer generators is relatively low and is insufficient for practical applications.

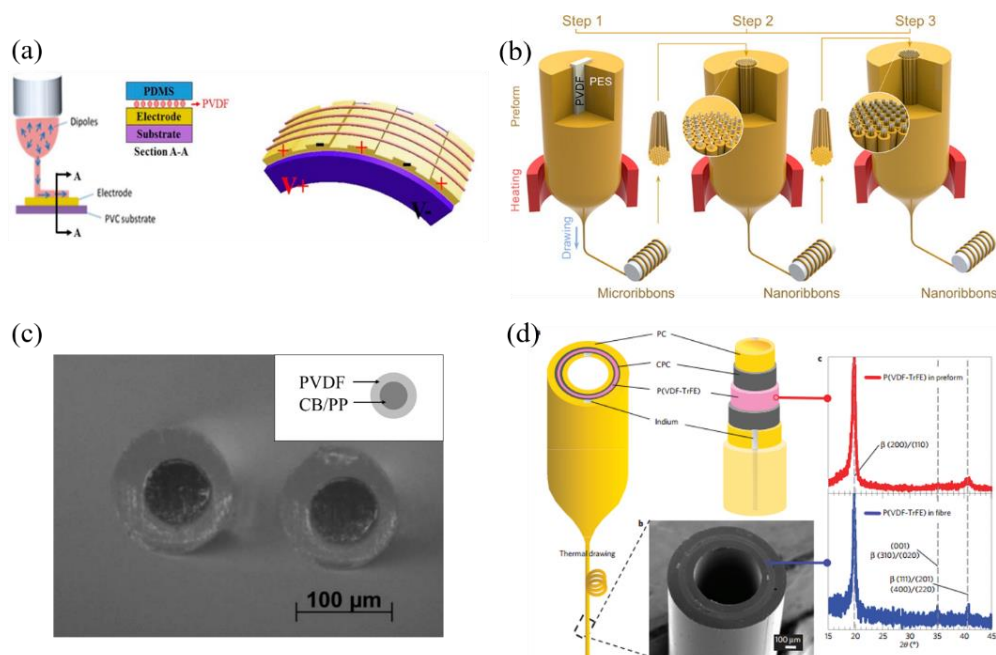
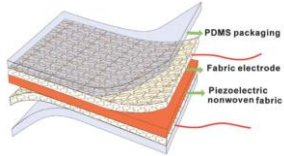
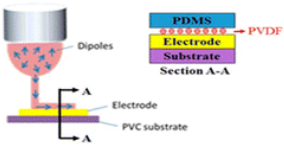
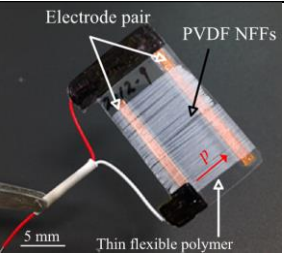
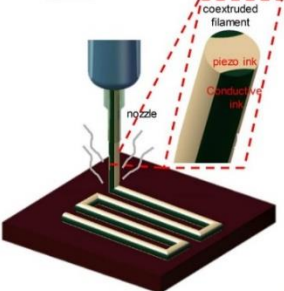


Figure 2.3: Summary of the piezoelectric polymer fibers. (a), Schematic of the direct-write, and electrical poling PVDF fibers *via* NFES. Reprinted from Ref [83]. (b), Schematic of the fabrication

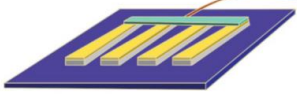
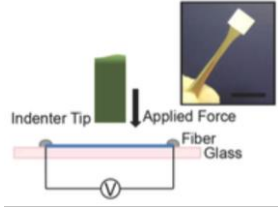
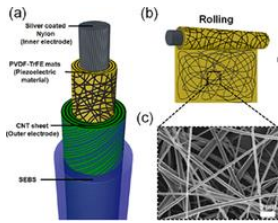


of the piezoelectric PVDF micro- and nanoribbons using iterative size reduction technique. Reprinted from Ref [93]. (c), Cross-section of the PVDF fiber that uses carbon-black (CB)/polypropylene (PP) as the core. Reprinted from Ref [63]. (d), Schematic of the fabrication of the piezoelectric microstructured PVDF fiber using fiber drawing technique. Reprinted from Ref [66].

Table 2.1: The comparison between the different types of wearable piezoelectric generators based on piezoelectric polymers

Type of piezoelectric materials	Photo (diagram) of the generators	Applied force type and area	Generated electrical signals	Comments	Ref
PVDF		Applied cyclic pressure of 0.2 MPa; 2.5×2.5×0.2 cm	3.2 V; 4.2 $\mu$ A	Poor stability	[75]
		Stretching-releasing deformations at a strain of 0.5%; 3.5 cm × 1 cm × 2 $\mu$ m	4 V; 390 nA	Use metallic electrodes	[83]
		Bending-releasing deformations at a strain of 0.05%; Fiber length of 1 mm, fiber diameter of ~200 $\mu$ m	25 mV; 7.5 nA	Poor stability	[81]
		Wing vibration at 0.5 Hz; Fiber length of up to 20 mm	0.2 V	No reports about the output currents	[100]



	 <ul style="list-style-type: none"> <li>PES cladding</li> <li>PVDF microribbon</li> <li>Gold coating</li> <li>Si wafer</li> <li>Ag paste</li> <li>Cu wire</li> <li>PDMS</li> </ul>	Finger tapping-releasing actions; 50 $\mu\text{m}$ thick	$\sim 2.5 \mu\text{A}$ ; $\sim 5\text{V}$	The fabrication process is complex	[93]
PVDF-TrFE		Applied cyclic load of 1 mN; Fiber length of $\sim 80 \mu\text{m}$	$\sim 0.3 \text{ mV}$	No reports about the output currents	[97]
		Applied cyclic pressure of 160 kPa; Fiber length of 10 mm	$\sim 2.6 \text{ V}$ $\sim 15 \text{ nA}$	The fiber has a simple core-sheath structure	[98]

### 2.2.2 Wearable piezoelectric generators based on piezoelectric ceramics

The wearable generators based on piezoelectric ceramics have drawn a lot of interest due to their high energy conversion efficiency and their capacity to harvest energy from small movements [76]. Generally, the piezoelectric ceramics can be divided into two categories [76]: (1) perovskite structured piezoelectric materials, such as barium titanate ( $\text{BaTiO}_3$ ) [38, 101], lead zirconate titanate (PZT) [102, 103], potassium niobate [104, 105], and sodium niobate [104, 106]; (2) semiconductor piezoelectric materials, including Zinc oxide ( $\text{ZnO}$ ) [107, 108], zinc sulfide ( $\text{ZnS}$ ) [109], gallium nitride ( $\text{GaN}$ ) [110, 111] and indium nitride ( $\text{InN}$ ) [112]. However, bulk piezoelectric ceramics are rigid, brittle, and thus unsuitable for wearable applications. In order to circumvent this barrier, flexible devices are fabricated by directly using ceramic nanofibers ( $\text{BaTiO}_3$ , PZT) or nanowires ( $\text{ZnO}$ ) grown on flexible substrates (polymers [113], papers [114], fibers [115], or textiles [116]), or by impregnating piezoelectric micro-/nanoparticles into soft polymers [76, 114].

#### Wearable piezoelectric generators based on perovskite ceramics



In what follows, I will give a brief review of piezoelectric generators based on perovskite ceramics including BaTiO<sub>3</sub> and PZT. Among the advantages of these piezoelectric generators are their low cost, ease of fabrication and high piezoelectric performance.

### **(1) Barium titanate (BaTiO<sub>3</sub>)**

BaTiO<sub>3</sub> is a perovskite crystal, whose structure is schematized in Fig. 2.4a. Each crystal is composed of a small, tetravalent metal ion placed inside a lattice of larger divalent metal ions and O<sup>2-</sup>. Above a critical temperature, which is known as the “Curie temperature”, each perovskite crystal in the heated ceramic element exhibits a simple cubic symmetry with no dipole moment, as demonstrated in Fig. 2.4a [117]. At temperatures lower than the Curie temperature, each crystal has a tetragonal symmetry and exhibits a dipole moment. If a BaTiO<sub>3</sub> tetragonal crystal is placed in a strong DC electric field at a temperature below the Curie temperature, the dipoles will be aligned in the same direction of the electric field. Even after the electric field is removed, the oriented domains maintain the permanent polarization. When the mechanical compression or tension is applied on the BaTiO<sub>3</sub>, the polarization density in the crystal would change, thus generating a piezoelectric potential. As shown in Fig. 2.4b, compression along the direction of polarization, or tension perpendicular to the direction of polarization, could generate voltage of the same polarity as that of the poling voltage. Tension along the direction of polarization, or compression perpendicular to that direction, would generate a voltage with its polarity opposite to that of the poling voltage (Fig. 2.4b) [117].

Bulk BaTiO<sub>3</sub> is brittle and thus can't be directly used as mechanical energy harvesting materials. Instead, piezoelectric generators based on BaTiO<sub>3</sub> are usually fabricated by dispersing BaTiO<sub>3</sub> nanoparticles into flexible polymers [70, 114, 118, 119]. For instance, Park *et al.* [120] demonstrated a planar generator based on BaTiO<sub>3</sub> nanoparticles (NPs) and graphitic carbons (Fig. 2.5a). In this work, the BaTiO<sub>3</sub> nanoparticles and carbon were dispersed in polydimethylsiloxane (PDMS) solution. After drying, the obtained polymer film is sandwiched between two electrode films into a wearable piezoelectric generator. This wearable device could generate the output voltage of ~1.5 V and current of ~150 nA under a pressure of ~ 57 kPa. Here graphitic carbons plays multiple roles, such as improving the dispersion of BaTiO<sub>3</sub> NPs in the host polymer, as well as reinforcing the stress applied to nanoparticles.



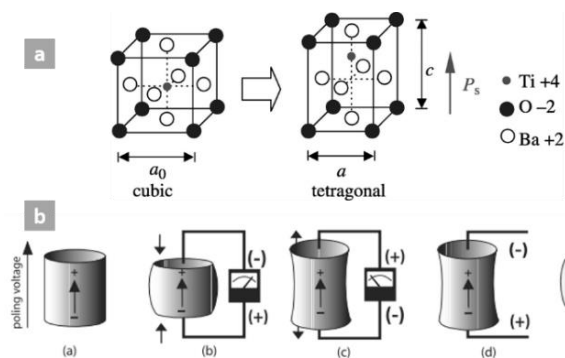


Figure 2.4: (a), Change of unit cell of a BaTiO<sub>3</sub> crystal during spontaneous polarization. (b), Reaction of a poled piezoelectric element to applied stimuli. Reprinted from Ref [117].

To further improve the piezoelectric response, wearable BaTiO<sub>3</sub> generators have been fabricated by combining BaTiO<sub>3</sub> nanostructures with piezoelectric polymers. For instance, Zhao *et al.* [70] reported a flexible generator by dispersing BaTiO<sub>3</sub> NPs into the PVDF matrix using the solvent evaporation method. In this device, PVDF not only functions as a binder for BaTiO<sub>3</sub> NPs, but also plays a part in generating piezoelectric potential. The highest open-circuit voltage and short-circuit current achieved were 150 V and 1500 nA respectively, while a stress of 10 MPa was applied to the piezoelectric generator. Recently, Chen *et al.* [121] demonstrated a flexible device by vertically aligning BaTiO<sub>3</sub>/PVDF micropillar arrays onto parallel multiwall-CNT (MWCNT) electrodes (Fig. 2.5 b,c). This device could generate an enhanced voltage of 13.2 V and a current density of 0.33  $\mu\text{A}/\text{cm}^2$ , which is more than 7-times larger than that of the pristine PVDF bulk films.



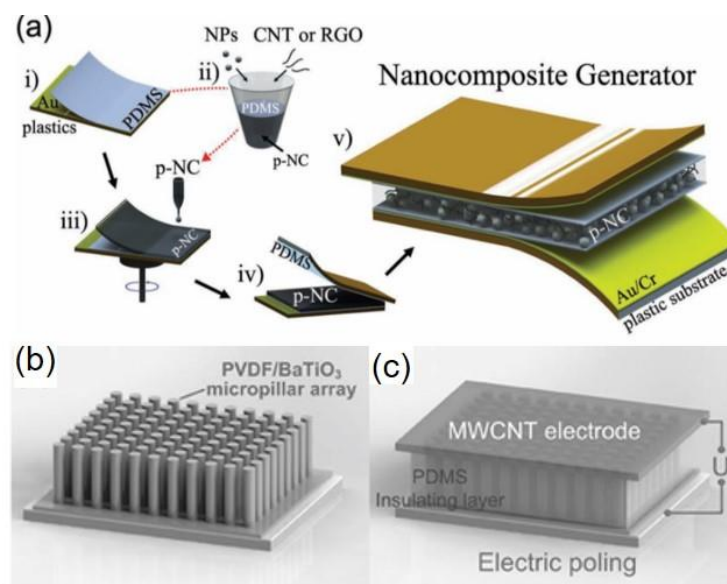


Figure 2.5: Wearable BaTiO<sub>3</sub> generators. (a), Schematics of the fabrication process of the BaTiO<sub>3</sub>-graphitic carbons nanocomposite generator. Reprinted from Ref [120]. (b, c), SEM images of the cross-section of the piezoelectric generator based on BaTiO<sub>3</sub>/PVDF micropillar arrays. c), A magnified top view of the SEM image of MWCNT layer. Reprinted from Ref [121].

## (2) Lead zirconate titanate (PZT)

Similar to barium titanate, lead zirconate titanate ( $\text{Pb}[\text{Zr}_x\text{Ti}_{1-x}]\text{O}_3$ , PZT) also features a perovskite crystal structure, and can be considered as one of the most promising piezoelectric materials due to its higher piezoelectric coefficient compared to that of other piezoelectric materials [122, 123]. Actually, the piezoelectric coefficient ( $d_{33}$ ) of bulk poled PZT can be as large as 289 pm/V, which is ten times higher than that of PVDF [124, 125].

Wearable PZT generators can be fabricated using a scalable transfer printing method. In this approach (Fig. 2.6), high-quality PZT thin films are first grown onto rigid crystal wafers, and then printed onto flexible films of plastic, graphene, or rubber [76]. In this method, a pre-fabricated stamp with the desired features is used to transfer the PZT structures from the rigid wafer to the soft substrate. A conformal contact between the stamp and the substrate enables high fidelity when transferring the material to the surface. The stamp can be made from PDMS, and epoxy, to name a few. Using this method, Kwon *et al.* [126] fabricated a flexible generator based on PZT nanoribbons. In their work, a good quality crystalline PZT was firstly deposited on a Pt/Ti/SiO<sub>2</sub>/Si wafer, which was subsequently etched, and then PZT nanoribbons were transferred onto a flexible



plastic substrate. To improve the electrical performance, a pair of graphene electrodes were used to collect electrical signals. The fabricated piezoelectric generators generated a high output voltage of up to  $\sim 2\text{V}$ , a current density of  $\sim 2.2\ \mu\text{A}/\text{cm}^2$ , and a power density of  $\sim 88\ \text{mW}/\text{cm}^3$  at an applying force of  $\sim 9\ \text{N}$ . This method is effective for large-scale assembly of piezoelectric crystalline ceramics onto flexible substrates. The merits are obvious; however, this technique also has drawbacks. For example, the crystallization of PZT typically requires a high temperature (higher than  $650^\circ\text{C}$ ) to maximize power generation efficiency, which makes the fabrication process expensive and complex.

Another approach begins with electrospinning PZT into nanofibers, following by assembling or packing the nanofibers with soft polymers. This method involves the steps including preparing precursor solutions, electrospinning and subsequently calcining at suitable temperatures to form highly crystalline PZT nanofibers, and finally assembling PZT nanofibers with soft polymers [127-129]. Chen *et al.* [127, 128] demonstrated the wearable generators following this route. In their work, PZT nanofibers with a diameter of  $\sim 100\ \text{nm}$  and a length of  $\sim 70\text{-}100\ \mu\text{m}$  were prepared by electrospinning the sol-gel of PZT and polyvinylpyrrolidone (PVP). Then, the nanofibers were annealed at  $650^\circ\text{C}$  to obtain the perovskite phase. Subsequently, a soft polymer (polydimethylsiloxane, PDMS) was spin-coated on top of the PZT nanofibers. This generator could generate an output voltage of  $1.63\ \text{V}$  and power of  $0.03\ \mu\text{W}$ , under periodic finger press-release actions. Recently, vertically aligned PZT nanowires were prepared by electrospinning [41, 113, 129], and the performance of the as-fabricated piezoelectric generators was greatly improved. Generally, the fabrication of aligned PZT nanowires was performed on multipairs of parallel electrodes using electrospinning (Fig. 2.6d), in which Coulomb force plays a very important role in obtaining parallel nanowires between parallel electrodes [113, 129]. Using this method, Gu *et al.* [113] demonstrated a wearable generator based on ultra-long PZT nanowire arrays. Such generators with an area of  $2.25\ \text{cm}^2$  can produce a maximum peak voltage of  $198\ \text{V}$  for an external load of  $100\ \text{M}\Omega$  and a peak output current of  $17.8\ \mu\text{A}$  for an external load of  $100\ \Omega$ . Moreover, this generator can directly lighten a commercial LED with a working voltage of  $1.9\ \text{V}$  even without the use of storage circuits.



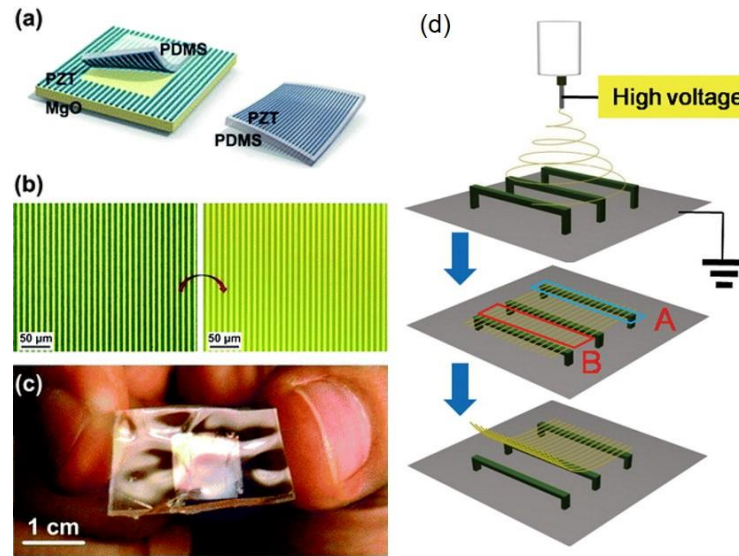


Figure 2.6: Wearable PZT generators. (a, b, c), Transfer printing of PZT nanoribbons onto flexible substrates. (a), A high-quality crystalline PZT was firstly deposited on an MgO host substrate, which was subsequently etched, and then PZT nanoribbons were transferred onto flexible plastic substrate using a PDMS stamp. (b), Optical micrograph of PZT ribbons on MgO substrate before transfer, and PZT ribbons on PDMS after transfer printing. (c), Photograph of a flexible PZT generator. Reprinted from Ref [76, 130]. (d), Schematic diagram of the process for fabricating a PZT textile using electrospinning. Reprinted from Ref [129].

### Wearable piezoelectric generators based on Zinc oxide (ZnO)

Zinc oxide (ZnO) is one of the most attractive semiconductor piezoelectric materials, due to its promising properties including low-cost, bio-safety, and biocompatibility. The growth of ZnO nanostructures is quite simple, and abundant configurations of nanostructures based on ZnO are possible, such as nanowires, nanobelts, nanosprings, and nanobows, to name a few [131, 132]. In the following section, I will give a brief overview of wearable devices based on ZnO nanomaterials.

The working principle of ZnO is shown in Fig. 2.7. Generally, piezoelectric ZnO has hexagonal wurtzite (WZ) structure [133]. Initially, the center of gravity of the negative charges is placed at the center of the crystal. When mechanical pressure or tension is applied on the crystal, as shown in Fig. 2.7b, the tetrahedron will experience a distortion, and thus, its center would be no longer the same as that of gravity of the negative charges. In this way, the electric dipoles could



be induced. In response to that, the corresponding positive and negative charges would be generated on two opposite faces of the crystal.

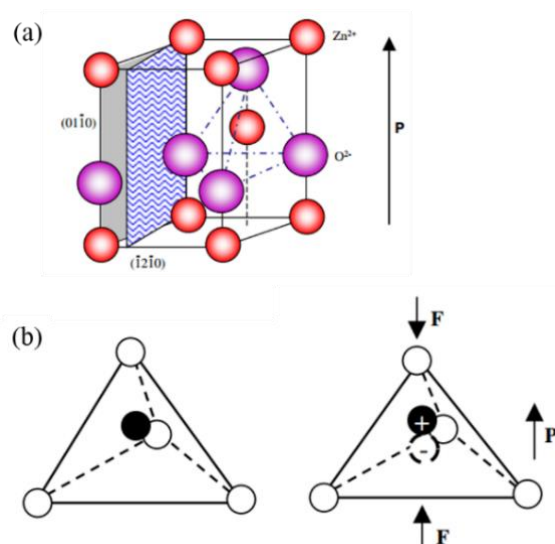


Figure 2.7: (a), The wurtzite structure model of ZnO. (b), Schematic diagrams showing the piezoelectric effect in a tetrahedrally coordinated cation–anion unit. Reprinted from Ref [133].

The first ZnO nanogenerator was demonstrated by deforming an individual ZnO nanowire (NW) with an atomic force microscopy (AFM) tip [134]. In this publication, the vertically aligned ZnO NWs were grown using a vapor-liquid-solid (VLS) process. After that, the fiber generators were demonstrated by growing ZnO on the surface of the textile fiber using a hydrothermal method. For instance, Yin *et al.* [135] presented a fiber-type generator fabricated by growing ZnO nanorods on a copper wire. This generator can generate a current of  $50 \text{ nA} \cdot \text{cm}^{-1}$  at low frequencies (such as  $<10 \text{ Hz}$ ) for more than 5 seconds. However, this fiber generator suffers from poor mechanical reliability due to its stiff metallic core. To address this issue, carbon filaments later have been adopted as the fiber cores because of their good mechanical flexibility. Lee *et al.* [51] reported a fiber-type generator comprising a carbon filament core and ZnO nanowires (NWs) sheath (Fig. 2.8). In this generator, the carbon fiber played the role of an inner electrode, while ZnO NWs served as the piezoelectric-potential generator. A thin layer of metal was deposited on the surface of ZnO NWs, functioning as the outer electrode. This generator ( $\sim 2 \text{ cm}$ ) produced an open-circuit voltage of  $0.1 \text{ V}$  during repeated folding and releasing events of a human elbow. To make further improvements to the wearable applications, a 2D woven nanogenerator was demonstrated using two microfibers [116]. In this generator, one microfiber was covered with ZnO NWs that could



generate electricity from bending movements, while the other microfiber was covered with ZnO NWs together with Au or Pd that could be used as the electrode. However, for all the fiber generators mentioned above, frequent bending/releasing motions may damage the ZnO nanostructures, or even cause cracks of the coating, which would greatly decrease the reliability of these fiber generators [136]. Hence, significant improvements in the mechanical robustness of the fiber structure are necessary in order to achieve a practical, flexible, and reliable power generator for wearable applications.

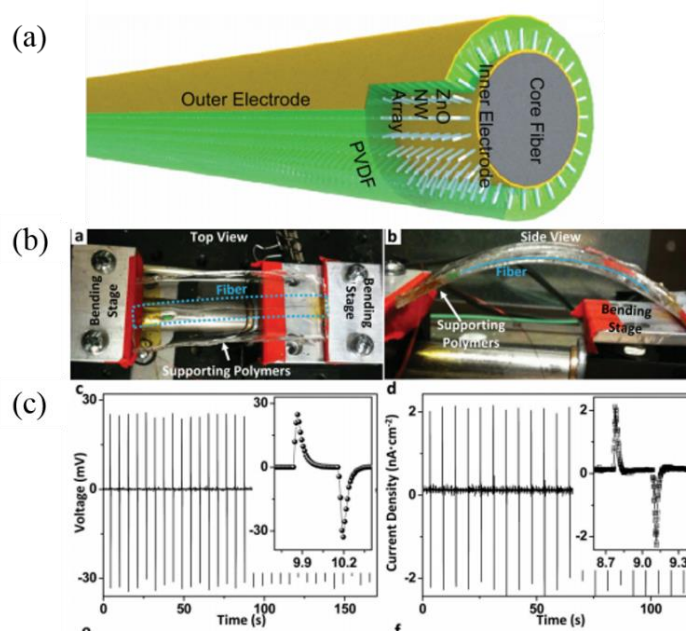
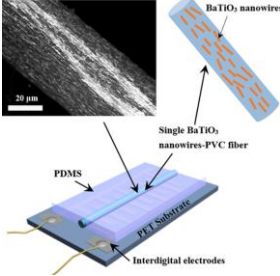
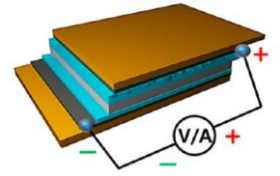
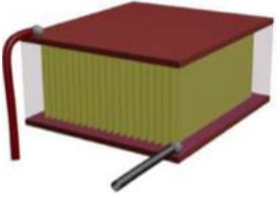
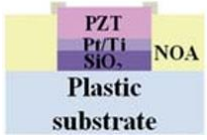
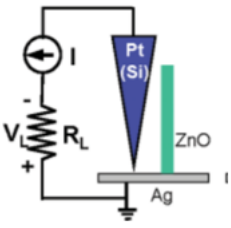


Figure 2.8: Wearable ZnO generator. (a), 3D Schematic diagram depicting the structure of a hybrid-fiber nanogenerator. (b), Image of the experimental setup. (c), Open-circuit output voltage and short-circuit output current density of a fiber device under a strain of  $\sim 0.1\%$ . Reprinted from Ref [51].

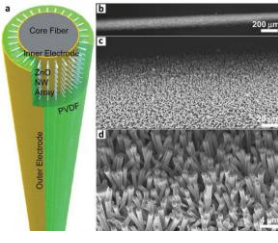
Table 2.2 summarizes the wearable piezoelectric generators based on the different types of the piezoelectric ceramics. Generally speaking, the piezoelectric ceramic generators can have high output power. However, significant progress must be made to achieve a practical, robust and flexible generator, as well as the mass production of self-powered systems. Moreover, novel fabrication techniques require to be developed for integrating the piezoelectric nanostructures into flexible textile fibers.



Table 2.2: The comparison between the different types of wearable piezoelectric generators based on piezoelectric ceramics

Type of piezoelectric materials	Photo (diagram) of the generators	Applied force type and area	Generated electrical signals	Comments	Ref .
BaTiO <sub>3</sub>		Finger bending-releasing actions; ~5 cm × 1 cm	~ 1 V; ~ 10 nA	No reports about the durability tests	[101]
		Applied cyclic pressure of ~0.23 MPa; ~2.2 cm <sup>2</sup>	~75 V; ~ 15 μA	Use metallic electrodes	[118]
PZT		Applied cyclic pressure of 0.53 MPa; 2.25 cm <sup>2</sup>	198 V; 17.8 μA	The fabrication process is complex	[113]
		Applied cyclic force of 0.53 MPa; 1 cm <sup>2</sup>	2 V; 8.82 μA	No reports about the durability tests	[126]
ZnO		Deform an individual ZnO nanowire (NW) with an atomic force microscopy (AFM) tip; Fiber length of ~0.5 μm	~9 mV	No reports about the output currents	[134]



		Repeated folding and releasing events of a human elbow; 2 cm <sup>2</sup>	~0.1 V ~10 $\mu$ A	The fiber is fragile	[51]
--	---	---	-----------------------	----------------------	------

## 2.3 The motivation and objectives

### 2.3.1 The motivation

As discussed in the section 2.2, the piezoelectric polymers are soft, flexible and can be processed at low temperatures. Nevertheless they suffer from poor stability due to the weak binding force between the polymer and the electrodes, as well as the low figure of merit. Alternatively, the piezoelectric ceramics have relatively higher piezoelectric coefficients than that of piezoelectric polymers. However, they are rigid, brittle and require high processing temperature, some being toxic and scarce. On the other hand, piezoelectric composite fibers are light, deformable in three-dimensional manner and processible at moderate temperatures. Most of all, in principle, these piezoelectric fibers can be such designed that they feature both a very high energy conversion efficiency, close to that of piezoelectric ceramics, and a very high mechanical flexibility, close to that of piezoelectric polymers. However, up-to date, very few studies have been reported about such piezoelectric fibers due to the technical difficulties of integrating the piezoelectric micro- and nanostructures into a textile fiber.

The fiber drawing is one of the possible approaches to fabricate the micro- and nanostructured fibers. Using this technique, kilometer-long piezoelectric fibers could be drawn from a multimaterial preform with a length of several tens of centimeters. Our proposed piezoelectric fibers feature a soft hollow polymer core surrounded by a spiral multilayer cladding consisting of alternating layers of piezoelectric nanocomposites and conductive polymer. The multilayer structure of the piezoelectric fiber will greatly increase the active area for the energy generation, thus resulting into higher energy generation efficiency. Other advantages of the proposed fibers, such as the low cost, large-active-area, mechanical reliability, and the possibility of cost-effective mass production, will open an important commercialization opportunity. Particularly, the unique fiber-form-factor allows piezoelectric fibers to be woven into low-cost



textiles using conventional weaving looms or knitting machines. By bending or stretching the piezoelectric textiles, piezoelectricity can be generated. The potential applications of the piezoelectric fibers and textiles could be imaged in the field of wearable, military and automotive industries.

### **2.3.2 The objectives**

In my doctoral research, I will concentrate on the fabrication of piezoelectric planar generators using electrospinning, as well as the fabrication of multimaterial piezoelectric fibers using fiber drawing. The piezoelectric planar generators will be fabricated by sandwiching the piezoelectric electrospun mat between two conductive polymer electrodes. Using fiber drawing, tens of metres of the piezoelectric fibers featuring alternating piezoelectric/conductive multilayers will be thermally drawn from a macroscopic preform. Moreover, novel soft, deformable piezoelectric textiles will be demonstrated by integrating the piezoelectric fibers into the cotton textiles using a classical loom. Finally, I will study the potential applications of the piezoelectric fibers and textiles in the wearable, military, automotive and aerospace industries.

#### **Specific objectives:**

##### **1. Design and fabricate piezoelectric planar generators with high piezoelectric performance using electrospinning**

We will use electrospinning to fabricate the piezoelectric mats, and then assemble the piezoelectric mats into the planar piezoelectric generators. We will characterize the structure and properties of the piezoelectric electrospun mats by the analytical methods, including XRD, SEM, and FT-IR, etc. Also, the electrical properties of the piezoelectric planar generators will be evaluated using our Ivium electrochemical station. Moreover, we will study the effect of nanofiller concentration and electrical poling on the piezoelectric response of the planar generators. Additionally, the charge separation mechanism and effective electric model of the piezoelectric planar generators will be proposed and discussed.

##### **2. Design and fabricate piezoelectric fiber generators with high piezoelectric performance using fiber drawing technique**

We will use fiber drawing technique to fabricate the piezoelectric fibers, and then assemble the piezoelectric fibers into the fiber generators. Similar to that of the piezoelectric planar



generators, the electrical properties of the piezoelectric fibers will be studied using the Ivium electrochemical station. The cross-sectional geometry of the drawn fiber will be studied using SEM and optical microscopy. Also, the effect of the nanofiller type and concentration, and electrical poling on the piezoelectric response of the piezoelectric fibers will be discussed. Moreover, the charge separation mechanism of the piezoelectric fibers in the bend-release measurements will be proposed and discussed.

### **3. Demonstrate prototypes of the textile piezoelectric power generator using the drawn fibers**

The piezoelectric textiles will be fabricated by integrating the piezoelectric fibers into the cotton textiles. The electrical properties of the piezoelectric textiles will be evaluated. We will also study the potential applications of the piezoelectric fibers and textiles in the field of remote sensing and energy generation.



## CHAPTER 3 METHODOLOGY

In this thesis, I demonstrated the fabrication and potential applications of planar piezoelectric generators, micro- and nanostructured piezoelectric fibers and piezoelectric textile generators using several material combinations. The planar generators were assembled by sandwiching the electrospun piezoelectric nanocomposite between two carbon-loaded-polyethylene (C-LDPE) films. The piezoelectric micro- and nanostructured fiber was fabricated *via* drawing of the multilayer fiber preform, and features a swissroll geometry that has several alternating piezoelectric and conductive layers. The piezoelectric textiles were fabricated by integrating the piezoelectric fibers into cotton textiles using a classical Dobby loom. Here the Dobby loom is a type of floor loom that weaves the fibers and yarns into the textiles. In the section that follows, I will introduce the fabrication methodology in detail.

### 3.1 Fabrication

#### 3.1.1 Preparation of piezoelectric nanocomposites using electrospinning

The fabrication of both piezoelectric planar generator and micro-/nano- structured piezoelectric fibers begins with the preparation of the piezoelectric nanocomposites. Here I used the electrospinning technique to fabricate the BTO-PVDF, PZT-PVDF and CNT-PVDF nanocomposites. The PVDF polymer used in this experiment was a semicrystalline PVDF (pellet, Sigma-Aldrich) which has an average molecular weight of ~275,000. Dimethylformamide (DMF) and acetone solvent were purchased from Sigma-Aldrich. BTO nanoparticles (average diameter of 200 nm) were purchased from US Research Nanomaterials Inc. PZT micropowders (50-100  $\mu\text{m}$ , APC 850) were purchased from APC Inc. Multi-walled carbon nanotubes (CNT) were purchased from Sigma-Aldrich.

##### Step 1. Preparation of the suspensions

*The BTO-PVDF suspension.* BTO of defined amount was dispersed in DMF solvent (Sigma-Aldrich) using a probe-type ultrasonicator (Fisher Scientific Inc.; Fig. 3.1) at 100 W in 5 s intervals (3 s pulse on, 2 s pulse off) for 1 h. Here the ultrasonicator is used to improve the dispersion of the BTO nanoparticles. PVDF was dispersed in acetone using a magnetic stirrer for 10 min. Then, the BTO solution and the PVDF solution were mixed together while being heated at



100 °C using a magnetic stirrer for 1 h. Subsequently, the BTO-PVDF solution was sonicated at 75 W in 5 s intervals (3 s pulse on, 2 s pulse off) for 15 min and then put in a vacuum chamber for 5 min to remove air bubbles. In our experiments, the weight concentration of PVDF in the solution was 20 wt%, and weight concentration of BTO in the as-spun BTO-PVDF composite mats was varied from 5 to 25 wt% with a 5 wt% interval. The DMF/acetone volume ratio was 2/3.

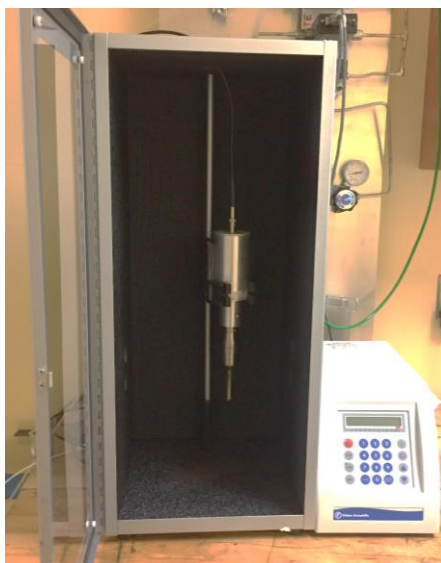


Figure 3.1: The probe-type ultrasonicator (Fisher Scientific Inc.)

*The PZT-PVDF suspension.* PZT powders have a size ranging from 10 to 50  $\mu\text{m}$ . To reduce the PZT particle size and thus enhance their piezoelectric functionality, PZT powders were milled using a ball-milling machine (MSK-SFM-2, MTI Corporation) for 10 h with a milling speed of 200 rpm. 10  $\text{ZrO}_2$  balls with a diameter of 10 mm were used as the milling medium. The weight ratio of PZT powders to the milling balls was 1:20. The milled PZT powders could be then used for the preparation of PZT-PVDF solutions, which follows exactly the same procedures as the case of BTO-PVDF solutions.

*The CNT-PVDF suspension.* Multi-walled carbon nanotubes of defined amount was dispersed in DMF solvent using an ultrasonicator for 15 min. PVDF was dispersed in acetone using a magnetic stirrer for 10 min. Then, the CNT solution and the PVDF solution were mixed together while being heated at 100 °C using a magnetic stirrer for 1 h. Subsequently, the CNT-PVDF solution was sonicated at 75 W in 5 s intervals (3 s pulse on, 2 s pulse off) for 15 min and then put in a vacuum chamber for 5 min to remove air bubbles. In our experiments, the concentration of



PVDF in the solution was 20 wt%, and weight concentration of CNTs in the as-spun BTO-PVDF composite mats was 0.2, 0.4, and 0.6 wt% respectively. The DMF/acetone volume ratio was 2/3.

## **Step 2. Fabrication of piezoelectric mats *via* electrospinning**

Electrospinning is an efficient and versatile fabrication and manufacturing method for the preparation of micro- and nanofibers [6, 11]. A range of materials could be utilized in the electrospinning process including polymers, metals, ceramic material and nanoparticles [6, 11, 79-84]. A typical electrospinning setup includes three important components, which are a syringe with a needle or nozzle, a high voltage power supply and a grounded collector. In the electrospinning process, the polymer solution is charged by the high voltage (typically in the range of 10 to 30 kV), and pumped out through the syringe needle using a computer-controlled mechanical pump. When the electrical field between the droplet towards the needle and the grounded collector is high enough, the electrostatic repulsion within the charged solution would overcome the surface tension, and thus the droplet towards the needle would be stretched [81, 82]. At a critical point, a stream of polymer jet erupts from the surface of the droplet; that point of eruption is known as the Taylor cone [137]. As the polymer jet evaporates, polymer micro- and nanofibers are collected by the fiber collector. The morphology and properties of the resulting fibers are influenced by the following three main categories [138]: (1) the properties of the applied solutions such as molecular weight, solubility, viscosity, dielectric constant, conductivity, surface tension, and evaporation rate [79-81]; (2) the set-up parameters such as the applied voltage, the feeding rate of solution, the needle gauge, and needle tip-to-collector distance [83, 84]; (3) the ambient parameters including temperature, humidity, and air velocity in the chamber [79-81].

In this thesis, the electrospinning was done in a commercial electrospinning workstation (MTI Corporation<sup>®</sup> MSK-NFES-3) as schematically demonstrated in Fig. 3.2. This electrospinning workstation consists of a high voltage supply, a glass syringe (20 mL) with a blunt metallic needle (22 gauge) and a grounded metallic drum (diameter: 5 cm). The drum for collecting piezoelectric fibers was set at a rotating speed of 200 rpm. In the electrospinning, the polymer suspensions were charged by a high voltage of 15 kV, and the distance between the needle tip and the drum collector was 15 cm. Electrospinning was done with an ejection rate of 1 *ml/h* from the syringe. The temperature in the electrospinning chamber was controlled at 25 °C. After the electrospinning, the electrospun mats were vacuum dried at room temperature for 24 h.



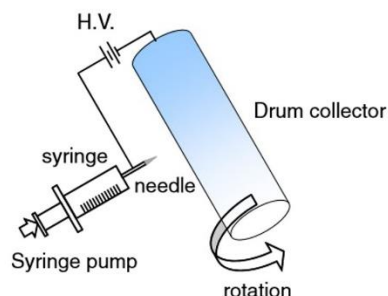


Figure 3.2: Schematic of the electrospinning. Reprinted from Ref [139].

### 3.1.2 Fabrication of the piezoelectric planar generators

As shown in Fig. 3.3, the piezoelectric planar generator has a laminated structure, comprising of a carbon black filled low-density polyethylene film (C-LDPE) as the top electrode ( $\sim 85\mu\text{m}$  thick;  $2.2\ \Omega\cdot\text{m}$ ; Bystat inc.), an electrospun nanocomposite ( $\sim 100\ \mu\text{m}$  thick), a C-LDPE counter electrode, a Kapton film ( $\sim 125\ \mu\text{m}$  thick; McMaster Inc.) and a supporting polystyrene (PS) substrate ( $\sim 1\ \text{mm}$  thick; McMaster Inc.). The PS substrate was attached to the devices for delivering identical strains throughout the active piezoelectric layer.



Figure 3.3: The design of piezoelectric planar generators

### 3.1.3 Fabrication of the micro-/nano- structured piezoelectric fibers *via* fiber drawing technique

Micro- and nanostructured piezoelectric fibers could be fabricated using the fiber drawing technique [91]. In this method, a geometrically complex multimaterial fiber preform with a length of tens of centimeters is first assembled using stacking of tubes, rods, multilayered films, or other functional components [91]. Then, the preform could be drawn into fibers using a fiber drawing tower. Geometry of the resultant fibers depends on parameters in the drawing process such as the temperature distribution in a furnace, the fiber drawing speed and the preform feed velocity, pressurization of the preform, as well as application of the electromagnetic fields [92, 93]. In the



following section, I will introduce the fabrication steps of micro- and nanostructured piezoelectric fibers in detail.

### **Step 1. Assembly of the fiber preforms**

The fabrication of the micro-/nano- structured piezoelectric fibers starts with the assembly of the fiber preform. As illustrated in Fig. 3.4, the preform was fabricated by co-rolling four alternating electrospun PVDF-based piezoelectric mats and C-LDPE conductive films around a PC tube with the outer diameter of 2.54 cm. In our choice of the materials for fiber fabrication we used two criteria. First, to obtain the fibers with high piezoelectric performance, the active material should have high piezoelectric coefficient. Second, to maintain the high degree of control over drawing of the kilometer-long piezoelectric fibers the materials in the fiber preform should be thermo-mechanically compatible. Thus, PVDF was chosen as the host material for the piezoelectric layers, as it is a low-cost, stable thermoplastic polymer that can exhibit the relatively high value of the piezoelectric coefficient. The PVDF-based piezoelectric nanocomposite mats used in fiber preform assembly were fabricated using electrospinning as this process allows fine-tuning of the thermo-mechanical properties of nanocomposites by changing the polymer molecular weight, the concentration of the nanofillers and the processing conditions. C-LDPE was selected as the conductive materials, as it is both thermoplastic and electrically conductive (volume resistivity:  $2.2 \Omega \cdot \text{m}$ ). The PC polymer was used as the fiber core, acting as the mechanical support for the active layers during fiber drawing.

After assembly, the co-rolled preform was consolidated in a vacuum oven at a temperature of  $110^\circ \text{C}$  for more than 12 hrs. The resulting piezoelectric fiber preforms typically feature  $\sim 10$  bilayers of C-LDPE films and PVDF-based piezoelectric layers that are wrapped around a PC core (Fig. 3.4). The two C-LDPE electrode layers were extended to the opposite sides of the exposed preform surface for convenience of the electrical connectorization.



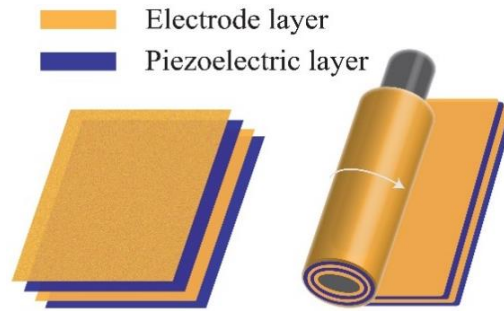


Figure 3.4: Assembly of the fiber preform

### Step 2. Fiber drawing process

As shown in Fig. 3.5, the as-assembled preform was placed into the vertical furnace of the fiber drawing tower. Upon heating, the preform tip melts, and forms a blob that later falls down under the force of gravity, thus creating a slender fiber that can be pulled from the molten preform tip. In actuality, a clamp tractor is used to continuously pull the fiber at a constant speed. The final diameter of a resultant fiber depends on the parameters used in the fiber drawing process including the fiber drawing speed, temperature distribution in the furnace, preform feeding speed, as well as overpressure to the fiber preform during drawing. Experimentally, we set the drawing speed as 500 mm/min, and used an air-pressure of 3 mbar to pressurize the fiber core during drawing. A high voltage of up to 5 kV was applied to the preform to promote the  $\beta$  phase transformation in the PVDF layer.

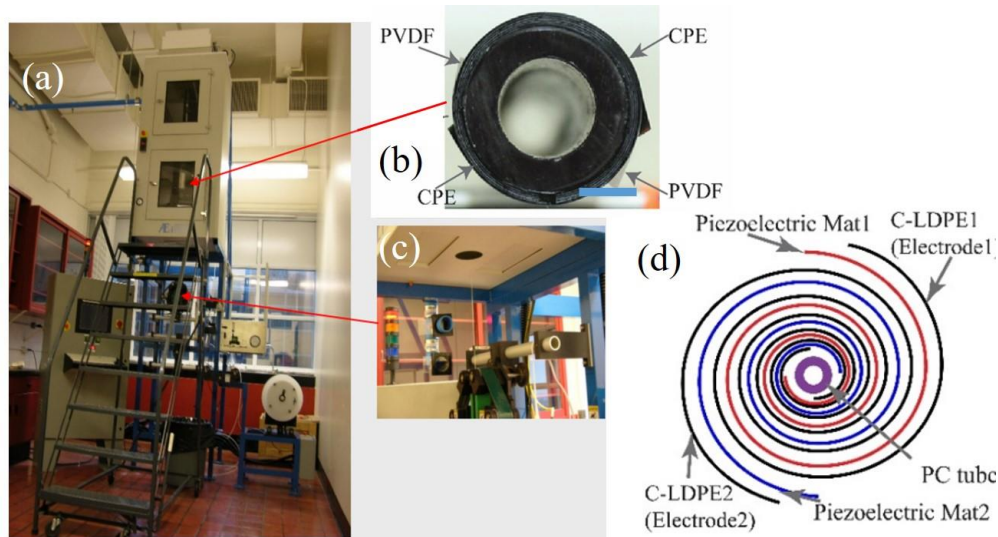


Figure 3.5: The fiber drawing process. (a), image of the fiber drawing tower. (b), image of the fiber preform cross-section. The blue scale bar is of  $\sim 1$  cm. (c), image of the clamp tractor. (d),



schematic of the fiber cross-section. The preform is fabricated by co-rolling electrospun polyvinylidene fluoride (PVDF) mat and C-LDPE film around a polycarbonate tube (PC tube).

### 3.1.4 Fabrication of piezoelectric fiber generators

The structure of piezoelectric fiber generators is schematically demonstrated in Fig. 3.6. It consisted of a 1-mm-thick polystyrene (PS) substrate (Mcmaster Inc.) and a 63.5  $\mu\text{m}$ -thick Kapton tape covering layer (Mcmaster Inc.). The PS plastic plate served as the bottom supporter and the Kapton tape is used to immobilize the piezoelectric fiber on the PS supporter and ensure the fiber to undertake the identical strain under a certain external stress.

To further increase the piezoelectricity, the as-fabricated piezoelectric planar and fiber generators were also poled after assembly. To prevent the electrical breakdown of the air, during the whole poling process, the poled devices were completely immersed into the silicone oil at a temperature of 80° C. The poling voltage was set at 1 kV for the first 12 hrs, then 5 kV for the next 12 hrs, and finally 9 kV for the last 24 hrs.

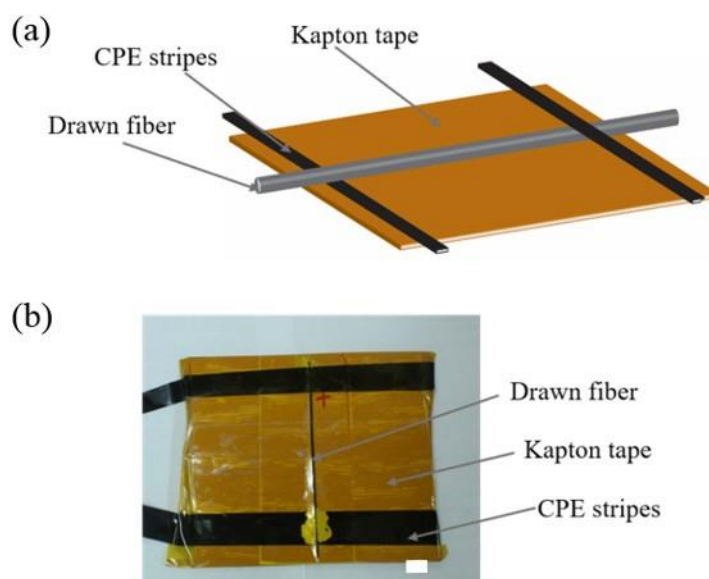


Figure 3.6 : (a) Schematic diagram and (b) Image of the piezoelectric fiber generator.

The scale bar is of ~ 1 cm.



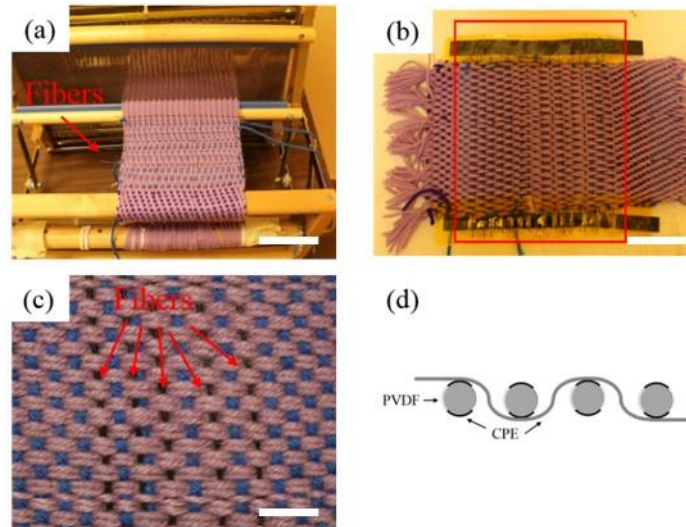


Figure 3.7: (a), The loom and a fabricated textile integrated with piezoelectric fibers. The scale bar is  $\sim 6$  cm. (b), The piezoelectric textile generators. The scale bar is  $\sim 5$  cm. (c), The image of the piezoelectric fiber. The scale bar is  $\sim 1$  cm. (d) Schematic of the electrodes connection (connected in series) at one fiber end.

### 3.1.5 Fabrication of the piezoelectric textiles

The as-fabricated piezoelectric fibers are flexible, and thus could be easily integrated into the cotton textiles using a traditional Dobby loom. As shown in Fig. 3.7a, purple cotton fibers were fixed in parallel on the loom as warp yarns, and twenty piezoelectric fibers, with the length of  $\sim 20$  cm, were integrated into the gaps of purple cotton fibers one by one. Finally, all these piezoelectric fibers were connected in series or in parallel using C-LDPE strips.

## 3.2 Characterization

### 3.2.1 Material characterization

In what follows I discuss the characterization of the electrospun nanocomposites using Fourier-transform infrared (FTIR) spectroscopy, X-ray diffraction (XRD) spectroscopy and Scanning electron microscopy (SEM).

#### Fourier-transform infrared spectroscopy (FTIR)



Poly(vinylidene fluoride) (PVDF) is a semi-crystalline polymer and has at least four phases. Among these phases, the polar phase  $\beta$  is the dominant one for its piezoelectric properties. Thus, to theoretically analyze the piezoelectric properties of the electrospun PVDF-based composite mat, we should first determine the degree of the  $\beta$  phase presenting in the samples.

Using a FTIR spectrometer, absorption spectra of samples in the infrared band were obtained, and several absorption bands can be overlapped. Among these bands, the 761 and 840  $\text{cm}^{-1}$  infrared absorption bands characterize the  $\alpha$  and  $\beta$  phases, respectively. The  $\beta$  phase content,  $F(\beta)$ , in the PVDF mats was calculated using the following Eq.: [140]

$$F(\beta) = \frac{X_\beta}{X_\alpha + X_\beta} = \frac{A_\beta}{\frac{K_\beta}{K_\alpha} A_\alpha + A_\beta}$$

where  $A_\alpha$  and  $A_\beta$  are the absorbances at 761  $\text{cm}^{-1}$  and 840  $\text{cm}^{-1}$  respectively, and  $X$  is the degree of crystallinity of each phase.  $K_\alpha$  and  $K_\beta$  are the absorption coefficient at the respective wavenumber, which are  $6.1 \times 10^4$  and  $7.7 \times 10^4 \text{ cm}^2 \text{ mol}^{-1}$ .

### **X-ray diffraction (XRD) analysis**

X-ray diffraction (XRD) spectroscopy can be used to identify crystalline phases in the nanocomposites. Using an X-ray diffractometer, scattering spectra of samples can be recorded. The characteristic pattern recorded by a typical X-ray diffractometer provides unique “fingerprint” of the crystals present in the tested samples [6]. In the case of PVDF mats, peaks at  $2\theta$  value of  $18.5^\circ$  and  $20.4^\circ$  are indexed to the  $\alpha$  phase [(020)] and  $\beta$  phase [(200)/(110)], respectively [91]. In my experiments, the X-ray diffraction patterns were recorded by a Bruker D8/Discover diffractometer equipped with a standard sealed tube producing Cu radiation ( $\lambda = 1.54178 \text{ \AA}$ ) running at 40 kV and 40 mA.

### **Microstructure characterization**

A scanning electron microscope (JEOL) was used to examine the surface morphology of the nanocomposites, and to determine the average length and diameter of the nanofibers. The samples were sputter coated with gold and examined at an accelerating voltage of 10 kV.



### 3.2.2 Electrical characterization

Here I characterized the electrical properties of the piezoelectric planar and fiber generators. In all tests, the open-circuit voltages and short-circuit currents generated by the piezoelectric devices were measured using an electrochemical station (Ivium Technologies) with a sampling time constant of 0.1 s.

#### **Bend-release tests**

Firstly, the electrical properties of the piezoelectric planar and fiber generators were determined by the bend-release tests. In the experiment, the tested generator was mounted on a bend-release setup as shown in Fig. 3.8. In the experiments, one end of the tested device was fixed on a stationary stage, while the other end of the tested device was fixed on a micropositioning stage which was controlled by a LabView program. The displacements of the micropositioning stage were set to be 5 cm, 10 cm, 15 cm, and 20 cm, respectively based on the characterization requirements. During each bend-release cycle, the bend motion lasted for 0.2 s, followed by a pause of 5 s at the maximum displacement (bent state); the release motion also lasted for 0.2 s, followed by a 5 s pause in the original position (released state). For the piezoelectricity characterization, the bend-release tests with different displacements were repeated at least 5 cycles. While for the durability test, the whole test lasted at least 3 days.

#### **Arm fold-release tests**

To demonstrate the wearable applications for energy harvesting, I performed the experiments as follows. Firstly, the piezoelectric fibers were woven into cotton textiles using a classic Dobby loom. Then, the as-fabricated piezoelectric textile was attached to the arm of an adult. The electrical properties of the piezoelectric textile were examined by multiple folding-releasing actions of human elbows at low frequencies.



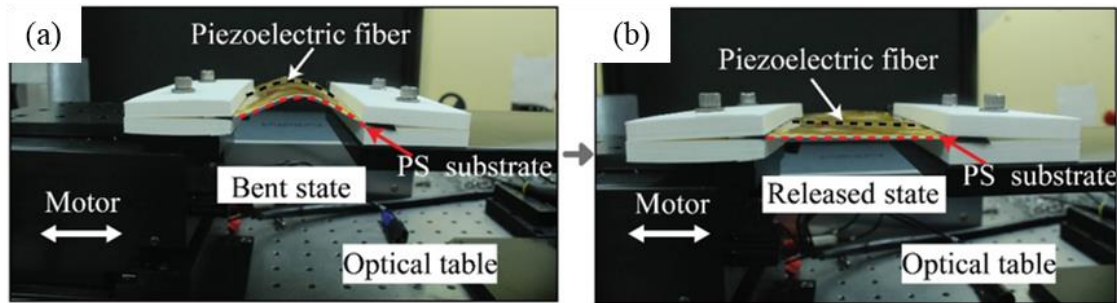


Figure 3.8: The experimental setup for the electrical characterization in (a) bent state and (b) released state.

### Sound tests

The piezoelectric fibers could be used as the ultrasensitive sound sensors. The sound is a type of mechanical vibrations that typically propagates through matter as an audible wave of pressure. When the sound wave strikes the piezoelectric fiber, it causes the piezoelectric fiber compressing and releasing, and thus, positive and negative voltages spikes could be observed. The functional relationship between the generated voltages and the parameters of the applied sound wave can be described as  $V^2 \propto P/f$ , where  $P$ ,  $V$ , and  $f$  are the power (which is defined as the input intensity of the sound wave multiplied by the surface area), the output voltage generated from the piezoelectric fiber, and the frequency of the applied sound wave, respectively [141].

In one experiment, the sound wave was generated by a speaker of a Dell laptop (XPS 13) and controlled by the commercial software (Adobe Audition). The tested piezoelectric fiber was fixed facing the speaker. The distance between the piezoelectric fiber and speaker is  $\sim 20$  cm. The experiment setup was put inside an anechoic chamber (Fisher Scientific). In another experiment, the sound wave (frequency:  $\sim 20$  kHz) was generated by an ultrasonic probe. The piezoelectric fiber generator was fixed in a water tank (dimension:  $60\text{ cm} \times 28\text{ cm} \times 15\text{ cm}$ ). The distance between the probe and the fiber was  $\sim 20$  cm. The sonication was repeated with a period of 6s (1 s on, 5 s off). Note that, to eliminate the environmental factors, the experiments were done in a closed room. The laptop was controlled using a remote-control software (Teamviewer).

### Airplane and vehicle tests

To explore the application in the area of automotive and transport, I conduct the following experiments. In the airplane test, the piezoelectric fiber with a length of  $\sim 15$  cm and a diameter of  $\sim 1$  mm was immobilized on the surface of an airplane model. During the tests, the airplane model



was fixed on a wooden table. As we turned on the airplane motor, the rotation of the airplane propeller resulted in the irregular vibrations of the piezoelectric fibers, thus generating the electric signal. In the vehicle test, the piezoelectric textile was fixed on the seat of a vehicle (Hyundai sedan), and a 22 kg sandbag was put on the surface of the textile. When the car is running, the traffic-induced vibration of the vehicle led to the distortion of the piezoelectric fibers in the textile, thus generating electric current. A simple full-wave bridge rectifier circuit was used to ensure that the current generated by the textiles with consistent polarity.



## **CHAPTER 4      ARTICLE 1: PIEZOELECTRIC MICRO- AND NANOSTRUCTURED FIBERS FABRICATED FROM THERMOPLASTIC NANOCOMPOSITES USING A FIBER DRAWING TECHNIQUE: COMPARATIVE STUDY AND POTENTIAL APPLICATIONS**

This chapter is based on my paper “Piezoelectric Micro- and Nanostructured Fibers Fabricated from Thermoplastic Nanocomposites Using a Fiber Drawing Technique: Comparative Study and Potential Applications” published in ACS Nano in 2017 [91]. I am the primary author of this paper, while this paper is co-written by Hang Qu and Maksim Skorobogatiy from Ecole Polytechnique de Montreal.

In this chapter, we report an all-polymer flexible piezoelectric fiber that uses both judiciously chosen geometry and advanced materials in order to enhance fiber piezoelectric response. The microstructured/nanostructured fiber features a soft hollow polycarbonate core surrounded with a spiral multilayer cladding consisting of alternating layers of piezoelectric nanocomposites (polyvinylidene enhanced with BaTiO<sub>3</sub>, PZT or CNT) and conductive polymer (carbon filled polyethylene). The conductive polymer layers serve as two electrodes and they also form two spatially offset electric connectors on the fiber surface designed for the ease of connectorization. Kilometer-long piezoelectric fibers of submillimeter diameters are thermally drawn from a macroscopic preform. The fibers exhibit high output voltage of up to 6V under moderate bending, and they show excellent mechanical and electrical durability in a cyclic bend-release test. The micron/nano-size multilayer structure enhances in-fiber poling efficiency thanks to the small distance between the conducting electrodes sandwiching the piezoelectric composite layers. Additionally, spiral structure greatly increases the active area of the piezoelectric composite, thus promoting higher voltage generation and resulting in 10-100 higher power generation efficiency over the existing piezoelectric cables. Finally, we weave the fabricated piezoelectric fibers into technical textiles and demonstrate their potential applications in power generation when used as a sound detector, smart car seat upholstery or wearable.



## 4.1 Introduction

Over the past decade, significant effort has been put into the R&D of energy harvesting and conversion devices that operate based on piezoelectric effect [142-145]. Unlike the energy harvesters utilizing solar or thermal energy, performance of piezoelectric generators is generally not limited by the environmental factors. An important driving force for developing piezoelectric energy generators is the growing popularity of the personal wearable electronics such as on-garment displays, wearable sensors in sports and medicine, virtual-reality devices, and smart watches and bracelets [11, 146-149]. In these devices, piezoelectric generators or transducers utilizing mechanical energy from human body motions could be used as power sources or sensor components. Another emerging field where piezoelectric generators could find niche applications relates to the self-energized electronics for automotive or aerospace industries. Piezoelectric generators harvesting energy from the traffic-induced vibrations or other parasitic mechanical movements motions could power on-board electronic systems such as wireless sensor networks (WSNs) with low-power consumption [150, 151]. Note that for these applications, piezoelectric generators in the form of fibers or strips are highly desired [75], as thanks to their flexibility, they could be weaved seamlessly into multifunctional fabrics for wearable or on-board applications, or, alternatively, coiled into compact energy generation cells.

Many attempts have been made to fabricate piezoelectric fibers. A simple method is directly depositing or wet-extruding ceramic piezoelectric materials such as ZnO nanowires (NWs), BaTiO<sub>3</sub> (BTO) NWs and Pb(Zr<sub>0.52</sub>Ti<sub>0.48</sub>)O<sub>3</sub> (PZT) NWs along a metallic wire/filament [51, 52, 152]. For instance, Qiu *et al.* reported a piezoelectric fiber fabricated by extruding a mixture of PNN-PZT powder and organic solvent along a Pt wire [152]. Wang and coworkers proposed a ZnO-based piezoelectric fiber fabricated by growing ZnO-NWs on an Au-coated Kevlar fiber using a hydrothermal method [52]. Note that the mechanical reliability of these piezoelectric fibers could be problematic, since frequent bending and surface abrasion would make the ceramic materials cracking and even peeling off from the fiber core. To improve robustness of the fibers, Wang and co-workers have proposed to cover the base of ZnO NWs with a protective polydimethylsiloxane (PDMS) layer using a method combining surface-coating and plasma-etching [136]. Instead of depositing piezoelectric layers onto a fiber/wire substrate, fabrication of piezoelectric fibers directly from piezoelectric polymers constitutes an alternative option. Compared to ceramic



materials, piezoelectric polymers generally have better flexibility, thus they are more suitable for wearable applications. Among all of the piezoelectric polymers, poly(vinylidene fluoride) (PVDF) and poly(vinylidene fluoride-co-trifluoroethylene) (PVDF-TrFE) are predominantly utilized in piezoelectric devices due to ease of their thermal processing, high flexibility, high strain level and good piezoelectric properties. Lund *et al.* used the melt-spinning method to fabricate a bicomponent fiber that had a PVDF sheath and a carbon-black impregnated polyethylene (CB-PE) core serving as the inner electrode [63, 65]. Recently, Liu *et al.* adopted an electrowetting-aided dry spinning method to fabricate a piezoelectric fiber featuring a metallic core covered by a thin PVDF or PVDF-TrFE layer [64]. Piezoelectric fibers produced *via* the traditional spinning methods typically adopt a simple core-sheath structure, and the as-spun fibers may require an additional deposition of a metallic layer as an outer electrode that may have reliability issues due to surface abrasion and repeated bending or stretching actions. Also note that for PVDF piezoelectric fibers, high-voltage poling of the PVDF layers has to be performed during (or after) the spinning process in order to promote the nonpolar  $\alpha$  to the ferroelectric  $\beta$  phase transition. In addition to electric poling of PVDF, one also uses stretching during poling process, thus further complicating the fabrication process. PVDF-TrFE, on the other hand, could spontaneously crystallize into  $\beta$  phase during its solidification during a spinning process; however, compared to PVDF, the price of PVDF-TrFE is considerably higher.

Piezoelectric polymer fibers could be also fabricated using the fiber drawing technique. In this method, a geometrically complex multimaterial fiber preform with a length of tens of centimeters is first assembled using stacking of tubes, rods, multilayered films, or other functional components. Then, the preform could be drawn into fibers using a fiber drawing tower (Fig. 4.1a). Geometry of the resultant fibers depends on parameters in the drawing process such as the temperature distribution in a furnace, the fiber drawing speed and the preform feed velocity, pressurization of the preform, as well as application of the electromagnetic fields. Fibers drawn from a macroscopic preform would generally retain the preform structure; however, sizes of the constituent elements will be reduced to micro- or even nanoscale. Therefore, various geometrically complex transverse structures that considerably enhance the fiber functionality could be realized within a fiber on a sub-micron scale by engineering the preform structure on a macroscopic scale and optimizing the conditions of the fiber drawing process. This, generally, cannot be accomplished by traditional fiber-spinning methods such as melt-spinning [153], or wet-spinning [154, 155]. As



an example, Egusa *et al.* demonstrated a multimaterial piezoelectric fiber using the fiber drawing technique [66]. This piezoelectric fiber featured a PVDF-TrFE piezoelectric layer sandwiched between two conductive polycarbonate (CPC) electrode layers and assembled with Tin microfilaments for electrical connection. The fiber also had an outermost isolating PC layer serving as the protective cladding. An acoustic transducer was developed based on this fiber, and showed a good response to acoustic waves with frequencies from kilohertz to megahertz. The fiber had several limitations, as it used very expensive PVDF-TrFE material, and it integrated in its structure a Tin metallic microfilament, thus reducing the fiber reliability with respect to flexing. Finally, connecting to such fibers is challenging, as it requires manipulation with built-in micron-sized metallic electrodes. In ref [93] it was proposed that spontaneous piezoelectricity can be achieved in PVDF nanoribbons, when using consecutive re-drawings of the same fiber under high voltage. The authors claimed that under such conditions PVDF could crystallize into an exotic piezoelectric  $\gamma$  phase. At this point, it is difficult to evaluate the robustness of this fabrication technique, as there were no further reports of using this fabrication method. Additionally, multiple re-drawing of the same fiber is needed for fabrication of PVDF nanoribbons, which could be labor intensive and of low yield. To improve the piezoelectric properties of the drawn fiber, while avoiding using expensive PVDF-TrFE, a PVDF impregnated with ceramic piezoelectric materials such as BTO and PZT could be used instead [34, 156, 157]. Although a higher concentration of the ceramic fillers generally results in enhanced piezoelectric performance of PVDF, it would at the same time affect the polymer viscosity [66], thus eventually leading to capillary break-up of the fiber during drawing. This is because, viscous liquids, due to their surface tension, seek to adopt a geometry that minimize their surface energy. This phenomenon was first discovered by Lord Rayleigh. The theory of Rayleigh instability indicates that the time constant of capillary instability growth is proportional to the feature size and viscosity, and inversely proportional to the surface tension. During the fiber drawing process, the preform diameter is becoming smaller and smaller, and thus, the capillary break-up may naturally occur. To enable a successful fiber drawing process, one should choose the materials with similar thermal-mechanical properties. And special attention should be paid to the maximal concentration of ceramic fillers. Furthermore, CNT could be also impregnated into PVDF in order to enhance its piezoelectric properties *via* spontaneous formation of the  $\beta$  phase crystals in PVDF [158-160]. Incorporation of a small amount of CNT can lead to remarkable improvements of the electrical and mechanical properties of the PVDF fibers as



reported in ref [161]. There, the authors argued that application of a shear stress to the polymer melt leads to the preferred orientation of the macromolecules, thus reducing the entropy of the polymer melt and leading to the flow-induced crystallization from the melt. Moreover, incorporation of CNT can promote the shear-induced crystallization behavior and enhance the formation of  $\beta$ -crystals in PVDF nanocomposites. Also, the CNT could induce charge accumulation at the interface during electrical poling process, thus further promoting the conversion of the PVDF molecules'  $\alpha$ -phase into the  $\beta$ -phase [158, 159, 162, 163]. Similar to the case of ceramic fillers, the maximum concentration of CNT is also limited by the fiber drawing process.

In this paper, we report fabrication of the multimaterial piezoelectric fibers from perovskite ceramic nanoparticles (BTO/PZT)-PVDF, and CNT-PVDF composites *via* fiber drawing. Furthermore, we perform a comparative study of the piezoelectric performance of thus fabricated fibers. The proposed fibers feature a spiral geometry that significantly increases the fiber piezoelectric response. Due to the judicious arrangement of the conductive layers, connecting to our fibers is easy as the two electrodes occupy the opposite sides of the exposed fiber surface. The use of conductive plastic composite electrodes also increases the fiber reliability. The proposed piezoelectric fibers feature a soft hollow PC core surrounded by a multilayer cladding consisting of the alternating sub-micron-sized piezoelectric/electrode layers as shown in Fig. 4.1d. PVDF, due to its low cost and availability is chosen as the principal component in the piezoelectric layers, while perovskite ceramic (BTO or PZT) nanoparticles or CNT are impregnated into PVDF layers in order to enhance their piezoelectric properties. This approach allows replacement of expensive PVDF-TrFE material, while resulting in the comparable or even superior piezoelectric response. The carbon-impregnated low-density polyethylene (C-LDPE) layers serve as electrode layers. By bending or stretching the fibers, piezoelectricity could be effectively generated. Experimentally, a piezoelectric generator using a 10 cm long BTO-PVDF (BTO concentration: 20 wt%) fiber could generate an open-circuit voltage of 1.4 V and a short-circuit current of 0.8 nA respectively, when the fiber tip is displaced transversely by 10 mm. The corresponding voltage and current were  $\sim 6$  V and  $\sim 4$  nA for a PZT-PVDF (20 wt% PZT) fiber generator, and  $\sim 3$  V and  $\sim 1.2$  nA for a CNT-PVDF (0.4 wt% CNT) fiber generator. Compared to the previous piezoelectric fibers reported in ref. [52, 62, 63, 65, 90], our fibers adopt a spiral structure, and thus have much larger active areas for piezoelectricity generation as well as smaller gaps between the electrodes. As a result, our fibers



could generate much higher piezoelectric currents, which are proportional to the number of turns in a spiral. Among other advantages of the piezoelectric fibers reported in this paper are low cost of the materials used in fabrication, lightweight, good durability, and possibility of mass production *via* fiber drawing. As examples of practical applications of the proposed piezoelectric fibers, we present energy harvesting textiles using BTO-PVDF fibers, and characterized their performance in the context of wearable and automotive microgenerators. Moreover, we also present detection of sound using CNT-PVDF fiber that feature piezoelectric voltage generated by sound wave to be proportional to the square root of the acoustic power.

## 4.2 Results and discussion

### 4.2.1 Fabrication of the piezoelectric micro-/nanostructured fibers

Fig. 4.1 summarizes the fabrication process of a piezoelectric fiber. A fiber preform is assembled by co-rolling two PVDF-based piezoelectric mats (thickness: 100  $\mu\text{m}$ ) sandwiched between two C-LDPE films (thickness: 85  $\mu\text{m}$ , volume resistivity:  $2.2 \Omega \cdot \text{m}$ , Bystat International Inc.) around a hollow PC tube (diameter: 25.4 mm, McMaster Carr) (Fig. 4.1b, c). Note, the bulk resistivity of conductive polymer layers can change significantly during drawing due to redistribution of the conductive fillers in the polymer matrix. In extreme cases, the conductive polymer layer can even lose its electrical conductivity after drawing. Therefore, care should be taken in the proper choice of drawing parameters. Our measurements suggest that volume resistivity of conductive layers in the drawn fibers are as  $\sim 2.5 \Omega \cdot \text{m}$ . The above-mentioned polymer materials are chosen for fiber fabrication because they have similar processing temperatures which is important for co-drawing. The conductive layers are spatially offset in order to produce two easily accessible electrodes on the preform surface after rolling the preform. The piezoelectric mats (Fig. 4.1f) used in the preform are BTO-PVDF, PZT-PVDF, or CNT-PVDF nanocomposites, which were fabricated in-house *via* electrospinning. Besides, we also varied the concentrations of BTO and CNT in the mats to study how they would affect the piezoelectric properties of the fabricated fibers. After assembly, the preforms were drawn into piezoelectric fibers using a plastic fiber drawing tower. During fiber drawing, we also explored applications of high voltage (up to 5 kV) to the preform electrodes in order to pole the drawn fibers directly during fabrication process. We found that while this only led to a modest improvement in the piezoelectric



functionality of the drawn fibers, (since the poling time is insufficient to provide a significant effect), using high voltage we could effectively control thickness of the layers in the piezoelectric fibers. This is because the conductive electrode layers in a softened preform have a tendency to attract to each other under voltage application, and, thus, very thin (sub  $1\ \mu\text{m}$ ) piezoelectric layers could be drawn.

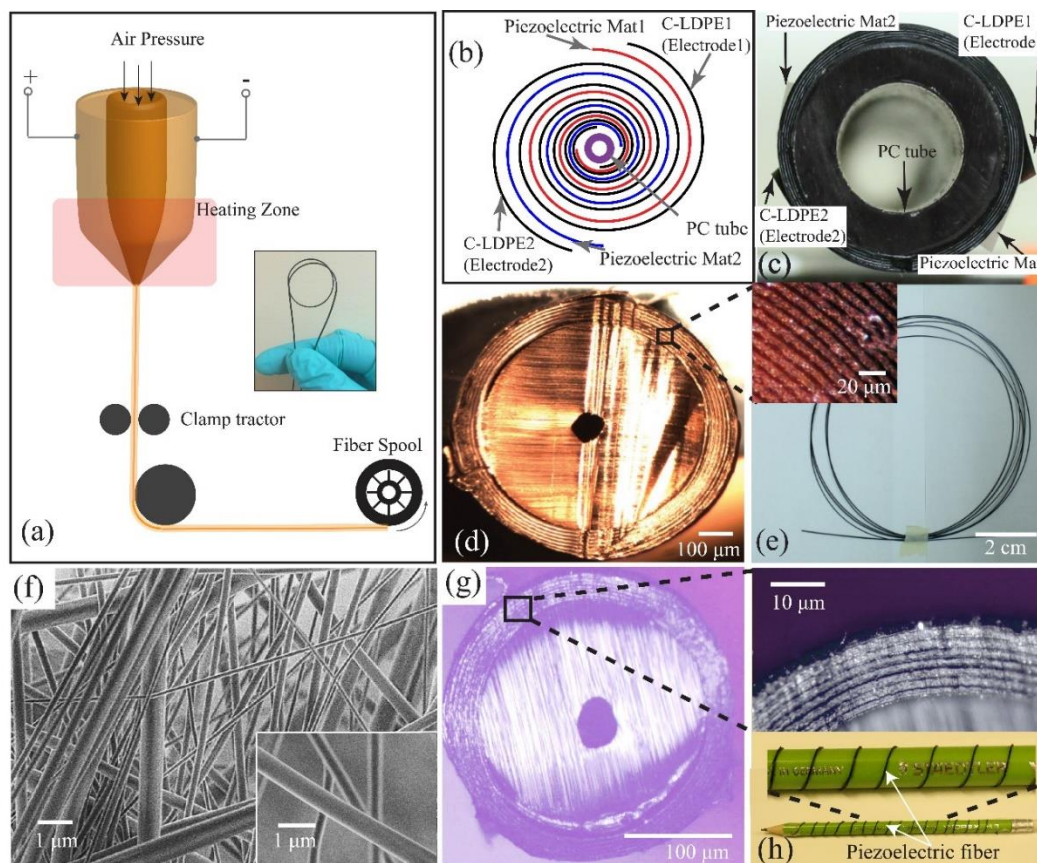


Figure 4.1: (a) Schematic of a fiber drawing process. (b) Schematic of the multilayer structure in the preform and in the drawn fiber. (c) Photo of a preform cross-section. (d) Photo of a cross section of the piezoelectric fiber with a diameter of  $\sim 900\ \mu\text{m}$  (drawn using 2 kV voltage on the preform electrodes). Inset: the magnified view of a multilayer structure. (e) A spool of a piezoelectric fiber. (f) SEM images of the CNT/PVDF electrospun mats at different magnifications. (g) Photo of a cross section of the piezoelectric fiber with a diameter of  $\sim 300\ \mu\text{m}$  (drawn using 5 kV voltage on the preform electrodes). Inset: the magnified view of a multilayer structure. (h) A piezoelectric fiber wrapped on a pencil.



In Fig. 4.1d, we show a typical cross-section of the piezoelectric fiber (diameter:  $\sim 900 \mu\text{m}$ ). The multilayer structure in the fiber cladding maintained well during drawing, while thicknesses of the individual piezoelectric or conductive layers typically ranged from 5 to  $10 \mu\text{m}$ . For those fibers drawn under 5 kV, the fiber diameters were reduced to  $\sim 300 \mu\text{m}$ , and thickness of the piezoelectric layers or conductive layers could be less than  $1 \mu\text{m}$  (Fig. 4.1g). Finally, in order to further enhance the fibers' piezoelectric property, they were poled in a silicone oil bath ( $80^\circ\text{C}$ ) using a voltage of 1 kV for 12 hours. The poling voltage was then increased to 5 kV for 12 hours and finally 9 kV for 12 hours. The poled fibers were then utilized for development of various piezoelectric generator and energy generation systems.

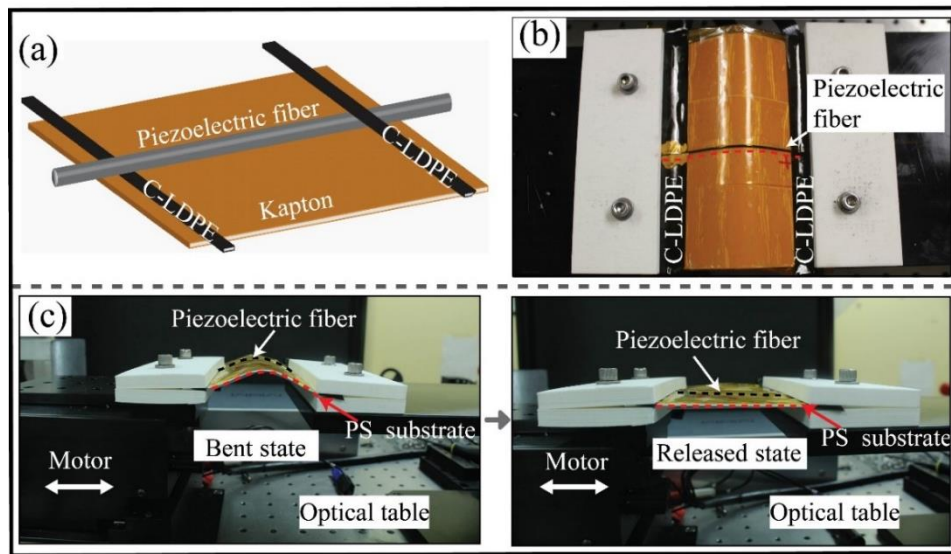


Figure 4.2: (a) Schematic and a photo (b) of a BTO-PVDF fiber test cell. (c) Fiber in the bent and released states.

## 4.2.2 Characterization of piezoelectric micro-/nanostructured fibers

### Structure of a Test Cell

In order to characterize fiber piezoelectric properties, we use the following testing method. The two ends of a piezoelectric fiber (length: 10 cm, diameter:  $\sim 1 \text{ mm}$ ) were glued to two C-LDPE strips as shown in Fig. 4.2a,b. Note that, by design the fiber features two exposed electrodes positioned on the opposite sides of the fiber surface (see Fig. 4.1c). Thus, before the connection, the piezoelectric fiber should be placed in a specific position: one fiber electrode is on the top while



the other fiber electrode is on the bottom (this can be achieved by rotating the fiber). Then, one C-LDPE strip was attached to the top side of the fiber, while the other one was attached to the bottom side of the fiber on the opposite end. In this way, the two strips would connect to the two different electrodes of the fiber. The piezoelectric fiber together with the C-LDPE strips were immobilized onto a 10 cm long, 1 mm thick PS substrate using Kapton tape. Due to asymmetry in the test cell structure, bending of the PS substrate would lead to a non-zero average strain in the piezoelectric fiber. Experimentally, one end of the PS substrate was fixed, while the other end was horizontally displaced by a micropositioning stage, thus bending the fibers (Fig. 4.2c). The generated voltage and current of the piezoelectric fiber were measured using an Ivium Electrochemical Workstation (Ivium Technologies).

### Charge Separation Mechanism in the Drawn Fibers

As the strain is applied along the microstructured fiber, corresponding positive peaks can be observed in both the output voltage and current measurements. This phenomenon can be explained by examining the charge separation mechanism and equivalent circuit model in Fig. 4.3. During poling, the dipoles of the piezoelectric layers are aligned in the direction of the local electrical fields. After the removal of the poling voltage, the oriented domains maintain a permanent polarization. The electric field of the dipole induces surface charge  $+Q$  at the top fiber electrode and  $-Q$  at the bottom fiber electrode. When the fiber is bent, mechanical strain leads to the change of polarization density, which induces change of induced surface charge ( $\pm\Delta Q$ ) in the fiber conductive layers [164, 165]. In response, the free charges in the fiber electrodes are forced to rebalance this change of charge at a speed set by both the external electric circuit and the built-in potential [82]. In the bent state, the initial increase in the voltage (current) gradually diminishes. Similar to that of piezoelectric film-type generators [120], this process can be modeled as the RC discharging process with two time constants ( $\tau$ ): a discharging time  $\tau_v = R_v C_f$  for open-circuit voltage spike and a discharging time  $\tau_c = R_f C_f$  for short-circuit current spike, where  $C_f$  is the effective capacitance and  $R_f$  is the effective resistance of the piezoelectric fiber, while  $R_v$  is the circuit resistance when fiber is connected to a voltmeter. From Fig. 4.3c, we observe that discharging time for the short-circuit current spike is considerably shorter than discharging time for the open-circuit voltage spike ( $\tau_c \sim 0.1s \ll \tau_v \sim 1s$ ), thus also signifying that  $R_f \ll R_v$ . When



the strain is removed, the free charges move in the opposite direction, generating a negative voltage (current) spike.

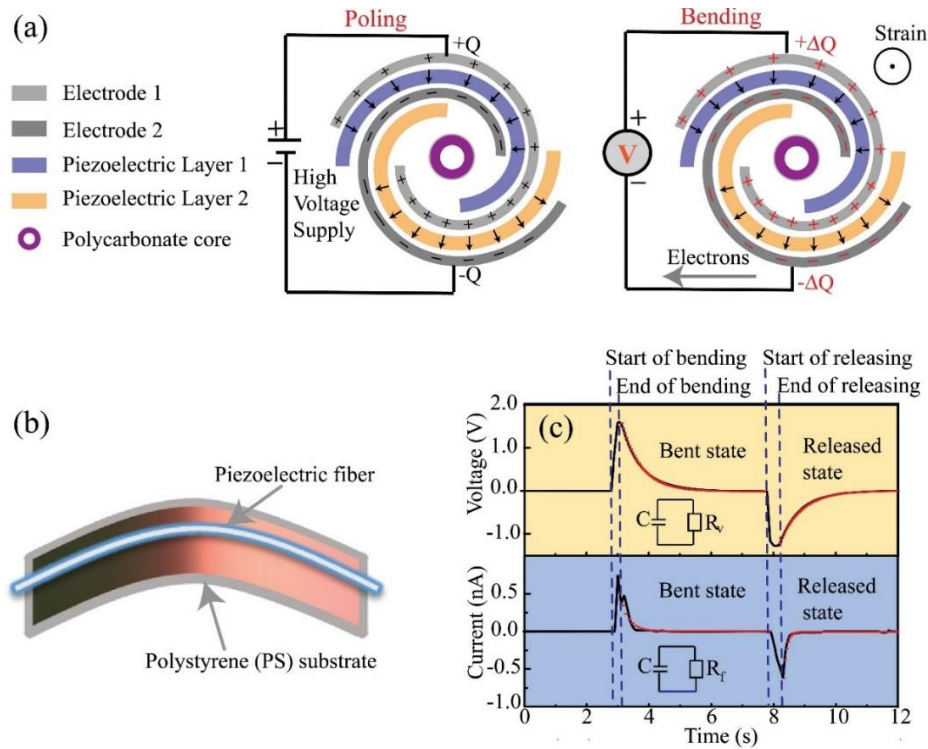


Figure 4.3: Schematics of the charge separation mechanism in the drawn fibers. (a) All dipoles are oriented in the direction of the local electric fields during electric poling (no bending). When mechanical strain is applied along the device by bending, the polarization density is changed and the electrons are forced to flow from one electrode to the other, thus generating voltage differential. (b) A schematic of a piezoelectric fiber in the bent state. The piezoelectric fiber was attached to a plane PS substrate and covered with Kapton tape in order to induce a uniform strain during bending. (c) The open-circuit voltage and short-circuit current of the piezoelectric fiber during the bend and release actions. The insert image shows the equivalent circuit of the piezoelectric fiber connected to a voltmeter or a current meter. The piezoelectric fiber is modeled as a capacitor  $C_f$ , the voltmeter is modeled as a resistor  $R_v$ , and the fiber resistance is  $R_f$ . The black line represents the measured output signals during the bend and release state. The red squares represent the modeled results during the bent and released state.

Note that characterization of the electrical properties of the piezoelectric generators is by far not an easy task and deserves a separate paper by itself. The fibers presented in this work have



internal structure similar to that of the capacitor fibers detailed in our prior work [166, 167]. There, we demonstrated that frequency-dependent electrical properties of the piezoelectric fibers can be modeled using an RC ladder network model. In this model, a fiber is considered as a collection of frequency-dependent transverse and longitudinal resistivities and capacitances, thus resulting in highly non-linear frequency dependence of the fiber effective complex impedance that cannot be interpreted in terms of simple electrical circuits. Therefore, for the sake of simplicity, in this paper we resort to qualitative arguments rather than exact derivations. In order to characterize fiber complex impedance, one has to perform an Impedance Spectroscopy analysis. However, we can approximate the value of the fiber impedance  $Z_f$  at low frequencies as a ratio of the open-circuit voltage to the short-circuit current thus resulting in the values of  $\sim 1 - 2.5 \text{ G}\Omega$ . Note, however, that this value does not correspond to the resistivity of the in-fiber electrodes, but rather represents a value of the complex impedance at a characteristic frequency corresponding to the fiber charge/discharge rate (1–10 Hz, see Fig. 4.3c). At the same time, longitudinal resistance of the in-fiber electrodes  $R_f$ , as well as fiber capacitance  $C_f$  can be estimated using simple expressions  $R_f \sim \rho \frac{L}{Sd} \sim 2.8 \text{ M}\Omega$ ,  $C_f \sim \frac{\epsilon_0 \epsilon L S}{d} \sim 46 \text{ nF}$ , where  $\rho$  is the bulk resistivity of the in-fiber conductive layers ( $\sim 2.5 \text{ }\Omega \cdot \text{m}$ ),  $L$  is the fiber length ( $\sim 10 \text{ cm}$ ),  $S$  and  $d$  are the conductive layer width and thickness respectively ( $S \sim 1.76 \text{ cm}$ ;  $d \sim 5 \text{ }\mu\text{m}$ ), while  $\epsilon$  is the dielectric constant of the piezoelectric films ( $\epsilon \sim 15$ ). Note that the value of  $R_f$  can be measured directly as a DC resistivity of a single fiber electrode. From this, we can also estimate a characteristic value for the charge/discharge time constant  $\tau_c = R_f C_f \sim 0.1 \text{ s}$ , which is in good correspondence to experimental measured value (see Fig. 4.3c). At the same time, when the fiber is connected to the voltmeter the charge/discharge time constant  $\tau_v = R_v C_f \sim 1 \text{ s} \gg \tau_c \sim 0.1 \text{ s}$ , which is consistent with the technical information from the voltmeter stating that  $R_v$  is in  $\text{G}\Omega$  range. To get a better qualitative comparison with the charge/discharge time constant when fiber is connected to the voltmeter, one has to consider more carefully the internal structure of the voltmeter and its effective complex impedance. Finally, for more details on the relation between the complex fiber impedance  $Z_f$  and the electrode resistivities, fiber capacitance, and frequency we refer the reader to the ref. [166, 167].

### **Characterization of the piezoelectric properties of the BTO-PVDF and PZT-PVDF fibers**



We first study the open-circuit voltage generated by the BTO-PVDF fiber generator as a function of the BTO concentration. As the concentration of BTO in the BTO-PVDF layer increased from 5 wt% to 25 wt%, the piezoelectric voltage of a fiber generator with its moving end displaced by 10 mm increased from  $\sim 0.15$  V to  $\sim 2.5$  V (Fig. 4.4a). We find that drawing fibers with BTO concentrations higher than 25 wt% is challenging, because at such high BTO concentrations the viscosity of a BTO-PVDF composite is affected significantly, thus resulting in capillary break-up during fiber drawing. Therefore, to maintain a stable fiber drawing while maximizing piezoelectric functionality, an optimal BTO concentration of 20 wt% was adopted in all our drawings. In Fig. 4.4d and 4.4e, we find that when the moving end of the fiber was displaced by 5 to 20 mm, the corresponding open-circuit voltage increased from  $\sim 1$  to  $\sim 1.7$  V, and the short-circuit current increased from  $\sim 0.7$  to  $\sim 1.3$  nA. Besides, we note that the electrical poling process plays major role in the functioning of the piezoelectric fibers. The fibers without poling exhibit an open-circuit voltage of  $\sim 1.5$  mV, which is three orders of magnitude smaller than that of their poled counterparts (Figure 4. 4b, c). A durability test was also conducted for fiber-based generators by continuously repeating the bend-release movements for 3 days. We find that the piezoelectric voltage and current generated by a fiber does not show degradation signs after the entire test that comprise  $\sim 26000$  bend/release cycles (Fig. 4.4f, g).

Next, piezoelectric generators based on PZT-PVDF piezoelectric fibers were studied. The advantage of PZT over BTO is its higher piezoelectric constant. We find that when the moving end of a PZT-PVDF (PZT concentration: 20 wt%) fiber generator is displaced by 10 mm, it generates an open-circuit voltage of  $\sim 6$  V and short-circuit current of  $\sim 4$  nA, which are  $\sim 4$  times higher than those generated by BTO-PVDF fibers (Fig. 4.5a, b). However, due to the high toxicity of PZT, PZT-PVDF fibers are probably not suitable for wearable applications.



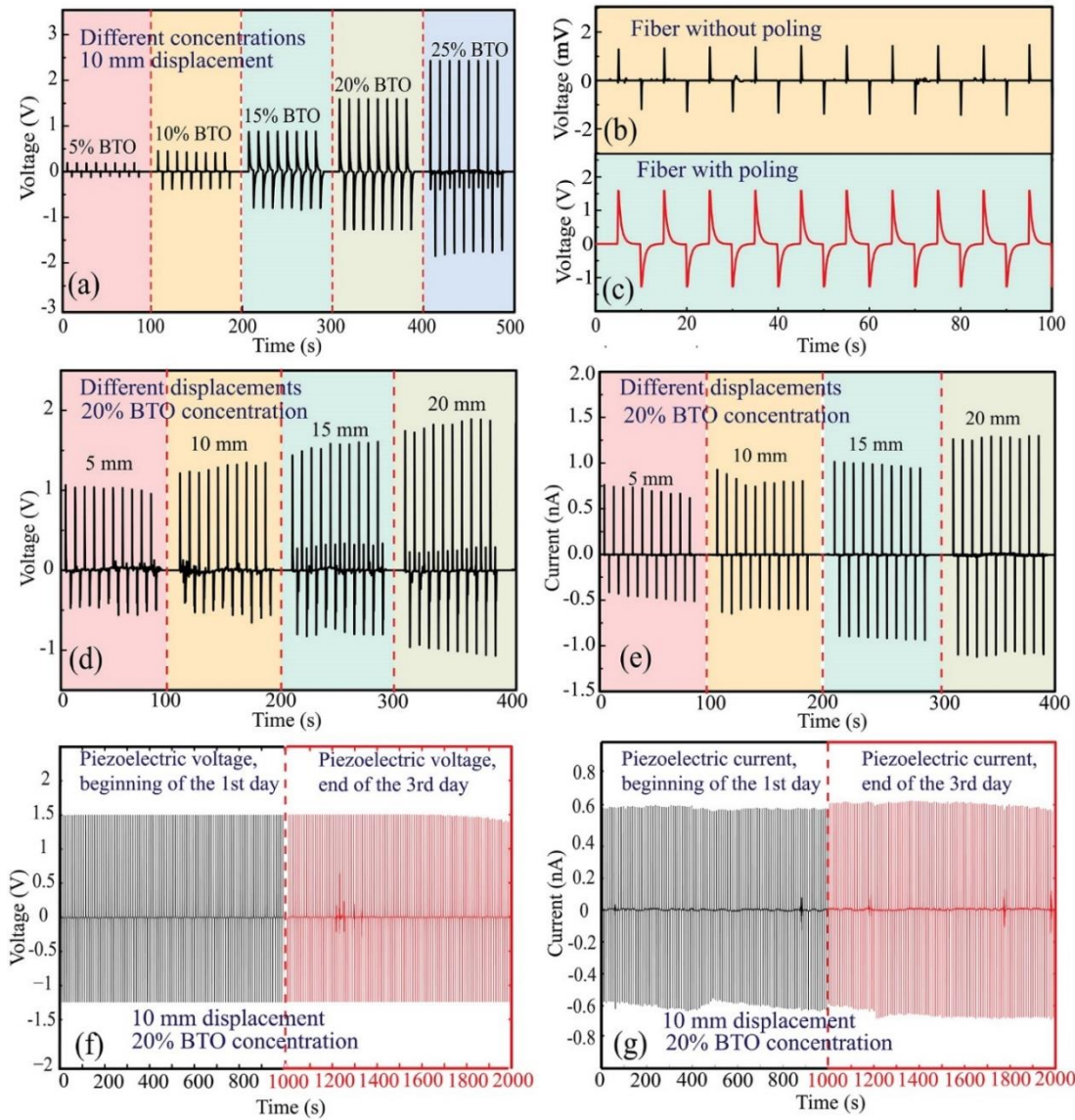


Figure 4.4: (a) Open-circuit voltage generated by a 10 cm long BTO-PVDF fiber with the BTO concentration of 5, 10, 15, 20, and 25 wt% subjected to a 1-cm displacement. (b-c) Comparison of the piezoelectric voltages generated by the poled BTO-PVDF fiber generator and the unpoled one. (d) and (e) show the open-circuit output voltage and short-circuit current generated by a 10 cm-long BTO-PVDF fiber generator (20 wt% BTO in the BTO-PVDF composite) when its moving end is displaced by 5, 10, 15, and 20 mm. (f-g) A durability test for the 10 cm long BTO-PVDF fiber (20 wt% BTO in BTO-PVDF composite) by continuously repeating 1 cm amplitude bend-release movements for 3 days. The open-circuit voltage and short-circuit current generated in a 1000 s period at the beginning of the first day (f) and at the end of the third day (g) are shown.



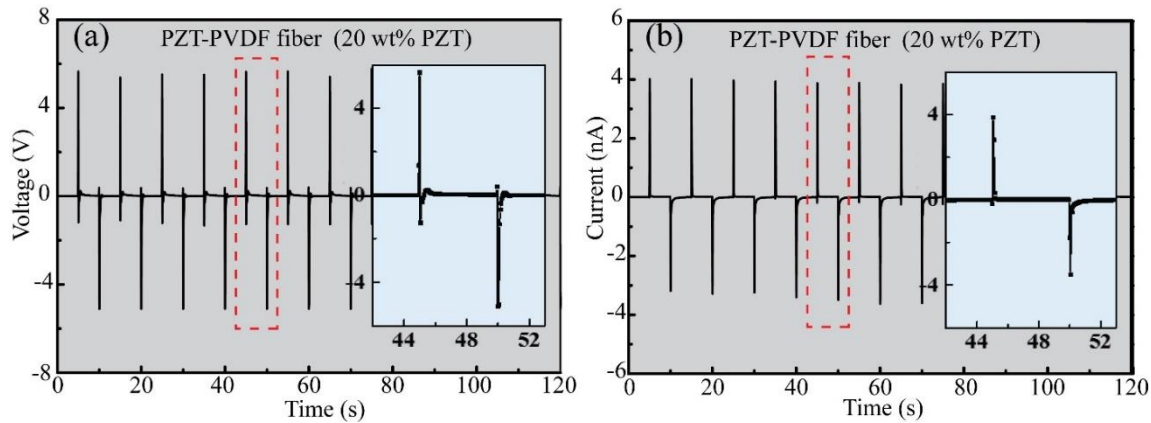


Figure 4.5: (a) and (b) show the open-circuit voltage and the short-circuit current generated by a 10 cm-long PZT-PVDF fiber generator (20 wt% PZT in the PZT-PVDF composite), when its moving end is displaced by 10 mm.

### Characterization of the piezoelectric properties of the CNT-PVDF composite fibers

Piezoelectric generators based on CNT-PVDF fibers were assembled following the same procedures described before. We first studied the dependence of the voltages generated by the CNT-PVDF fibers on CNT concentrations. As shown in Fig. 4. 6b, when the moving end of the fiber generators was displaced by 10 mm, the 10-cm long CNT-PVDF fiber generator containing 0.1 wt% CNT generated an open-circuit voltage of  $\sim 0.8$  V, while the generator containing 0.6 wt% CNT generated an open-circuit voltage of as high as  $\sim 6.8$  V. We, furthermore, find that the fibers with CNT concentrations higher than 0.6 wt% are challenging to fabricate, as they tend to break up during the drawing process. Thus, we adopted an optimal CNT concentration of 0.4 wt% for all our CNT-PVDF fibers that guaranteed the ease of drawing while maintaining high generated voltage. The Fig. 4.6c, d show that when the moving end of the CNT-PVDF (0.4 wt% CNT) fiber generator was displaced by 5 to 20 mm, the open-circuit voltage increased from  $\sim 1.7$  to  $\sim 3.7$  V, and the short-circuit current increased from  $\sim 0.2$  to  $\sim 0.7$  nA. From this we conclude the performance of the CNT-PVDF (0.4 wt% CNT) fiber generator is comparable to that of the BTO-PVDF (20 wt% BTO) fiber generator.



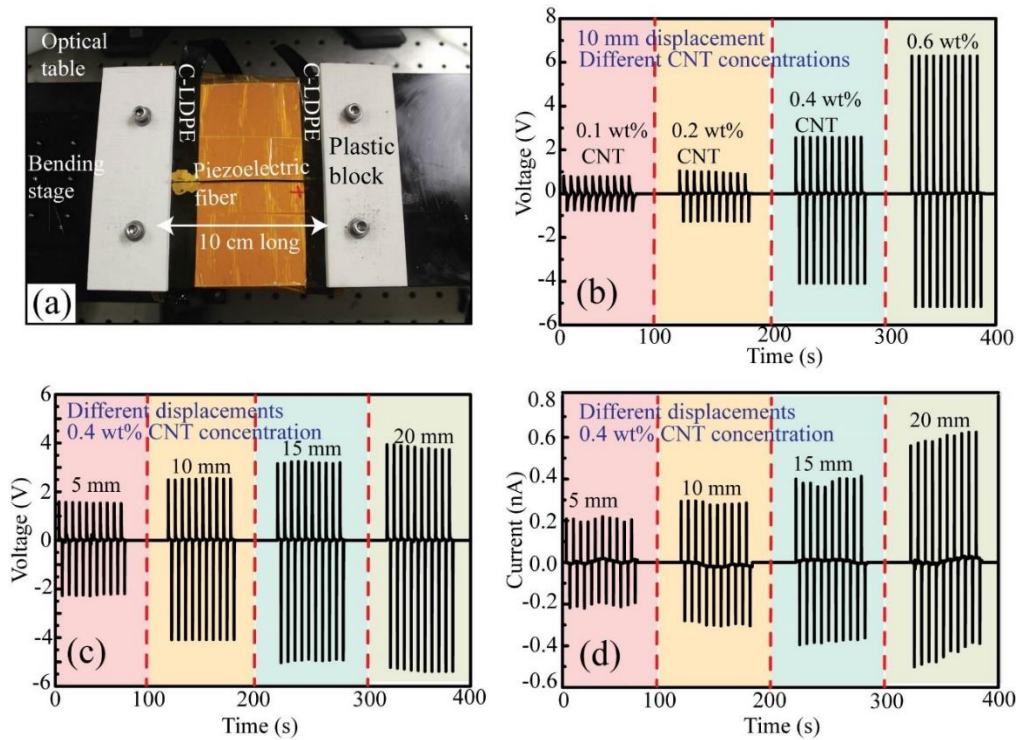


Figure 4.6 : (a) Photo of a CNT/PVDF fiber generator. (b) Open-circuit voltage of a 10-cm long CNT-PVDF fiber generators with CNT concentrations of 0.1, 0.2, 0.4 and 0.6 wt% under 10 mm displacement. (c) and (d) show the open-circuit voltage and short-circuit current of a 10-cm long CNT-PVDF fiber (CNT concentration: 0.4 wt%), when the moving end of the fiber was displaced by 5, 10, 15, 20 mm.

## 4.3 Examples of practical applications of piezoelectric fibers

### 4.3.1 Stand-off distributed sound detection

Our piezoelectric fibers can be used for stand-off sound detection, which opens various possibilities in security and defense applications. In our experiment, the sound wave was generated by a speaker (Dell computer speaker) and a software (Adobe Audition CC 2015). The distance between the fiber and speaker is  $\sim 20$  cm. Fig. 4.7 shows the structure of the sound wave and the output voltage obtained from the CNT/PVDF fiber (10 cm length). The sound pressure level (SPL) of the actuating sound was  $\sim 20$  dB (0.2 mPa) at 1 Hz where  $\text{dB} = 20\log_{10}(P/P_0)$ ,  $P_0 = 20 \mu\text{Pa}$ , and the amplitude of the fiber output voltage was in the range of 50 to 70 mV. The SPL of the actuating sound was measured using a sound level meter (Larson Davis model 831).



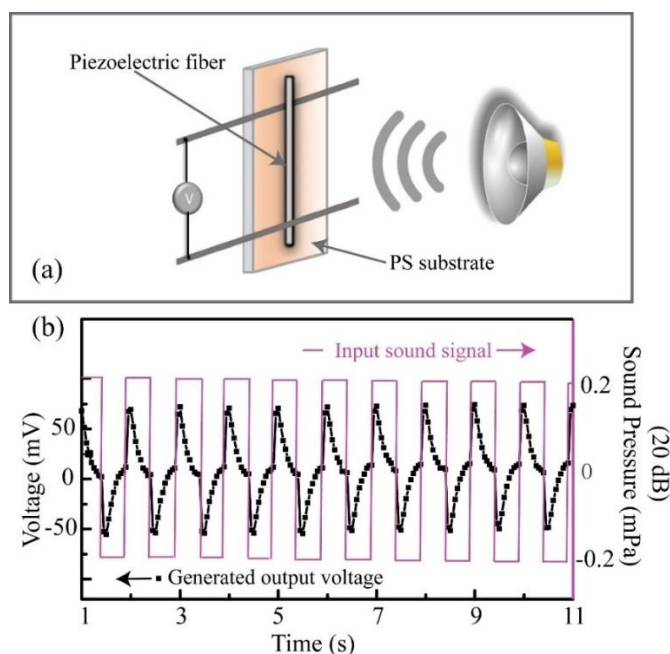


Figure 4.7 : (a) Schematics of the experimental setup. (b) The sound wave (Red) and the output voltage from the CNT/PVDF fiber actuated by the sound wave.

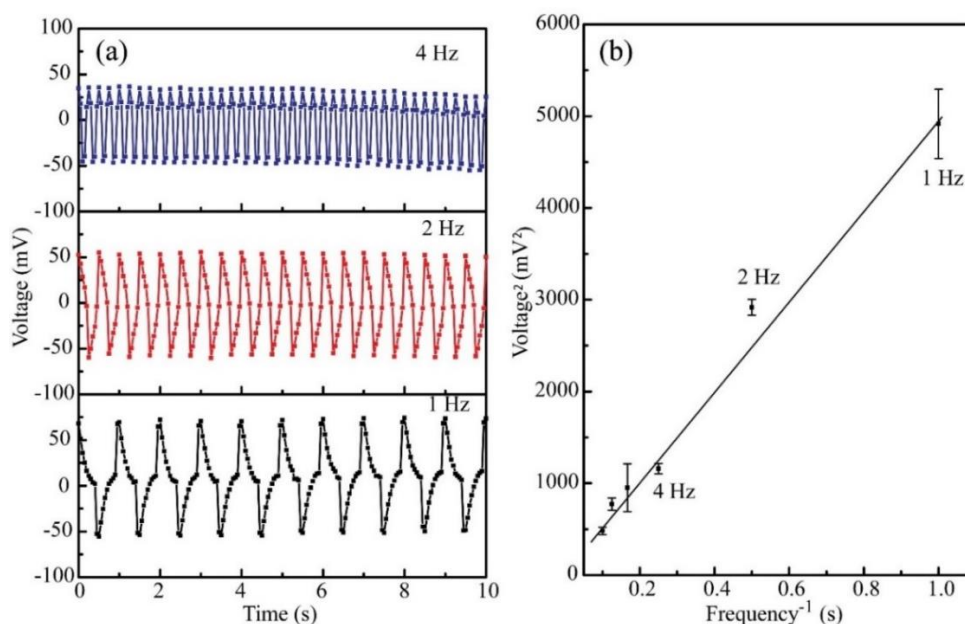


Figure 4.8 : (a) The output voltage generated by the CNT/PVDF fiber at the frequencies of the actuating sound wave of 1 Hz, 2 Hz and 4 Hz for SPL of  $\sim 20$  dB. (b) The square of the output voltage of the piezoelectric fiber vs. frequency of the sound wave. In the experiment, we measured



20 pulses, and the value of the mean voltage was calculated by averaging the peak value of the measured pulses. The error bar is calculated by the standard deviation (SD) of the peak value of measured pulses.

When a piezoelectric generator is actuated by the sound waves, the generated voltage  $V$  could be generally related to the acoustic power  $P$  incident onto the fiber as:  $V^2 \sim P/f$ , where  $f$  is the frequency of the applied sound wave, while the time average power incident on the fiber is given by  $P = AP_0^2/(2Z_0)$ , where  $P_0$  is the local value of the sound wave pressure,  $A$  is the fiber surface and  $Z_0$  is air impedance [141]. Fig. 4.8a shows the output voltage from the CNT/PVDF fiber under the frequencies of 1 Hz, 2 Hz, 4 Hz, 6 Hz, 8 Hz and 10 Hz respectively, when the input power level of the sound was held constant with the correspondent SPL at  $\sim 20$  dB. As shown in Fig. 4.8b, the  $V^2$  was linearly dependent on the frequency of the applied sound wave in accordance with ref [141].

Furthermore, we investigate performance of the sound-driven fiber generator under water. Experimentally, the two ends of a 10 cm long CNT-PVDF fiber were fixed in a water tank with a dimension of 60 cm $\times$ 28 cm $\times$ 15 cm. An ultrasonic probe was also immersed under water to emit ultrasound waves with a frequency of  $\sim 20$  kHz. The distance between the probe and the fiber was  $\sim 20$  cm. While the sonication was repeated with a period of 6 s (1 s on, 5 s off), the piezoelectric voltage generated by the fiber was continuously measured. As the power of the ultrasound wave increased, the amplitude of voltage generated by the CNT-PVDF fiber also increased (Fig. 4.9c, d) according to  $V^2 \sim P/f$ . We note that in Fig. 4.9c the generated voltage does not return to zero as the off time (5 s) is too short for all the water oscillations in the tank to subside. Normally, the off time should be longer than a minute to see the generation voltage to approach zero value.



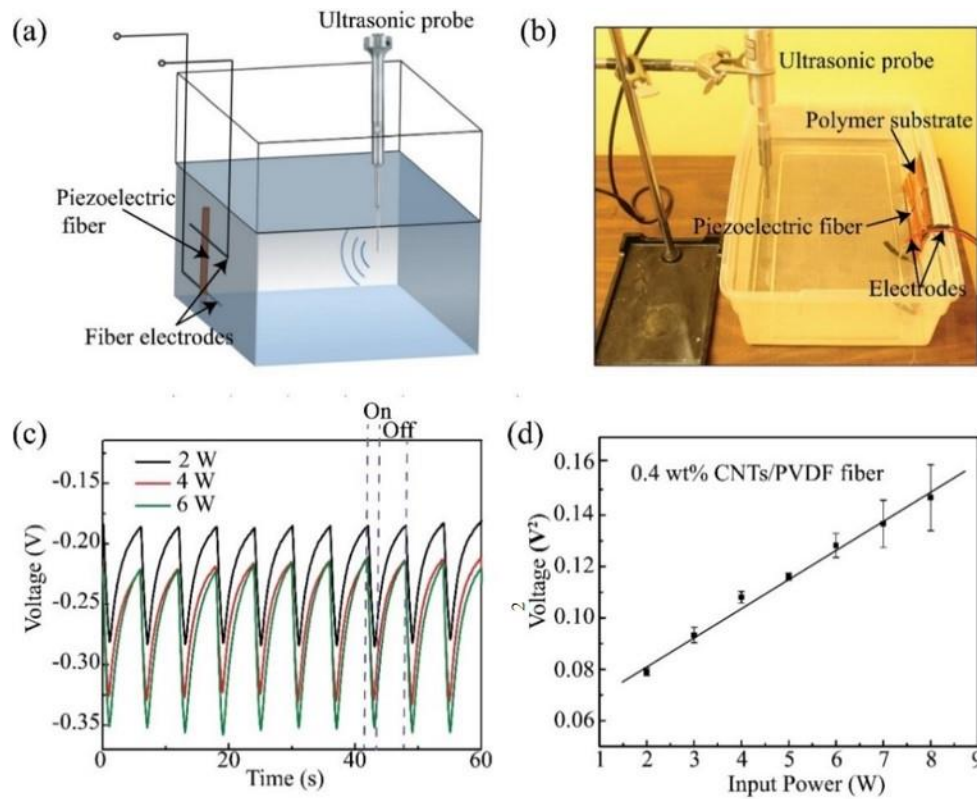


Figure 4.9: (a) Schematic and a photo (b) of experimental setup of the underwater ultrasound detection using a CNT-PVDF fiber. (c) Piezoelectric voltages generated by the fiber, when the source acoustic powers were 2 W, 4 W and 6 W. (d) The square of the piezoelectric voltage generated by the generator has a linear relationship with the acoustic power. In the experiment, we measured 20 pulses, and the value of the mean voltage was calculated by averaging the peak value of the measured pulses. The error bar is calculated by the standard deviation (SD) of the peak value of measured pulses.

### 4.3.2 Textile-based piezoelectric generators woven using BTO-PVDF fibers

Here, we present two prototypes of the flexible, textile-based piezoelectric generators. They were fabricated using individual piezoelectric BTO-PVDF fibers and a classic Dobby-loom weaving process (Fig. 4.10 a, b). We demonstrate that such textile generators could be potentially used as tactile or motion sensors for sport outfits or medical apparels; or for micro-power-generation in automotive and aeronautic industries for powering various electronic devices. In the first prototype, four 20 cm-long BTO-PVDF fibers (20 wt% BTO in BTO-PVDF composites) were weaved into a textile and then connected in series. The textile was then tightly wrapped around a



human elbow (Fig. 4.10c). In a 90 degree bend-release action of the elbow, the piezoelectric textile could generate open-circuit voltages of up to  $\sim 10$  V and short-circuit currents of 5-15 nA (Figure 4.10d, e).

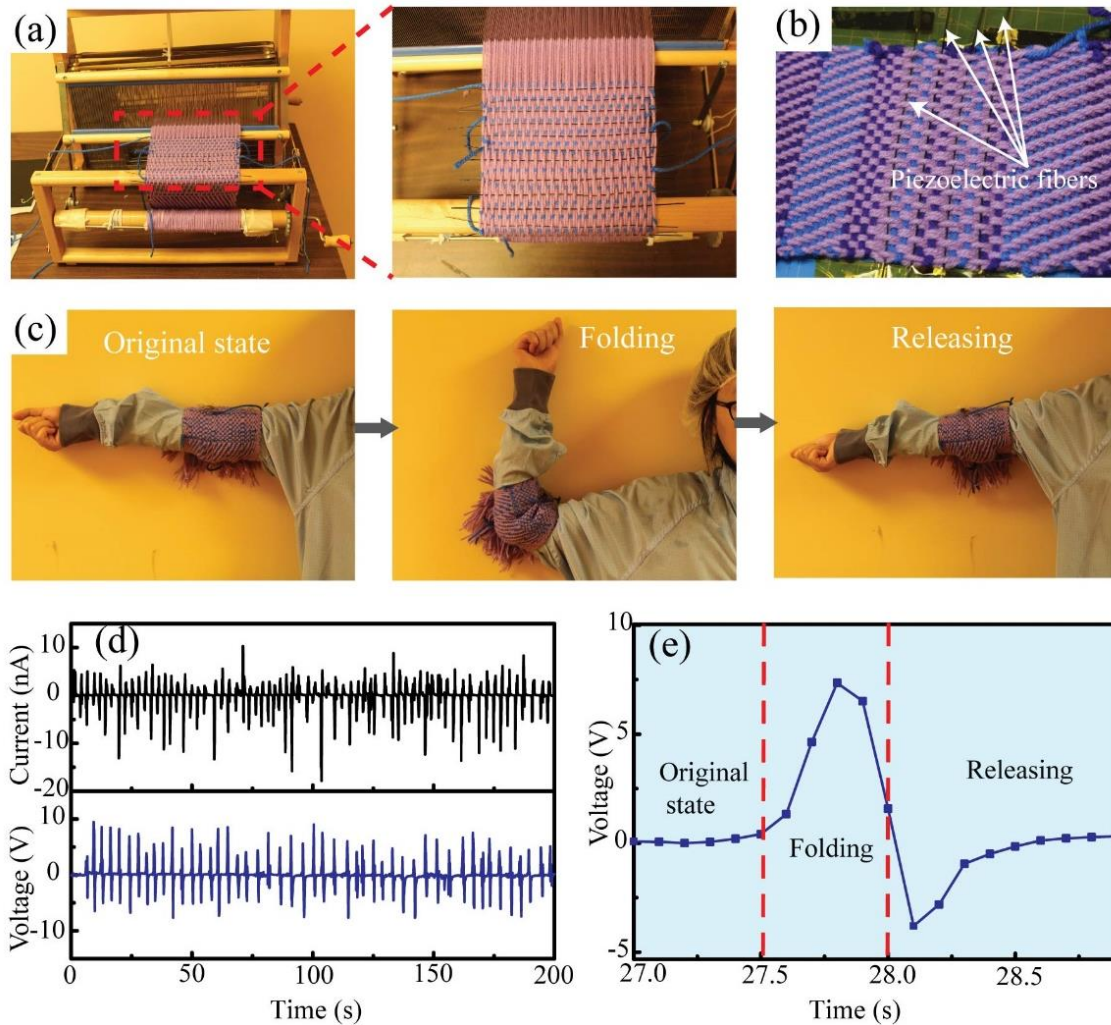


Figure 4.10: (a) Dobby loom was used to weave piezoelectric fibers into a cotton textile. During weaving, cotton yarns are used as a warp (longitudinal threads forming the textile base). Piezoelectric fibers are introduced during weaving as a weft by passing them through the warp cotton yarns. (b) A cotton-based textile containing 4 piezoelectric fibers woven using a Dobby loom. (c) Electrical properties of the piezoelectric textile in a 90° folding-release action of the elbow. (d) Open-circuit voltages and short-circuit currents generated by the piezoelectric textile during repeated fold-release motion of the elbow. (e) Open-circuit voltage of the piezoelectric textile in a fold-release elbow action.



In the second prototype, fifteen 20 cm-long fibers are weaved into a textile and connected in parallel. We then used this textile as a seat pad of a vehicle (Hyundai sedan) and put a 22 kg sandbag on it (Fig. 4.11a). As we drove the vehicle on urban roads, traffic-induced vibration of the vehicle led to distortion of the piezoelectric fibers in the textile, thus generating electric current. A simple full-wave bridge rectifier circuit was used to ensure that the current generated by the textiles would charge a 10  $\mu\text{F}$  capacitor with consistent polarity (Fig. 4.11c). During a 6000 s period of urban-road driving under regular traffic condition, the piezoelectric textile was able to charge the capacitor from 0 to  $\sim 0.3$  V (Fig. 4.11d). The charging rate could be further improved by adding more fibers to the power-generation pad.

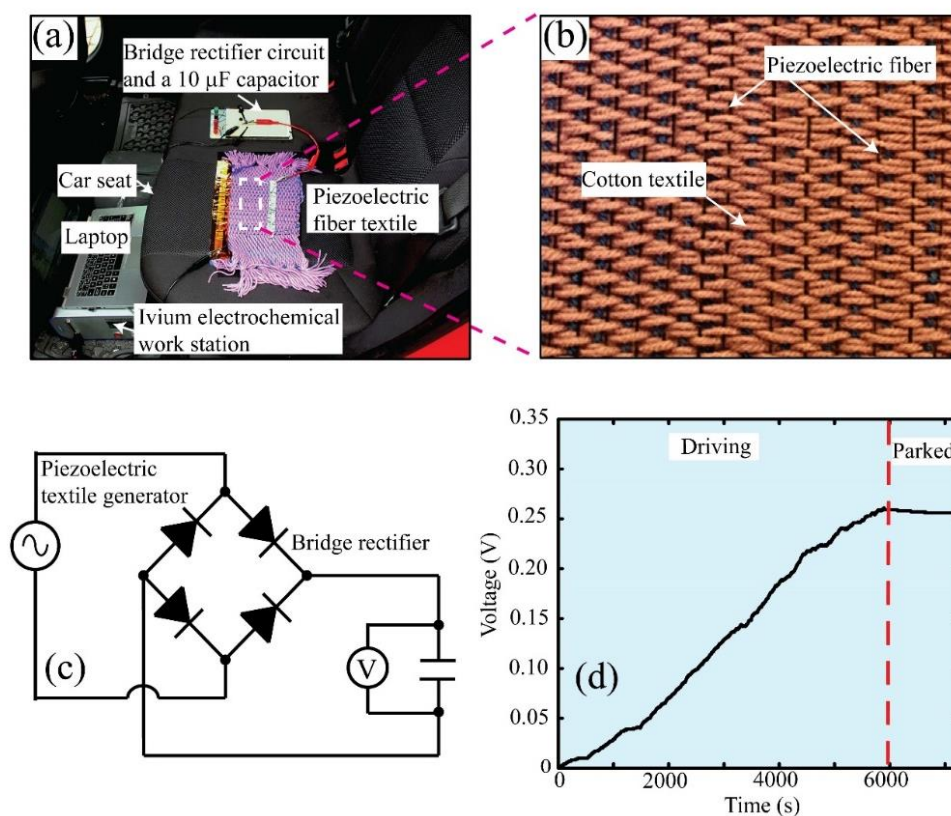


Figure 4.11: (a) Photo of the experimental setup for the in-car test. The piezoelectric fiber textile (b) (consisting of fifteen 20 cm-long piezoelectric fibers connected in parallel) was utilized as an automotive microgenerator pad to charge a 10  $\mu\text{F}$  capacitor *via* a bridge rectifier circuit shown in (c). (d) Voltage of the capacitor charged by a piezoelectric textile during driving and stationary state of the vehicle.



## 4.4 Conclusion

In summary, we have studied several material combinations, piezoelectric fiber designs and manufacturing techniques that allow fabrication of piezoelectric fibers with greatly enhanced piezoelectric properties compared to the existing counterparts. The micro-/nanostructured piezoelectric fibers presented here feature a soft hollow PC core surrounded by a multilayer cladding consisting of alternating PVDF-based nanocomposite layers and conductive C-LDPE layers. We have also performed comparative study of three material combinations. A BTO/PVDF microstructured fiber (10 cm long; BTO concentration: 20 wt%) could generate an open-circuit voltage of 1.4 V and a short-circuit current of 0.8 nA, when the moving end of the generator was displaced transversely by 10 mm. The corresponding voltage and current were  $\sim 6$  V and  $\sim 4$  nA for a PZT-PVDF (20 wt% PZT) fiber generator, and  $\sim 3$  V and  $\sim 1.2$  nA for a CNT-PVDF (0.4 wt% CNT) fiber generator. Perovskite ceramics (such as BTO and PZT) could improve the fiber performance owing to their high piezoelectric coefficient. On the other hand, CNT could induce the crystallization of polar phase in PVDF layers, thus leading to remarkable improvements in piezoelectric performance. Also we note in passing that the CNT/PVDF microstructured fibers are easier to draw to smaller diameters and they appear to have better mechanical flexibility. The resultant fibers exhibit excellent durability with high piezoelectric voltages (of up to 6 V) in a cyclic bend-release test (greater than 26000 cycles). Finally, we have present several examples of the practical applications of the proposed piezoelectric fibers: for distributed stand-off sound detector using CNT-PVDF fibers, and for energy harvesting using textile-based piezoelectric generators that incorporate BTO-PVDF fibers.

The microstructured fibers developed in this work have the following advantages compared to other existing piezoelectric fibers. Firstly, the proposed piezoelectric fibers adopt a spiral multilayer structure, which considerably increases the active areas of the piezoelectric materials, and, thus results in higher energy generation efficiency. The piezoelectric performance of the proposed fibers could be further improved simply by increasing the number of piezoelectric layers in the fiber structure. Secondly, the outermost C-LDPE layers serve as two spatially-offset electrodes on the fiber surface, thus greatly simplifying connectorization to our fibers. Thirdly, owing to thermal fiber drawing process, the dimensions of piezoelectric fibers can be as small as hundreds of microns, which enables their applications inside small tubes, such as blood vessels



[66, 168, 169]. Moreover, the soft piezoelectric fibers with well-controlled geometries can be woven into low-cost fabrics that allows wearable, portable and large-area applications. Other advantages include use of low cost materials during fabrication, high flexibility, good durability, and possibility of mass production using fiber drawing technique.

## 4.5 Experimental section

### 4.5.1 Solution preparation

*BTO-PVDF Solution Preparation.* BTO (nanoparticles with average diameter of 200 nm; US Research Nanomaterials Inc.) of defined amount was dispersed in dimethylformamide (DMF) solvent (Sigma-Aldrich) using a probe-type sonicator (Fisher Scientific Inc.) at 100 W in 5 s intervals (3 s pulse on, 2 s pulse off) for 1 h. PVDF (pellet, Mw ~275000, Sigma-Aldrich) was dispersed in acetone using a magnetic stirrer for 10 min. Then, the BTO solution and the PVDF solution were mixed together while being heated at 100 °C using a magnetic stirrer for 1 h. Subsequently, the BTO-PVDF solution was sonicated at 75 W in 5 s intervals (3 s pulse on, 2 s pulse off) for 15 min and then put in a vacuum chamber for 5 min to remove air bubbles. In our experiments, the concentration of PVDF in the solution was 20 wt%, and weight concentration of BTO in the as-spun BTO-PVDF composite mats was varied from 5 to 25 wt% with a 5 wt% interval. The DMF/acetone volume ratio was 2/3.

*PZT-PVDF Solution Preparation.* PZT powders (APC 850) purchased from APC Inc. generally have a size ranging from 10 to 50  $\mu\text{m}$ . To reduce the PZT particle size and thus enhance their piezoelectric functionality, PZT powders were milled using a ball-milling machine (MSK-SFM-2, MTI Corporation) for 10 h with a milling speed of 200 rpm. 10  $\text{ZrO}_2$  balls with a diameter of 10 mm were used as the milling medium. The weight ratio of PZT powders to the milling balls was 1:20. The milled PZT powders could be then used for the preparation of PZT-PVDF solutions, which follows exactly the same procedures as the case of BTO-PVDF solutions.

*CNT-PVDF Solution Preparation.* Multi-walled carbon nanotubes (Sigma-Aldrich) of defined amount was dispersed in DMF solvent using an ultrasonicator for 15 min. PVDF (pellet, Mw ~275000, Sigma-Aldrich) was dispersed in acetone using a magnetic stirrer for 10 min. Then, the CNT solution and the PVDF solution were mixed together while being heated at 100 °C using



a magnetic stirrer for 1 h. Subsequently, the CNT-PVDF solution was sonicated at 75 W in 5 s intervals (3 s pulse on, 2 s pulse off) for 15 min and then put in a vacuum chamber for 5 min to remove air bubbles. In our experiments, the concentration of PVDF in the solution was 20 wt%, and weight concentration of CNT in the as-spun BTO-PVDF composite mats was varied from 0.2, 0.4, and 0.6 wt%. The DMF/acetone volume ratio was 2/3.

#### **4.5.2 Electrospinning of BTO-PVDF, PZT-PVDF and CNT-PVDF solutions**

The as-prepared PVDF-based composite (BTO-PVDF, PZT-PVDF or CNT-PVDF) solutions were electrospun using an Electrospinning Workstation (MSK-NFES-3, MTI Corporation) to fabricate the corresponding mats. In electrospinning, the solution was first loaded into a glass syringe (Hamilton, 20 mL) equipped with a blunt metallic needle (Hamilton, 22 gauge). A high voltage of 15 kV was then applied to the syringe needle, while a drum collector (diameter: 5 cm) used as the substrate of the as-electrospun mat was grounded. The distance between the needle tip and the drum collector was ~15 cm. The spinning solution was delivered to the needle tip at a flow rate of 1 mL·h<sup>-1</sup>. To ensure uniformity of the thickness of the electrospun mat, the syringe was mounted onto a motor-driven platform that scans tangentially to the drum collector with a speed of 2 mm/s. A SEM image of the as-electrospun BTO-PVDF mats was shown in Fig. 4.1f.

#### **4.5.3 Preparation of the piezoelectric fiber preforms and fiber drawing**

To fabricate the fiber preform, four alternating PVDF-based composite mats (100  $\mu$ m-thick) and C-LDPE films (85  $\mu$ m-thick) are co-rolled around a hollow PC tube as shown in Fig. 4.1b. Before drawing, the preform was consolidated in a vacuum furnace at 110 °C for ~24 h. The preform was then drawn at 190 °C into piezoelectric fibers using the fiber drawing technique. In particular, the preform was placed into the vertical furnace of the fiber drawing tower, where the temperature is increased above the polymer softening temperature. As a consequence, the preform tip melts, and forms a blob that later falls down under the force of gravity, thus creating a slender fiber that can be continuously pulled from the molten perform tip. In actuality, a clamp tractor is used to continuously pull the fiber at a constant speed. The final size of a resultant fiber depends on the parameters used in the drawing process such as fiber drawing speed, temperature distribution in the furnace, preform feeding speed, as well as overpressure used during fiber fabrication.



Experimentally, we set the drawing speed as 500 mm/min, and used an air-pressure of 3 mbar to pressurize the fiber core during drawing.

#### 4.5.4 Electrical measurements

The open-circuit voltage and short-circuit current of the devices were measured by an electrochemical station (Ivium Technologies). The sampling time constant was 0.1 s. The bend/release actions of the devices were controlled by a micropositioning stage. The displacement velocity during bend/release cycles was 5 cm/s. The bend/release cycle was repeated every 10.4 s. During each cycle, the bend motion lasted 0.2 s, followed by a pause of 5 s in the bent state, followed by 0.2 s of the release motion, and finally followed by a 5 s pause in the released state.

### 4.6 Supporting information

Here we discuss in more details the effects of the fiber length on the output voltage and current of the piezoelectric devices reported in the main paper.

As shown in Fig. 4. 12, when the moving end of a CNT-PVDF (CNT concentration: 0.6 wt.%) fiber generator (10 cm long) is displaced by 10 mm, it generates an open-circuit voltage of  $\sim 6$  V and short-circuit current of  $\sim 0.4$  nA. Then, we cut the fiber generator into two 5 cm-long pieces and test the output characteristics of the individual fiber piece under 5 mm displacement. This displacement was chosen to provide the same bending strain as the case of the longer 10 cm fiber under 1 cm displacement. As a result, the short fiber generator generates an open-circuit voltage of  $\sim 3$  V and a short-circuit current of  $\sim 0.4$  nA.

From this we can conclude that the output voltage of the piezoelectric fiber increases with the fiber length, while the output current of the piezoelectric fiber remains constant.

This result can be easily rationalized by noticing that increasing the fiber length two folds is equivalent to join two shorter fibers in series, which results in a higher net open-circuit voltage and higher resistivity thus the same short-circuit current.



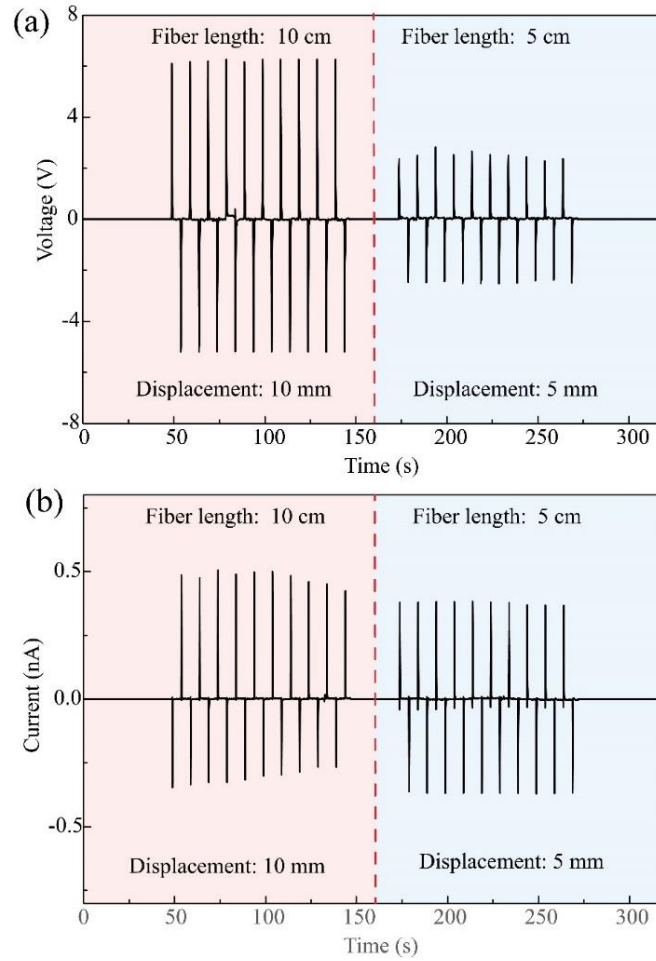


Figure 4.12 : The output characteristics generated by the 0.6 wt% CNT/PVDF fibers (Left: 10 cm-long fiber under 10 mm bending displacement; right: 5 cm-long fiber under 5 mm bending displacement).

Then we investigate how the electrical characteristics of the circuits made of several piezoelectric fibers depend on the type of the connection. In fact, we find that the piezoelectric fibers behave like classic voltage sources with internal resistances. In our experiments, we used two identical 10 cm long CNT-PVDF fibers. In Fig. 4.13, we present photos of experimental setup used in our studies. The two fibers were first placed on the Kapton tape parallel each other separated by 1 cm. The polystyrene substrate was placed under the Kapton tape similarly to the arrangement shown in Fig. 4.3. During the experiment, 1 cm displacement was used. As a result, we find that the output voltage generated by the two piezoelectric fibers connected in series is two times higher than that of the two fibers connected in parallel, while the output current generated by the two piezoelectric fibers connected in series is half of that generated by the two fibers connected in



parallel.

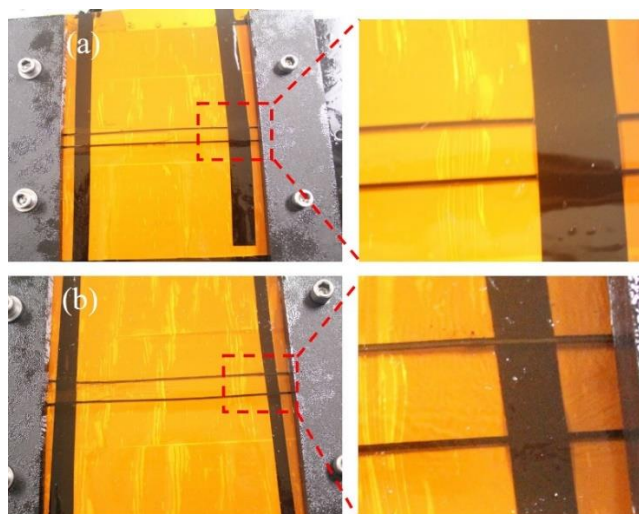


Figure 4.13 : (a) Two 0.4 wt% CNT/PVDF fibers (10 cm long) connected in parallel; (b) Two 0.4 wt% CNT/PVDF fibers (10 cm long) connected in series.



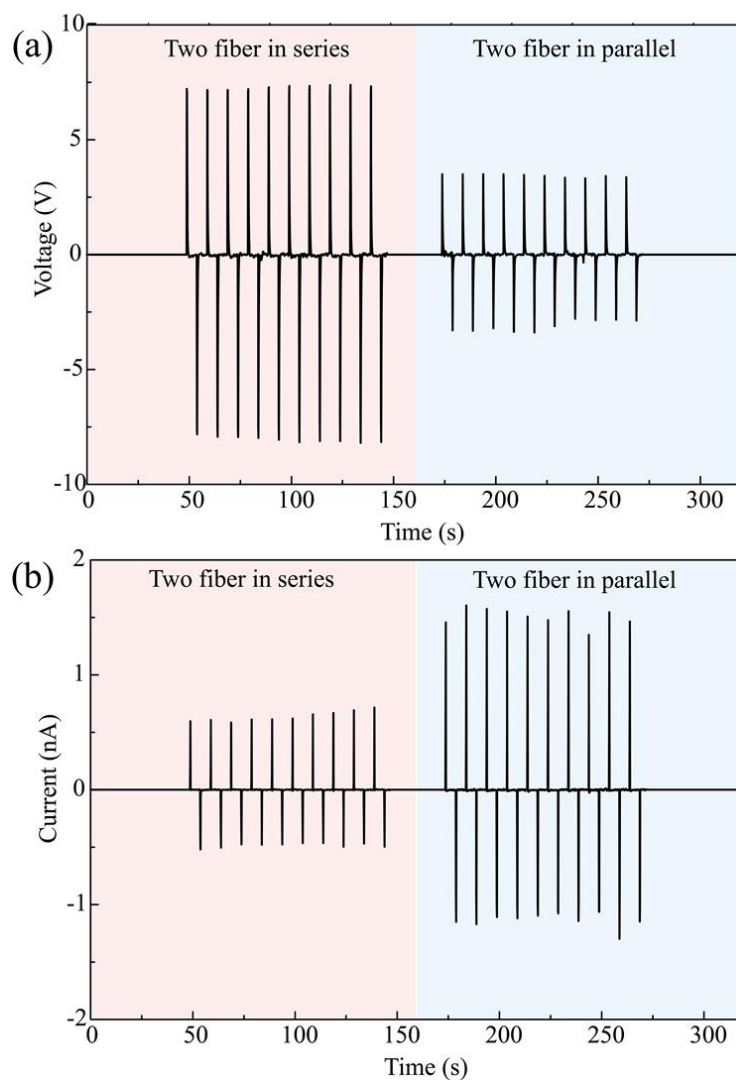


Figure 4.14 : The output characteristics generated by two 10 cm-long 0.4 wt% CNT/PVDF fibers, when the moving tip of the fiber generators is displaced by 10 mm (Left: two fibers are connected in series; Right: two fibers are connected in parallel).



## CHAPTER 5      ARTICLE 2: PIEZOELECTRIC MICROSTRUCTURED FIBERS VIA DRAWING OF MULTIMATERIAL PREFORMS

This chapter is based on the paper “Piezoelectric Microstructured Fibers *via* Drawing of Multimaterial Preforms,” published in Scientific Reports in 2017 [170]. I am the primary author of this paper, while this paper is co-written by Hang Qu and Maksim Skorobogatiy from Ecole Polytechnique de Montreal.

In this Chapter, we demonstrate planar laminated piezoelectric generators and piezoelectric microstructured fibers based on BaTiO<sub>3</sub>-polyvinylidene and carbon-loaded-polyethylene materials combinations. The laminated piezoelectric generators were assembled by sandwiching the electrospun BaTiO<sub>3</sub>-polyvinylidene mat between two carbon-loaded-polyethylene films. The piezoelectric microstructured fiber was fabricated *via* drawing of the multilayer fiber preform, and features a swissroll geometry that have ~10 alternating piezoelectric and conductive layers. Both piezoelectric generators have excellent mechanical durability, and could retain their piezoelectric performance after 3 days’ cyclic bend-release tests. Compared to the laminated generators, the piezoelectric fibers are advantageous as they could be directly woven into large-area commercial fabrics. Potential applications of the proposed piezoelectric fibers include micro-power-generation and remote sensing in wearable, automotive and aerospace industries.

### 5.1 Introduction

Driven by the ever-growing market of the personal wearable products such as on-garment displays, health-monitoring sensors [171], virtual-reality devices, smartwatches and bracelets, and intelligent glasses, extensive effort has been devoted to the R&D of soft and wearable electronics [61]. The development of wearable and portable electronics has inspired much work [172] in the design and fabrication of flexible fibers which could be used as power sources or sensor components. Among all of these fiber generators or sensors, piezoelectric fibers that operate based on piezoelectric effect [37] are especially attractive, because they could convert mechanical vibrations accessible in our daily life (i.e. walking [173], airflow [174, 175] and heart beating [176, 177]) into electrical signals. Another application of piezoelectric generators is related to automotive or aerospace industries [178]. Piezoelectric generators or sensors are implanted on the airplanes and vehicles, for the purpose of structural integrity monitoring [179, 180], as well as powering the



on-board electronic systems such as wireless sensor networks (WSNs) with low-power consumption [150].

To date, a number of piezoelectric fibers have been demonstrated. A straightforward route for fabrication of the piezoelectric fibers is to directly grow or wet-extrude piezoelectric ceramic materials such as ZnO nanorods or nanowires (NWs), BaTiO<sub>3</sub> (BTO) nanostructures and Pb(Zr<sub>0.52</sub>Ti<sub>0.48</sub>)O<sub>3</sub> (PZT) NWs along a metallic wire/microfiber [51, 52, 116, 136, 176]. For instance, Yin *et al.* report a piezoelectric fiber by depositing ZnO nanorods on a copper wire [135]. However, for these fibers, frequent and intensive mechanical movements may potentially damage the fiber structure (e.g. the continuous bending can make the piezoelectric layers cracking, and even peeling off from the fiber core). Thus, the as-fabricated fiber generators typically suffer from poor mechanical reliability, which makes them unsuitable for truly wearable applications. To improve robustness of the fibers, Zhang *et al.* have coated a thin layer of polydimethylsiloxane (PDMS) on the roots of ZnO NWs using surface-coating combined with plasma-etching [136]. An alternative route for fabrication of the piezoelectric fibers involves the utilization of piezoelectric polymers. In principle, piezoelectric fibers based on piezoelectric polymers usually feature better mechanical robustness and flexibility. Among all of these piezoelectric polymers, poly(vinylidene fluoride) (PVDF) and poly(vinylidene fluoride-co-trifluoroethylene) (PVDF-TrFE) are particularly attractive due to their ease of production, high chemical resistance, superior flexibility, and good piezoelectric performance. Most of the existing piezoelectric polymer fibers are fabricated by melt-spinning or extrusion. For example, Lund *et al.* reported the melt-spinning of a PVDF-yarn with a conductive carbon black/polypropylene (CB/PP) core [63, 65, 88, 89]. Using a similar method, Bian *et al.* demonstrated a metal-core piezoelectric fiber that had a PVDF sheath and a molybdenum filament core [181]. Recently, Martins *et al.* used the melt-coextrusion method to fabricate a piezoelectric fiber that has a piezoelectric PVDF layer sandwiched by two polypropylene-based conductive polymers [62]. Note that the piezoelectric fibers fabricated by traditional spinning methods typically adopt a simple core-sheath structure, in which a conductive filament constitutes the core, and a piezoelectric polymer layer constitutes the sheath. Besides, an additional conductive layer should be coated on the fiber as an external electrode that may limit the lifetime and applications of the as-spun fibers, since the metallic layer under repeated mechanical deformations generally results in fracture. In the case of fiber spinning/stretching, the stress applied on the fiber can induce the conversion of the nonpolar  $\alpha$  into the ferroelectric  $\beta$  phase.



Additionally, an electrical poling of the piezoelectric fibers during (or after) the spinning process can considerably promote the phase transformation.

Fabrication of the piezoelectric polymer fibers could be also achieved by fiber drawing technique (Fig. 5.1a). In this method, kilometer-long piezoelectric fibers of sub-millimeter diameters are thermally drawn from a geometrically complex multimaterial fiber preform. The fiber perform could be assembled using a variety of materials such as thermoplastic polymers, glass and even metals. The preform is then heated in a vertical furnace and drawn into the extended lengths of fiber. The resultant fiber generally preserve the perform structure but with a much smaller cross-section dimension. By engineering the fiber inner microstructure and optimizing the drawing conditions, the fibers produced from fiber drawing technique would provide various electrical functionalities as well as great mechanical flexibility. Egusa *et al.* [66] reported the fabrication of piezoelectric fibers based on PVDF-TrFE using the fiber drawing technique. In that fiber, the PVDF-TrFE layer was sandwiched between two carbon-loaded polycarbonate layers and assembled with Tin microfilaments as the electrodes. The fiber also covered with polycarbonate shell for the protective cladding. The limitations of these piezoelectric fibers are evident, as they use very expensive PVDF-TrFE material, and the integration of Tin microfilaments reduces the fiber reliability. Kanik *et al.* fabricated piezoelectric PVDF micro- and nanoribbons using iterative size reduction technique based on thermal fiber drawing [93]. In order to obtain spontaneously polar  $\gamma$  phase PVDF, one should redraw the same fiber multiply. At this point, the robustness and reproducibility of this fabrication technique would be major concerns; however, there were no further evaluations and reports of this fabrication method. Also, consecutive re-drawings of the same fiber would be time and labor consuming. Instead, a PVDF can be impregnated with piezoelectric ceramics such as BTO and PZT, in order to enhance the piezoelectric performance of the drawn fibers [34, 156, 157]. Although a higher concentration of the piezoelectric fillers typically leads to improved piezoelectric properties, it would also cause flow instabilities that eventually result in fiber breakage. Thus, to enable the stable drawings, one should properly choose the concentration of the piezoelectric fillers.

This paper describes the material combinations and processing employed in the preparation of piezoelectric laminated generators and piezoelectric fibers. We also present a detailed study of the piezoelectric properties of the as-fabricated laminated generators and fibers. The laminated piezoelectric generators were assembled by sandwiching an electrospun piezoelectric mat between



two conductive polymer films. The piezoelectric fibers were fabricated *via* drawing of the multilayer fiber preforms. In our choice of the materials for fiber fabrication we used two criteria. First, to obtain the fibers with high piezoelectric performance, the active material should have high piezoelectric coefficient. Second, to maintain the high degree of control over drawing of the kilometer-long piezoelectric fibers the materials in the fiber preform should be thermo-mechanically compatible. Thus, PVDF was chosen as the host material for the piezoelectric layers, as it is a low-cost, stable thermoplastic polymer that can exhibit relatively high value of the piezoelectric coefficient. BTO nanoparticles were impregnated into PVDF polymer to improve its piezoelectric properties. BTO-PVDF nanocomposite mats used in planar generators and fiber preform assembly were fabricated using electrospinning as this process allows fine-tuning of the thermo-mechanical properties of nanocomposites by changing the polymer molecular weight, the concentration of the BTO nanoparticles and the processing conditions. Carbon-impregnated low density polyethylene (C-LDPE) was selected as the conductive materials, as it is both thermoplastic and electrically conductive (volume resistivity:  $2.2 \Omega \cdot m$ ). The polycarbonate (PC) polymer was used as the fiber core, acting as the mechanical support for the active layers during fiber drawing. The resulting piezoelectric fibers typically feature  $\sim 10$  bilayers of C-LDPE films and BTO-PVDF piezoelectric layers that are wrapped around a polycarbonate core (Fig. 5.1b, d). The two fiber electrode layers were extended to the opposite sides of the exposed fiber surface for convenience of the electrical connectorization (Fig. 5.1b, c). The piezoelectric fibers could effectively convert mechanical energy into electricity. Experimentally, a piezoelectric fiber (20 wt% BTO-PVDF; 10 cm length) could generate an open-circuit voltage of  $\sim 1$  V and a short-circuit current of  $\sim 0.7$  nA, when subjected to a 10 mm-bending displacement in a cyclic bend-release test (0.1 Hz). More importantly, the piezoelectric fiber retained its performance even after three days' cyclic bend-release tests. Compared to other piezoelectric fibers [51, 63, 113, 182], the fibers presented in this work feature a swiss roll structure of the piezoelectric layer, which considerably increases the active surface area and reduces the layer thickness, this resulting in considerably higher voltages and currents (and consequently electric powers) that can be generated by such fibers. Large-area piezoelectric textiles could be fabricated by incorporating the drawn fibers into woven fabrics, thanks to their excellent mechanical properties (as they are made only of plastics), and the use of low-cost, high volume fabrication techniques (fiber drawing). Finally, we conclude the paper by detailing several technology demonstrators with potential applications for powering personal



electronics and wearable sensing in the smart garments, automotive and aerospace industries.

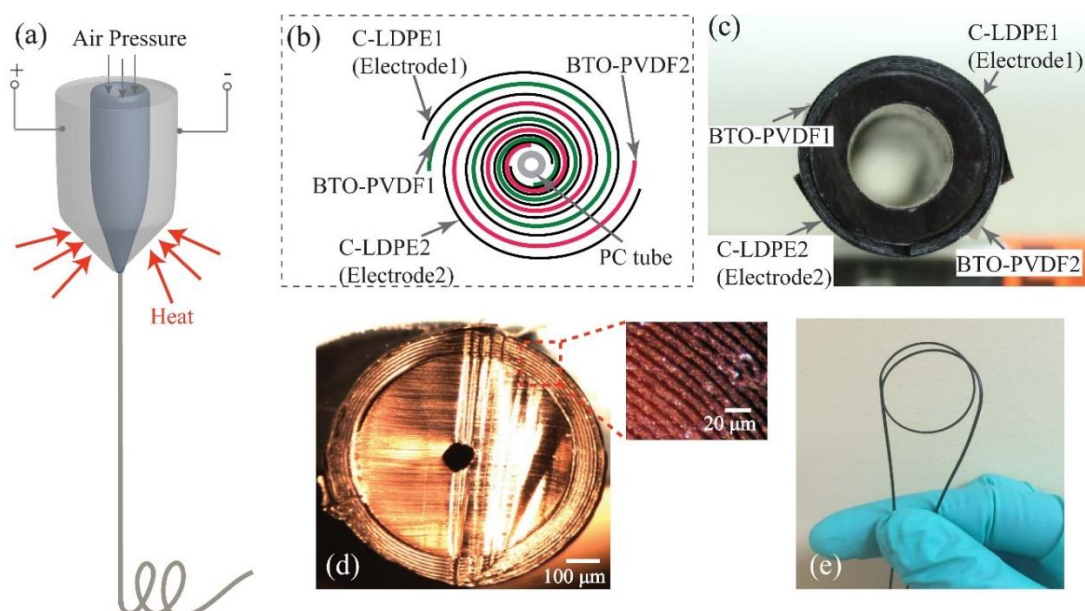


Figure 5.1: Fabrication of the piezoelectric microstructured fibers *via* drawing of the multimaterial preforms. (a) Schematic of the fabrication process of a piezoelectric fiber. (b) Schematic of the multilayer structure in the fiber preform and in the microstructured fiber. (c) Photo of a preform cross section. (d) Photo of a cross section of the piezoelectric microstructured fiber. Insert: the magnified view of a multilayer structure. (e) Photo of a piezoelectric microstructured fiber.

## 5.2 Results

### 5.2.1 Fabrication and characterization of the laminated piezoelectric generators

Before we present fiber-based piezoelectric generators, we first detail piezoelectric properties of the BTO-PVDF nanocomposites used in fiber fabrication. BTO-PVDF mats (Fig. 5.2b) were fabricated *via* electrospinning with the BTO concentrations of 5, 10, 15 and 20 wt%. The FTIR [140, 183-185] and XRD [140, 184, 186] studies of the BTO-PVDF mats are presented in Supplementary Note 1.



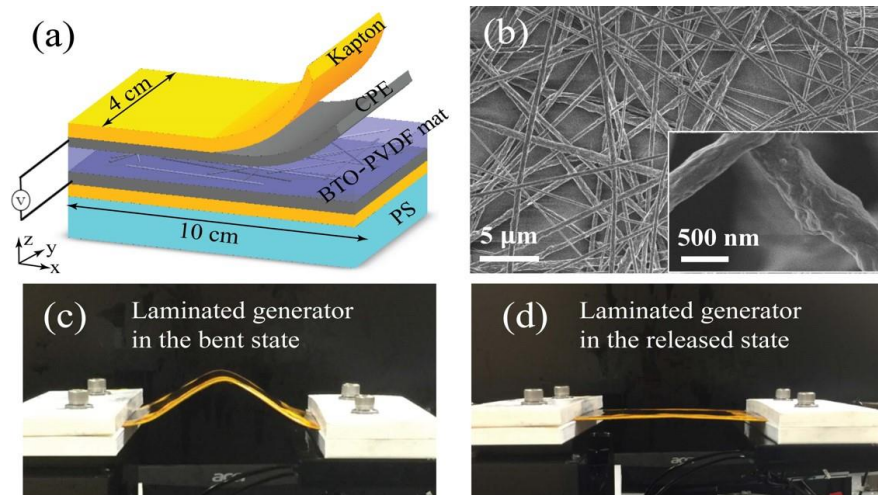


Figure 5.2: Design and performance of the laminated piezoelectric generators. (a) Schematic of a laminated BTO-PVDF generator that uses an electrospun piezoelectric mat. (b) SEM images of a BTO-PVDF mat at different magnifications. Insert: a magnified image of the BTO-PVDF nanocomposite. (c-d) Testing the laminated piezoelectric generator in its bent and released state.

A laminated piezoelectric generator was assembled by gluing an entire BTO-PVDF mat (thickness: 100  $\mu\text{m}$ ) between the two C-LDPE electrode films (thickness: 75  $\mu\text{m}$ ) using adhesive silver paste (Fig. 5.2a). And then the generators were poled in a silicone oil bath (80  $^{\circ}\text{C}$ ) under the voltage of 5 kV for 24 hours. We then immobilized the laminated generator on a 1 mm thick polystyrene (PS) substrate using Kapton tape. Due to asymmetry in the generator structure, bending of the PS substrate would lead to the non-zero average strain in the BTO-PVDF mat. Experimentally, one end of the PS substrate was fixed, while the other end was horizontally displaced by a micropositioning stage, thus bending the generator. The laminated generators were cut into a rectangular shape with dimensions of 10 cm (in x direction) by 5 cm (in y direction), and the moving end of a generator is displaced along the x direction as shown in Fig. 5.2c, d. A typical voltage and current generated by a 20 wt% BTO-PVDF laminated generator under a 10 mm-bending displacement is shown in Fig. 5.3a, b. When the moving end of the generator was displaced by 5 to 20 mm, the corresponding open-circuit voltage increased from  $\sim 4$  to  $\sim 8$  V, and the short-circuit current increased from  $\sim 18$  to  $\sim 50$  nA (Fig. 5.3c, d).



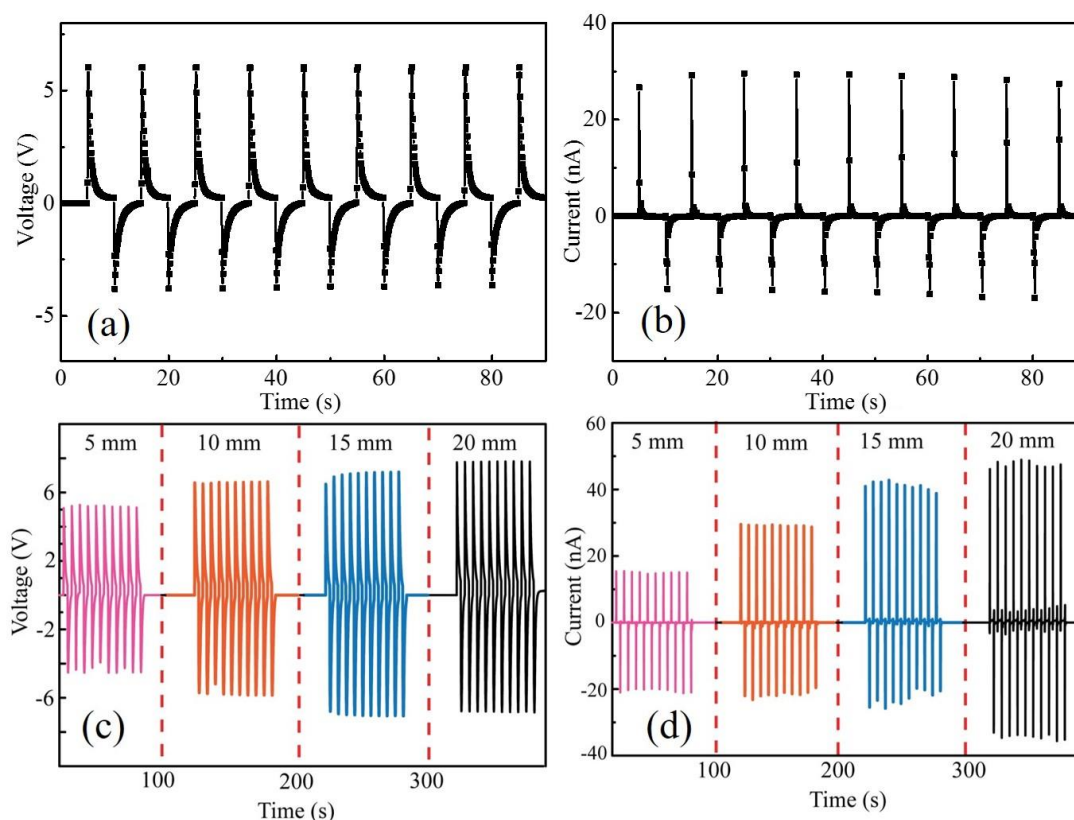


Figure 5.3: Performance of the laminated piezoelectric generators. (a) and (b) show the generated output voltage of the laminated planar generator under bending cycle at different bending displacements (5, 10, 15, and 20 mm). (c) and (d) show the output voltages and currents generated by a BTO-PVDF generator (20 wt.% BTO in the BTO-PVDF composite) when subjected to a 10 mm bending displacement.

The concentration of the BTO nanoparticles have a substantial effect on the piezoelectric properties of the mats. As the BTO concentration increased from 5 wt% to 25 wt%, the open-circuit voltage of the generator with its moving end displaced by 10 mm increased from  $\sim 0.5$  V to  $\sim 8$  V (Supplementary Fig. 5.8). We also note that the electrical poling process that would align the dipoles is critical to actuate the piezoelectric function. Compared to the case of the poled generators, the unpoled ones generally have a piezoelectric voltage one order smaller (Supplementary Fig. 5.9). Finally, we tested the durability of the generator by continuously repeating the bend-release measurements for 3 days. The generator retained well its piezoelectric voltage and current throughout the whole test that comprised  $\sim 26000$  bend/release cycles (Supplementary Fig. 5.10).



### 5.2.2 Electro-mechanical model of the planar piezoelectric generator

In what follows we describe the fundamentals of operation of the laminated piezoelectric generators and study the relationships between the generated voltages and currents with the applied stage displacements, piezoelectric mat width and thickness. As an example, we focus on the electrical signals generated during the release part of the bending cycle. Thus, in the bent state, the generator can be divided into three regions with the lengths of  $l/4$ ,  $l/2$  and  $l/4$ , according to the sign of the curvature of the generator. In the first and the third regions the generator is under stress, while in the second region the generator is under strain (see Fig. 5.4a), therefore generating  $(\Delta Q, -2\Delta Q, \Delta Q)$  fixed surface charges in the piezoelectric mat. In the equilibrium state of a generator, these charges are compensated by the opposite free charges in the electrodes. Therefore, at the beginning of the generator release (when the stress on the piezoelectric layer is suddenly released and the generator is flattened), mobile surface charges  $(-\Delta Q, 2\Delta Q, -\Delta Q)$  will be present on the conductive electrodes. Consequent charge equilibration in the generator can then be approximated in terms of the effective electrical circuit shown in Fig. 5.4b, where  $C$  is the generator capacitance,  $R_e$  is a single electrode resistance, while  $R_L$  is the resistance of the load.

In the case of a planar piezoelectric mat of length  $l$ , width  $w$ , thickness  $d_p$ , and dielectric constant  $\epsilon_p$ , the generator capacitance is  $C = \frac{\epsilon_p \epsilon_0 l w}{d_p}$ . At the same time resistance of the electrode resistance that covers the mat is  $R_e = \rho \frac{l}{w d_e}$ , where  $d_e$  is the electrode thickness and  $\rho$  is the electrode material bulk resistivity. Using standard analysis of the basic electric circuits (Supplementary Note 2), we can derive the following expressions for the open circuit voltage  $V^{oc}(t) \sim V_{max}^{oc} e^{-2\frac{t}{\Delta t^{oc}}}$  and the short circuit currents  $I^{sc}(t) \sim I_{max}^{sc} e^{-2\frac{t}{\Delta t^{sc}}}$  with the following maximal values of the open circuit voltage and short circuit currents, as well as equilibration times  $\Delta t^{oc}$ , and  $\Delta t^{sc}$ :

$$\begin{aligned}
 \text{Open-circuit voltage:} \quad & V_{max}^{oc} = V^{oc}(0) = -\frac{4\Delta Q}{C} \\
 & \Delta t^{oc} \sim 2\tau_0 \\
 \text{Short-circuit current:} \quad & I_{max}^{sc} = I^{sc}(0) = \frac{\Delta Q}{\tau_0} \\
 & \Delta t^{sc} \sim 1.5279\tau_0
 \end{aligned} \tag{1}$$



where the time constant is defined as:

$$\tau_0 = \frac{R_e C}{8} = \frac{\rho \epsilon_p \epsilon_0}{8} \frac{l^2}{d_p d_e} \quad (2)$$

According to ref. [34], fixed charges  $\Delta Q$  induced on the surface of a piezoelectric mat of length  $l/4$  (see Fig. 5.4a) can be calculated as:

$$\Delta Q = d_{31} Y_p \epsilon w \cdot \frac{l}{4} \quad (3)$$

where  $d_{31}$  is the piezoelectric coefficient of a piezoelectric mat,  $Y_p$  is the Young's modulus of the piezoelectric material,  $w$  is the width of the piezoelectric mat, and  $\epsilon$  is the applied strain. From Eq. (1), we can then conclude that the peak open-circuit voltages have a liner relationship with the applied strain  $\epsilon$ :

$$\begin{aligned} |V_{max}^{oc}| &= \epsilon \frac{d_{31} Y_p w l}{C} = \epsilon d_p \frac{d_{31} Y_p}{\epsilon_p \epsilon_0} \\ |I_{max}^{sc}| &= \frac{\Delta Q}{\tau_0} = 2\epsilon \frac{w \cdot d_p d_e}{l} \frac{d_{31} Y_p}{\rho \epsilon_p \epsilon_0} \end{aligned} \quad (4)$$

The evaluation of the applied strain  $\epsilon$  is presented in the (Supplementary Note 3). By using a model for the buckling of thin beams, according to ref. [51, 187], the strain in the PVDF mat can be determined as:

$$\epsilon \approx 2\pi \frac{d_{PS} \sqrt{\Delta l}}{l^{3/2}} \quad (5)$$

where  $d_{PS}$  is the polymer substrate thickness,  $\Delta l$  is the stage displacement, and  $l$  is the length of the laminated piezoelectric generator. Finally, remembering a relationship between the maximal open circuit voltage and the strain given by Eq. (4), we conclude that generated voltages and currents depend in a non-linear manner with the generator displacement, namely:

$$\begin{aligned} |V_{max}^{oc}| &= \epsilon d_p \frac{d_{31} Y_p}{\epsilon_p \epsilon_0} = 2\pi \frac{\sqrt{\Delta l} d_{PS} d_p}{l^{3/2}} \frac{d_{31} Y_p}{\epsilon_p \epsilon_0} \\ |I_{max}^{sc}| &= \frac{\Delta Q}{\tau_0} = 4\pi \frac{w \sqrt{\Delta l} d_{PS} d_p d_e}{l^{5/2}} \frac{d_{31} Y_p}{\rho \epsilon_p \epsilon_0} \end{aligned} \quad (6)$$

To test our theoretical model against experimental measurements, we first characterized the laminated generators ( $w: \sim 5$  cm;  $l: \sim 10$  cm) under different stage displacements. In Fig. 5.4c, d we



plot the peak voltages ( $|V_{max}^{oc}|$ ) and currents ( $|I_{max}^{sc}|$ ) as a function of the displacements ( $\sqrt{\Delta l}$ ) as calculated using Eq. (6) and observe an almost linear dependence in good agreement with theory. Note that, for each displacement, we repeated the bend-release cycles for 20 times; and the value of  $|V_{max}^{oc}|$  and  $|I_{max}^{sc}|$  are the average of these measured peaks. Then, we studied the relationship between the measured voltages (currents) and the piezoelectric mat width. We cut a generator along its longitudinal direction, and thus obtained smaller pieces with 1/2, 1/4 and 1/8 of the original widths and the same mat length. In Fig. 5.4e we find that the output voltage ( $|V_{max}^{oc}|$ ) is independent of the piezoelectric mat width ( $w$ ), while generated current increases with the mat width although the dependence is not linear and depends strongly on a sample. Finally, we investigated the relationship between the measured voltages and piezoelectric mat thickness. The thickness of the piezoelectric mat could be increased by using a longer electrospinning time, while keeping other processing conditions the same. Here, the electrospinning time and materials utilized in the fabrication of  $\sim 100$   $\mu\text{m}$ -thick piezoelectric mat was twice of that of  $\sim 50$   $\mu\text{m}$ -thick piezoelectric mat. In Fig. 5.4f we observe that the output voltage ( $|V_{max}^{oc}|$ ) is indeed proportional to the thickness of piezoelectric mats ( $d_p$ ), which is again in accordance with our theory. Finally, from Eq. (6) and almost linear behavior of the output voltage to the displacements ( $\sqrt{\Delta l}$ ) value (see Figure 5.4c) we can estimate the value of the  $d_{31}$  piezoelectric coefficient to be  $d_{31} \sim 13$  pC/N which is lower than the  $d_{31}$  of BaTiO<sub>3</sub> nanoparticles ( $\sim 80$  pC/N), but higher than that of the commercial piezoelectric PVDF films ( $\sim 6$  pC/N). Here, the dielectric constant ( $\epsilon_p$ ) of BTO/PVDF mat was estimated using the Bruggeman (BG) formulation:

$$c \cdot \frac{\epsilon_{BTO} - \epsilon_p}{\epsilon_{BTO} + 2\epsilon_p} + (1 - c) \cdot \frac{\epsilon_{PVDF} - \epsilon_p}{\epsilon_{PVDF} + 2\epsilon_p} = 0$$

where  $\epsilon_p$  is the complex effective dielectric constant of BTO suspension in the PVDF matrix,  $\epsilon_{BTO}$  and  $\epsilon_{PVDF}$  are the complex constants of the pure bulk BTO and PVDF, respectively. We note that thus found value of the  $d_{31}$  coefficient should only be considered as rough estimate as its value was found using the predictions of several approximate models designed to explain general trends in the electro-mechanical operation of the planar piezoelectric generators.



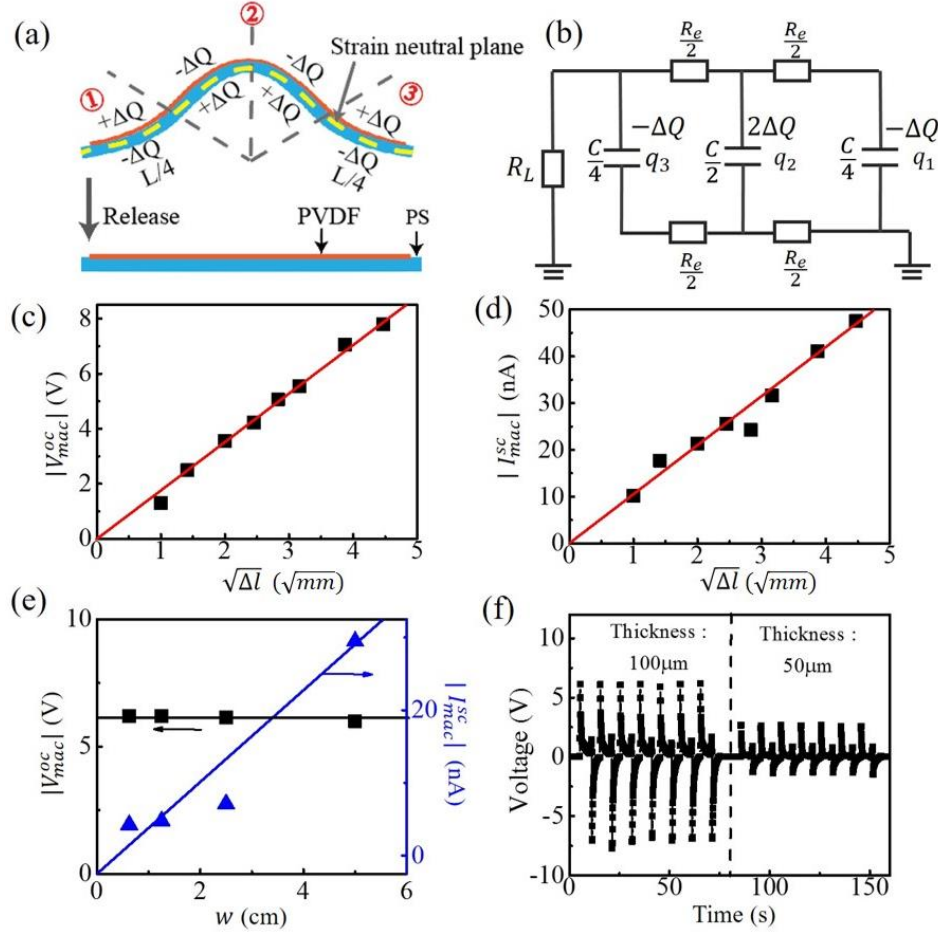


Figure 5.4: Electrical properties of the laminated piezoelectric generators under bending. (a), Schematic of charge separation in the piezoelectric mat under bending. (b), Equivalent electric circuit of the generator with a resistance load  $R_L$ . (c, d), The measured output voltages (c) and currents (d) generated by a laminated generator (BTO concentration: 20 wt%) under different displacements ( $\sqrt{\Delta l}$ ) compared to the calculated ones (red lines) using Eq. (6). (e, f), The relationship between the output voltage (current) and piezoelectric mat width  $w$  (e), and piezoelectric mat thickness  $d_p$  (f).

### 5.2.3 Fabrication of the piezoelectric fibers via drawing of the multimaterial preforms

Fig. 5.1 summarizes the fabrication process of the piezoelectric fibers. The first step is to assemble a fiber preform using the commercial and home-made materials. Two BTO-PVDF mats (thickness: 100  $\mu m$ ) and C-LDPE films (thickness: 85  $\mu m$ ) were co-rolled onto a hollow



polycarbonate rod with an outer diameter of 2.54 cm, in order to create a multilayer cladding having  $\sim 10$  alternating piezoelectric-conductive layers (Fig. 5.1b, c). After assembly, the structure was then vacuum consolidated into a solid preform at 110°C. Subsequently, the resulting fiber preform was thermal-mechanically drawn into meters of piezoelectric microstructured fibers using a fiber drawing tower. Here the BTO-PVDF mats were fabricated in-house *via* electrospinning. We differed the BTO concentrations in the BTO-PVDF mats from 5% to 20% with a 5 wt% interval, in order to investigate the effects of BTO nanoparticles on the properties of the final fibers. The C-LDPE films were purchased from Bystat International Inc. and had a volume resistivity of  $2.2 \Omega \cdot m$ . Note that, the carbon fillers in the polyethylene matrix will be re-arranged, and thus the conductive network will be altered during fiber drawing. After drawing, the bulk resistivity of the polymer composite in the drawn fiber will be increased dramatically. Thus, it is important to optimize the drawing parameters. In the drawings of piezoelectric fibers, the drawing temperature is set at 190 °C and the drawing speed is 500 mm/min, at which conditions the formation of conductive network during fiber drawing could be facilitated. Our measurements suggest that the volume resistivity of the conductive layers in the piezoelectric fiber is  $\sim 2.5 \Omega \cdot m$ . The application of the electrical field during drawing would also affect the piezoelectric properties of the drawn fibers, because the electrical poling together with mechanical stretching could promote the  $\beta$  phase transformation in the PVDF layer. In our experiments, a voltage of up to 5 kV was applied to the preform. However, the results suggested that the polarization during fiber drawing is not effective as the drawing time is too short. On the other hand, we find the application of the high voltage could effectively control the layer thickness in the drawn fibers, since the two conductive layers in the molten polymer were forced to pull together due to the strong electrical force. In this way, the piezoelectric fibers with several tens of nm layer thicknesses could be obtained. Optical images of fiber cross section (Fig. 5.1d) show that the multilayer structure retained well after drawing, while the layer thicknesses typically ranged from 5 to 20  $\mu m$ . The obtained fibers were then immersed in silicone oil bath (80 °C) for further polarization. After applying a voltage of 9 kV for 12 h, the fibers were slowly cooled down to room temperature.

#### 5.2.4 Characterization of the piezoelectric microstructured fibers

We then characterized the performance of the piezoelectric microstructured fibers. A piezoelectric microstructured fiber (length:  $\sim 10$  cm, diameter:  $\sim 1$  mm) was used to assemble the



fiber-based generator. As shown in Fig. 5.5a, b, two C-LDPE strips were used to connect the fiber electrodes. Particularly, one C-LDPE strip was glued to the top side of the fiber, while the other one was glued to the opposite side. Similar to the laminated piezoelectric generators, the fiber-based devices also consisted of a PS substrate (10 cm long, 1 mm thick) and Kapton tapes. Experimentally, the fiber-based generators were periodically bent and released in the horizontal direction using a linear motor. During the bend/release motions, the PS substrate worked as the bottom supporter and the Kapton tape covered the piezoelectric fibers. The mechanical strain was applied along the piezoelectric fiber by displacing one fiber end. The working principle of the fiber-based generators is discussed as follows. When the piezoelectric fiber is bent and released, positive and negative voltage spikes are observed (Fig. 5.5c). To explain this phenomenon, one needs to examine the charge separation mechanism and equivalent circuit model of the piezoelectric fiber. In the electrical poling, the dipoles of the piezoelectric domains in the BTO-PVDF layers are aligned in one direction. Due to the presence of the electric field of the dipoles, surface charges  $+Q$  and  $-Q$  are induced on the top and bottom electrode respectively. When a tensile stress is applied along the piezoelectric fiber, the polarization density of piezoelectric layers will change, thus inducing  $\pm\Delta Q$  changes in the surface charges of the fiber electrodes. In response to that, the electrons are forced to flow from one electrode to the other, thus generating voltage differential. (Fig. 5.5d). In the bent state, the output voltage (current) gradually return to zero. Similarly, to the planar piezoelectric generators in the absence of the external load resistance, the charge relaxation processes in the generator can be considered as the RC charging/discharging with the two different time constants, one for the open-circuit voltage equilibration  $\tau_{co}$  and the other for the short-circuit current equilibration  $\tau_{sc}$ .



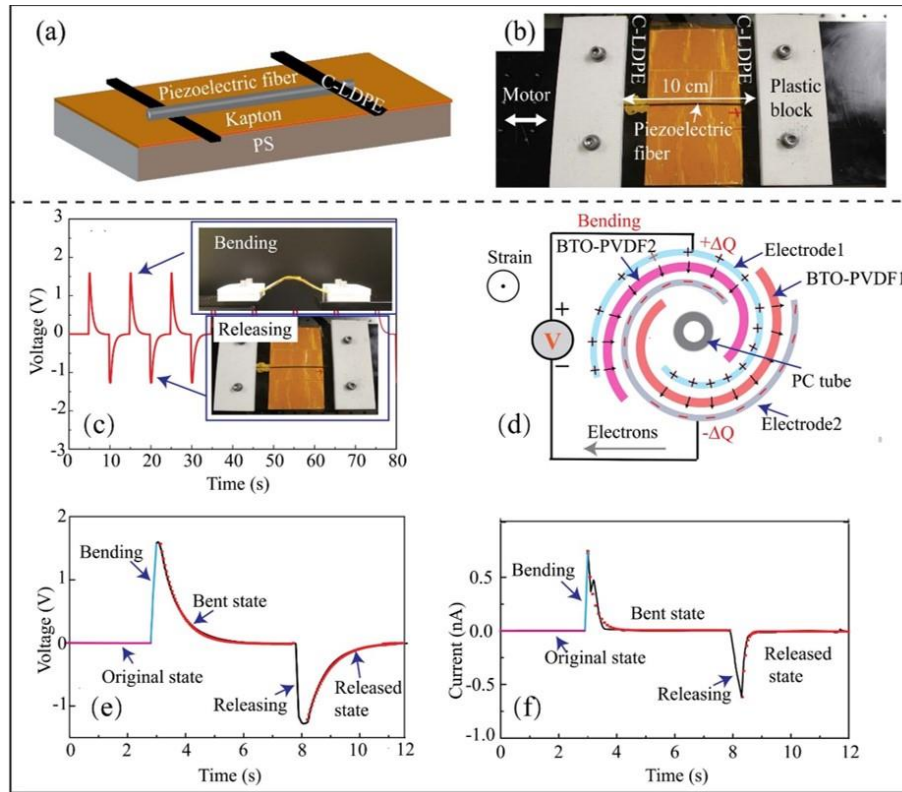


Figure 5.5: Design and working principles of the fiber-based piezoelectric generators. (a), Schematic of a BTO-PVDF fiber-based generator. (b), Setup for testing of microstructured fiber generator. (c), Measured voltage response of the piezoelectric fiber under cycling bending at 0.1 Hz. The top and bottom insets show photographs of the fiber during bending and release, respectively. (d), When mechanical strain is applied along the fiber by bending, the polarization density of the BTO-PVDF layer is changed and the electrons are forced to flow from one electrode to the other, thus generating voltage differential. (e, f), The open-circuit voltage (e) and the short-circuit current (f) of the piezoelectric fiber during the bend and release actions. Relaxation of the short circuit current and open circuit voltage on time can be described as single exponential decays with two distinct time constants (red curve fits).

The electrical outputs of the fiber-based generators are also affected by the BTO concentrations. Experimental results (Supplementary Fig. 5.11) suggest that the open-circuit voltage of the piezoelectric fiber-based generators increased from  $\sim 0.15$  V to  $\sim 2.5$  V when subjected to a 10 mm-bending displacement, while the BTO concentration in the piezoelectric fiber increased from 5 wt% to 25 wt%. However, we find that drawing fibers with BTO concentrations



higher than 25 wt% is challenging. Within the fiber drawing process, the preform is softened above the glass transition temperature, and then pulled into a fiber at a specified speed. When the BTO concentration is too high, during drawing the nanoparticles will aggregate in the melt and form multiple macroscopic domains. While the preform diameter is being reduced, these domains serve as defect centers that cause flow instabilities that eventually result in fiber breakage. Thus, there is a trade-off between BTO concentration and the availability of fiber drawing process. All the drawings in this paper used the 20 wt% BTO concentration, since at this condition the drawing is stable while the piezoelectric functionality of the as-drawn fibers is maximized. Similar to the laminated generators, the performance of the fiber-based generators is also affected by the bending displacements. The piezoelectric voltage and current generated from the microstructured fibers increased from  $\sim 1$  to  $\sim 1.7$  V and  $\sim 0.7$  to  $\sim 1.3$  nA respectively, when the bending displacements increased from 5 mm to 20 mm (Fig. 5.6a,b). Besides, the electrical poling process is also required for the improvement of the piezoelectric fiber performance, since the electrical poling can align the piezoelectric domains in the same direction. As stated in Supplementary Fig. 5.12, the output voltage of non-poled fibers was  $\sim 1.5$  mV, which was much smaller than that of poled ones ( $\sim 1$  V). The mechanical stability of the piezoelectric fibers was estimated by conducting continually bend-release tests for 3 days. The amplitudes of output voltages and currents exhibit high stability for 25920 bend/release cycles (Supplementary Fig. 5.13). This phenomenon is probably attributed to the flexibility and robustness of the polymer materials utilized in the fiber fabrication. The properties of the piezoelectric fibers could be improved by using piezoelectric materials with higher piezoelectric coefficients. According to the literature, PZT has a higher piezoelectric coefficient than BTO. The PZT-PVDF (20 wt% of PZT in the PZT-PVDF composite layer) fibers were thus fabricated and then characterized using the same procedures as used for BTO-PVDF fibers. Experimentally, when subjected to the same bending displacements, the output signals generated from PZT composite fibers is  $\sim 4$  times higher than that from BTO composite fibers (Fig. 5.6c, d). However, the toxicity of PZT may limit the potential applications.



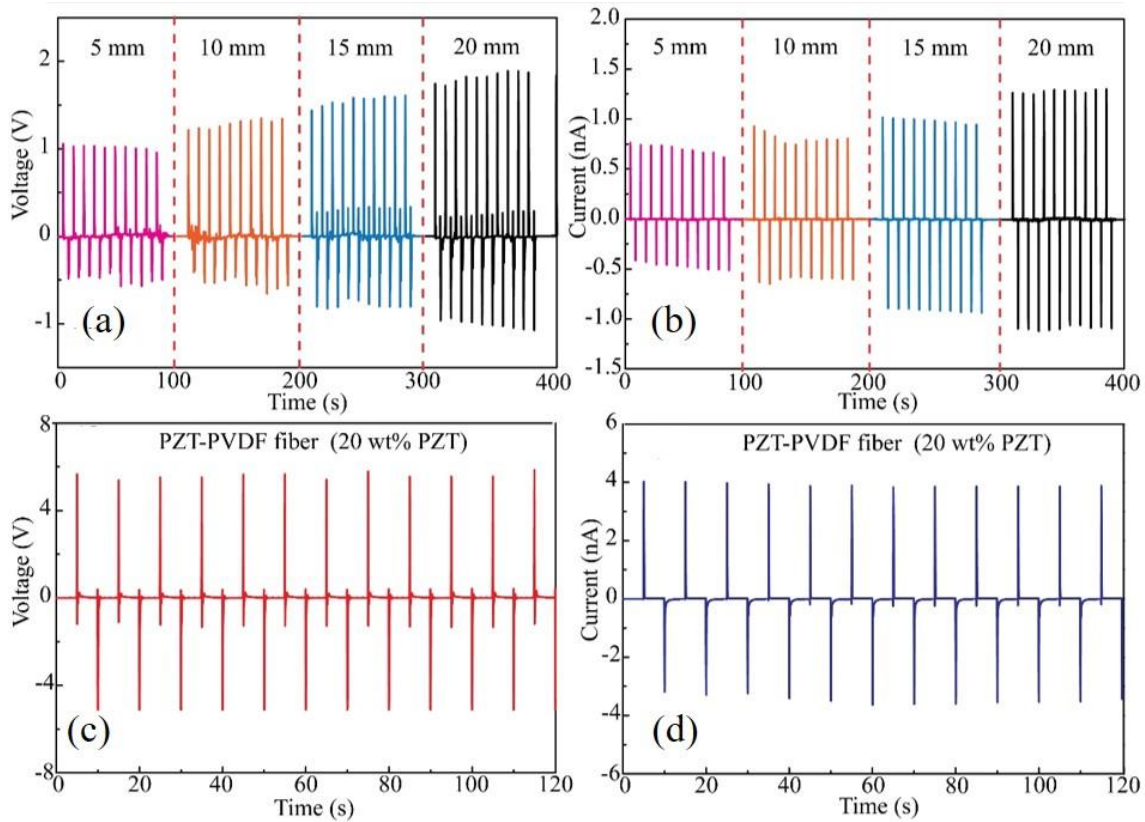


Figure 5.6: Performance of the piezoelectric microstructured fibers. (a) and (b) show the generated output voltage of the fiber-based generator under bending cycle at different bending displacements (5, 10, 15, and 20 mm). (c) and (d) show the output voltages and currents generated by a 10 cm-long PZT-PVDF fiber generator (20 wt.% PZT in the PZT-PVDF composite) when subjected to a 10 mm bending displacement.

### 5.3 Examples of the potential applications of the piezoelectric fiber generators

Piezoelectric microstructured fibers could be easily integrated into large-area cotton textiles using traditional textile fabrication techniques, thanks to the excellent mechanical properties of the drawn fibers. In this paper, the piezoelectric textiles were fabricated using a classic Dobby-loom (see Video 1). Here we discuss two prototypes of the fiber-based generators and demonstrated their possible applications as micro-generators or sensors for the wearables and automotive/airspace applications. In the first prototype, four piezoelectric fibers (length:  $\sim 15$  cm; diameter:  $\sim 1$  mm) were woven into a cotton fabric and then connected in series (Fig. 5.7b). The piezoelectric textile



could generate open-circuit voltages up to  $\sim 5$  V and short-circuit currents of 2-10 nA, during the repeated irregular deformations caused by the human hand tap-release actions (Fig. 5.7d, e). In the second prototype, the piezoelectric fiber (length:  $\sim 15$  cm; diameter:  $\sim 1$  mm) was glued on the exterior of the airplane model. Note that, the tiny and flexible piezoelectric fibers could be implanted on the any parts of the airplane (Fig. 5.7f, g). During the tests, the airplane model was fixed on the wooden table. As we turned on the airplane motor, the rotation of the airplane propeller resulted in the irregular vibrations of the piezoelectric fibers, thus generating electric signal (see Video 2). The output voltages of the piezoelectric fibers are highly dependent on the rotation speed of the airplane motor. As the propeller rotation speed increased to the maximum, the open-circuit voltage of the piezoelectric fiber increased from 0 to 2V (Fig. 5.7h, i).

## 5.4 Conclusion

In this work, we have demonstrated both planar piezoelectric generators and piezoelectric fibers. The piezoelectric laminated generators were assembled first in order to study energy harvesting properties of the piezoelectric electrospun nanocomposites. Such planar generators can generate open-circuit voltages of up to 8 V and short-circuit voltage of up to 40 nA with an active area of several tens of  $\text{cm}^2$ . Then, using electrospun nanocomposites as building materials, all-polymer piezoelectric microstructured fibers were fabricated using fiber drawing technique. The fabricated fibers feature a hollow PC core surrounded by a multilayer cladding consisting of the alternating BTO-PVDF and conductive C-LDPE layers. A swiss roll structure of the piezoelectric layer used in our fibers, considerably increases the active surface area and reduces the piezoelectric layer thickness, thus resulting in high voltages of up to 6V and currents of up to 4 nA that can be generated by our fibers with only several  $\text{cm}^2$  of the active area. Finally, we have demonstrated that the large-area piezoelectric textiles could be fabricated by incorporating piezoelectric fibers into the woven fabrics, thanks to the fiber excellent mechanical properties. The fabricated textiles and fibers were then used to highlight several of their potential applications as micro power generators or sensors in smart textile apparel and avionics.



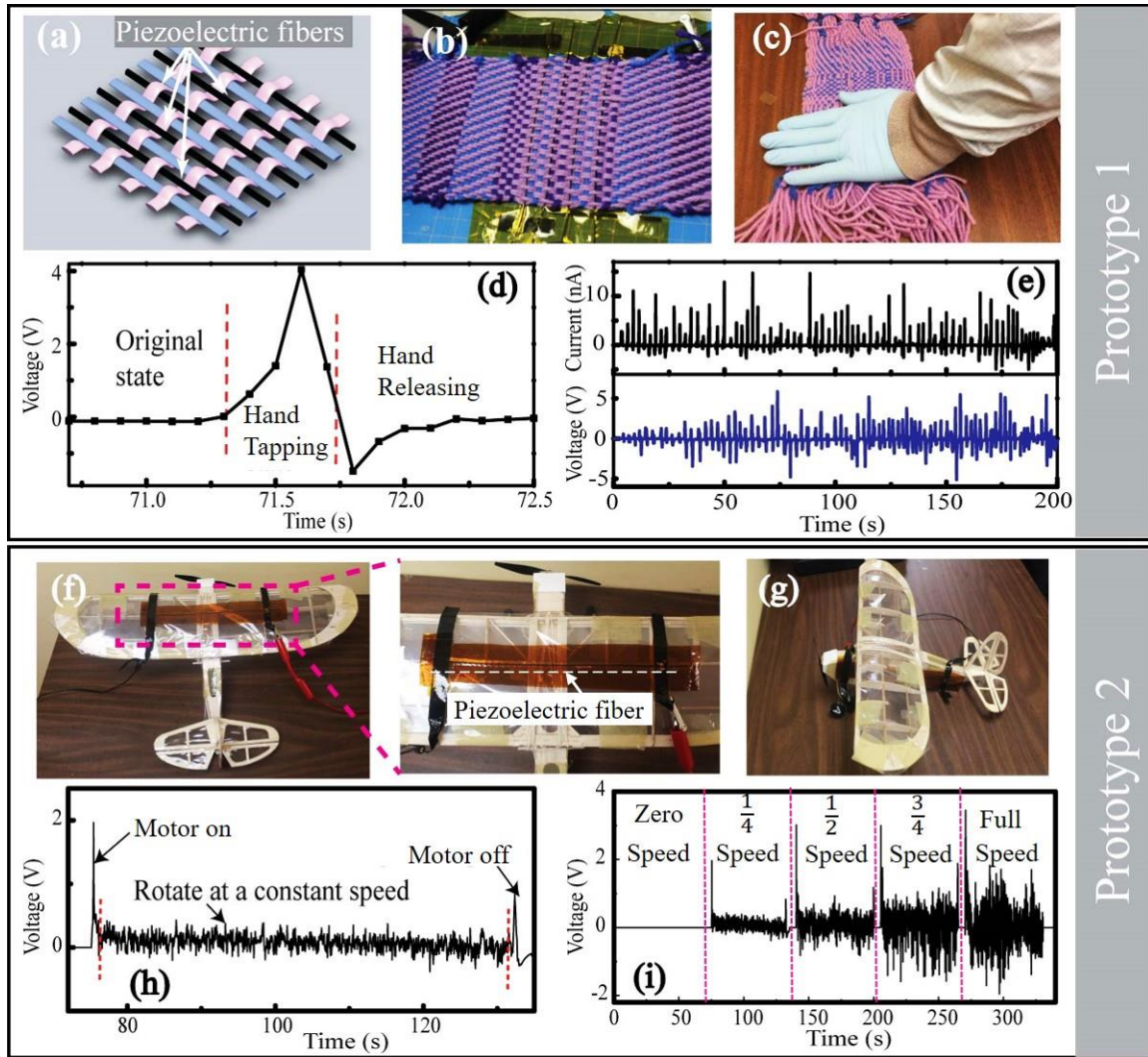


Figure 5.7: Potential applications of the piezoelectric fiber generators. (a, b), A cotton-based textile containing piezoelectric fibers woven using a Dobby loom. (c), Electrical properties of the piezoelectric textile actuated by the human hand tapping. (d), Open-circuit voltages of the piezoelectric textile in a hand tapping-releasing actions. (e), Open-circuit voltages and short-circuit currents generated by the piezoelectric textile during repeated hand tap-release motions. (f, g), Piezoelectric fibers implanted on the airplane wing (f) and the airplane body (g). (h), Open-circuit voltages generated by the piezoelectric fibers during rotation of the airplane propeller. (i), Open-circuit voltages generated by the vibrations induced by the airplane motor operation with the motor speeds set at zero,  $1/4$ ,  $1/2$ ,  $3/4$  of its maximum speed.



## 5.5 Methods

### 5.5.1 Materials

The PVDF polymer used in this experiment was a semicrystalline PVDF (pellet, Sigma-Aldrich) which has a number average molecular weight of  $\sim 275,000$ . Dimethylformamide (DMF) and acetone solvent were purchased from Sigma-Aldrich. BTO nanoparticles (average diameter of 200 nm) were purchased from US Research Nanomaterials Inc. PZT micropowders (50-100  $\mu\text{m}$ , APC 850) were purchased from APC Inc.

### 5.5.2 Preparation of polymer solutions

#### Preparation of BTO-PVDF suspensions

A good dispersion of inorganic particles in polymer matrix is necessary to achieve the best possible performance of the polymer nanocomposite. We use the ultrasound to improve the dispersion of the BTO nanoparticles. A suspension of BTO-DMF was ultrasonically irradiated using a probe-type sonicator (Fisher Scientific Inc.) at 100 W for 1 h. To prevent the DMF solvent from heating, the suspension was irradiated in 5 s intervals (3 s pulse on, 2 s pulse off). PVDF was swelled in acetone using a magnetic stirrer for 10 min. Then, the two suspensions were mixed together using a magnetic stirrer while being heated at 100  $^{\circ}\text{C}$  for 1 h. Finally, the mixed suspension was ultrasonically irradiated at 75 W in 5 s intervals (3 s pulse on, 2 s pulse off) for 15 min, and then transferred to a vacuum chamber to remove the air bubbles. Here, the PVDF concentration was 20%, the BTO concentrations in the BTO-PVDF nanocomposites were ranges from 5 to 25 wt% with a 5 wt% variation. The DMF/acetone volume ratio was 2/3.

#### Preparation of PZT-PVDF Suspensions

The PZT micropowders were milled using a ball-milling machine (MSK-SFM-2, MTI Corporation). The milling time is 10 h, while the milling speed is 200 rpm. The weight ratio of ball-to-PZT was 20:1. The as-milled PZT micropowders were then utilized in the preparation of PZT-PVDF suspensions, following the same procedures proposed for the preparation of BTO-PVDF suspensions.



### 5.5.3 Electrospinning

The Electrospinning Workstation (MSK-NFES-3, MTI Corporation) consists of a high voltage supply, a glass syringe (20 mL) with a blunt metallic needle (22 gauge) and a grounded metallic drum (diameter: 5 cm). The drum rotating at a speed of 200 rpm was used to collect the piezoelectric nanofibers. In the electrospinning, the polymer suspensions were charged by a high voltage of 15 kV, and the distance between the needle tip and the drum collector is 15 cm. Electrospinning was done with an ejection rate of 1 *ml/h* from the syringe. The temperature in the electrospinning chamber was controlled at 25 °C. After the electrospining, the electrospun mats were vacuum dried at room temperature for 24 h.

### 5.5.4 Preforms and fibers fabrication

The preform and fiber structure is illustrated in Fig. 5.1b, c. The fabrication of the preform started with co-rolling of four alternating BTO-PVDF electrospun mats and C-LDPE conductive films. The preform was then vacuum consolidated at a temperature of 110 °C. The as-assembled preform was subsequently thermally drawn in a two temperature-zone verticle furnace. The bottom temperature is 190 °C, while the top temperature is 150 °C. The drawing speed was set at 500 mm/min. And an air-pressure of 3 mbar is used to maintain the fiber core during the drawing.

## 5.6 Supplementary Figures and Notes

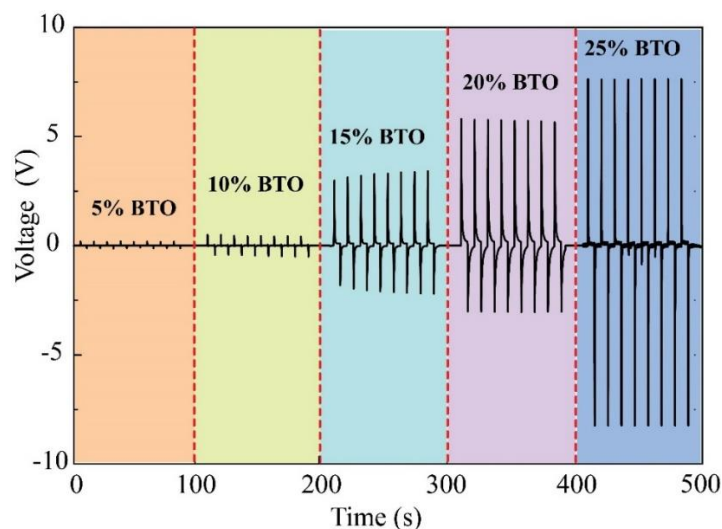


Figure 5.8 : Open-circuit voltage generated by the laminated BTO-PVDF generators with the BTO concentration of 5, 10, 15, 20, and 25 wt%. 10 mm-displacement was used in all tests.



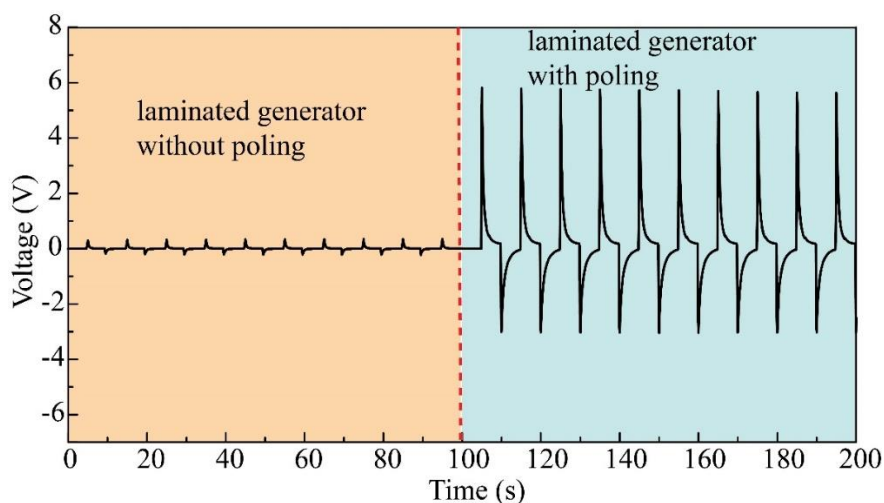


Figure 5.9: Comparison of the open-circuit voltage generated by the poled laminated BTO-PVDF (20 wt% BTO) generator to that of the unpoled one.

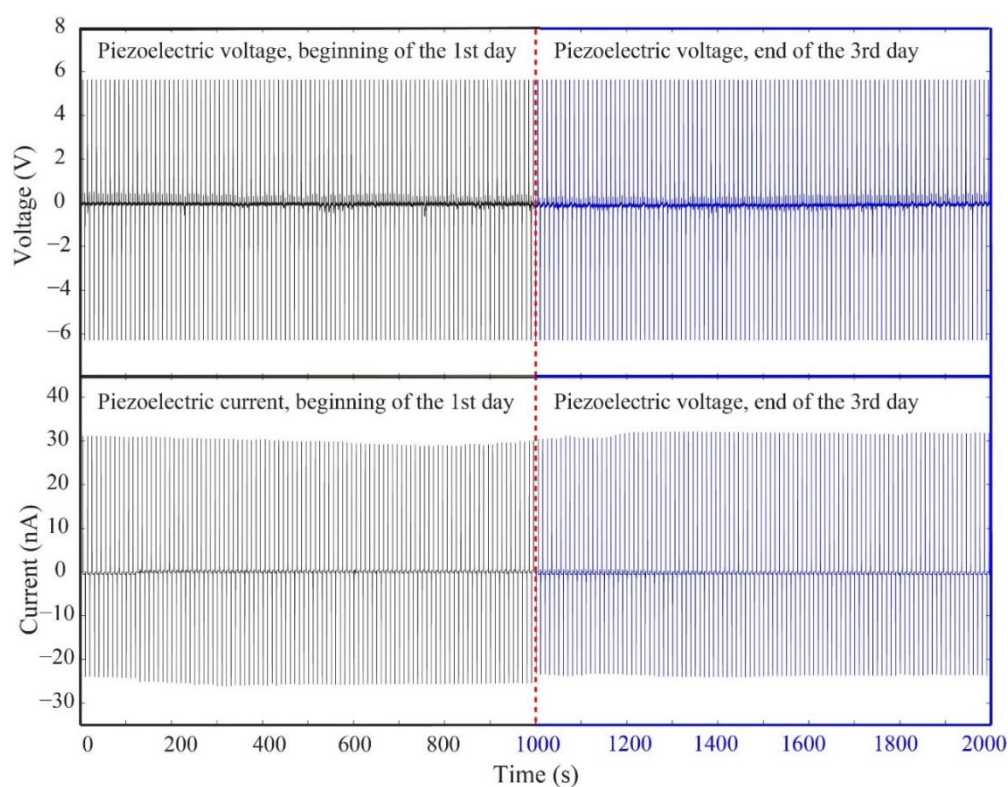


Figure 5.10 : A durability test was carried out for the laminated BTO-PVDF generator (20 wt% BTO) by continuously repeating the bend-release test for 3 days. In each bend-release motion, the moving end of the generator was displaced by 10 mm. The open-circuit voltage and short-circuit



current generated in a 1000 s period at the beginning of in the first day and at the end of the third day are shown. Overall, 25920 bend/release cycles were performed during 3 days.

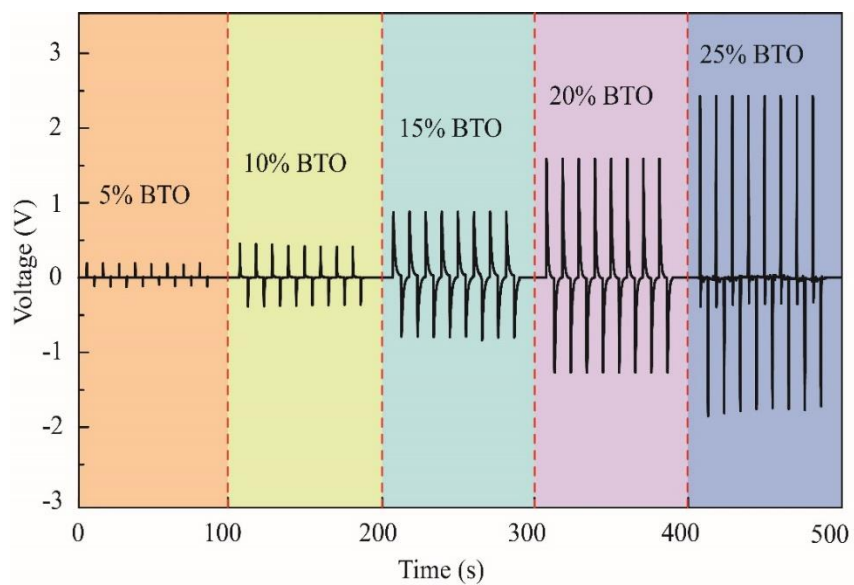


Figure 5.11 : Open-circuit voltage generated by BTO-PVDF microstructured fiber with the BTO concentration of 5, 10, 15, 20, and 25 wt%.



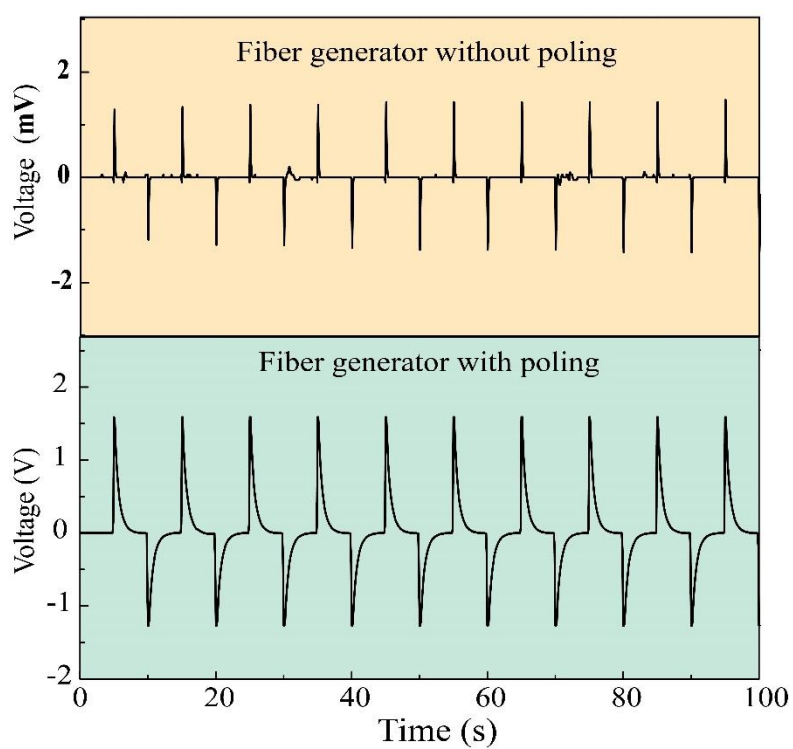


Figure 5.12 : Comparison of the open-circuit voltages generated by the poled BTO-PVDF microstructured fiber and the unpoled one.



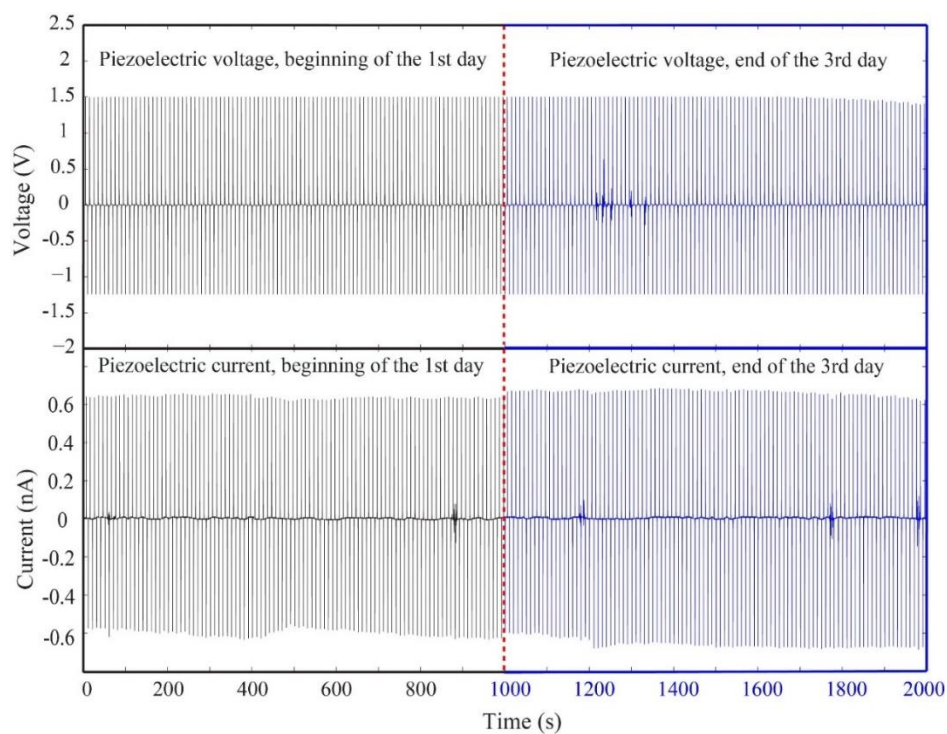


Figure 5.13 : A durability test was carried out for the BTO-PVDF microstructured fiber (20 wt% BTO in BTO-PVDF composite) by continuously repeating the bend-release test for 3 days. The open-circuit voltage and short-circuit current generated in a 1000 s period at the beginning of the first day and at the end of the third day are shown.



### Supplementary Note 1. Piezoelectric properties of the BTO-PVDF mats

In the following we detail dependence of the piezoelectric properties of the BTO-PVDF mats on the concentration of the piezoelectric nanofillers using FTIR and XRD techniques.

#### FTIR of BTO-PVDF mats

Fourier transform infrared (FTIR) spectra were recorded on a FTIR spectrometer (FTLA2000-104, ABB Inc.). The vibration bands at 761 (CF<sub>2</sub> bending and skeletal bending), 796 (CH<sub>2</sub> rocking), 870, 974, 1146 and 1383 cm<sup>-1</sup> correspond to  $\alpha$  phase; whereas vibration bands at 840 and 1274 cm<sup>-1</sup> (CH<sub>2</sub> rocking) are assigned to  $\beta$  phase [140, 183-185].

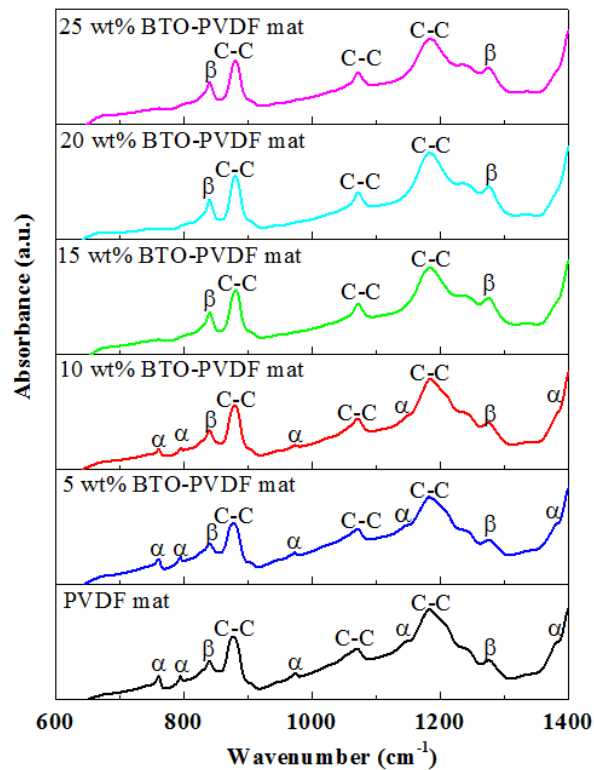


Figure 5.14 : FTIR spectra of BTO-PVDF electrospun mats at different BTO concentrations

As shown in Supplementary Fig. 5.14, when the BTO concentration is higher than 15%,  $\alpha$  phase could be hardly observed. When the BTO concentration is lower than 10%,  $\alpha$  phase and  $\beta$  phase coexist in the nanocomposite. The  $\beta$  phase content,  $F(\beta)$ , in the PVDF mats was calculated using the following Eq.: [140]

$$F(\beta) = \frac{X_{\beta}}{X_{\alpha} + X_{\beta}} = \frac{A_{\beta}}{\frac{K_{\beta}}{K_{\alpha}} A_{\alpha} + A_{\beta}}$$



where  $A_\alpha$  and  $A_\beta$  are the absorbance at  $761\text{ cm}^{-1}$  and  $840\text{ cm}^{-1}$  respectively, and  $X$  is the degree of crystallinity of each phase.  $K_\alpha$  and  $K_\beta$  are the absorption coefficient at the respective wavenumber, which are  $6.1 \times 10^4$  and  $7.7 \times 10^4\text{ cm}^2\text{ mol}^{-1}$ . From calculation, we find that the  $\beta$  crystal phase content increased from 56% to 70%, when the BTO concentration increases from 0 to 10 wt%.

### XRD of BTO-PVDF mats

The X-ray diffraction patterns were recorded by a Bruker D8/Discover diffractometer equipped with a standard sealed tube producing Cu radiation ( $\lambda = 1.54178\text{ \AA}$ ) running at 40 kV and 40 mA. The peaks at  $2\theta$  values of  $18.5^\circ$ ,  $20.4^\circ$  are indexed to the  $\alpha(020)$ ,  $\beta(200/110)$  reflections of PVDF respectively [97, 140], while the other characteristic peaks can be assigned to the tetragonal phase of  $\text{BaTiO}_3$  [186].

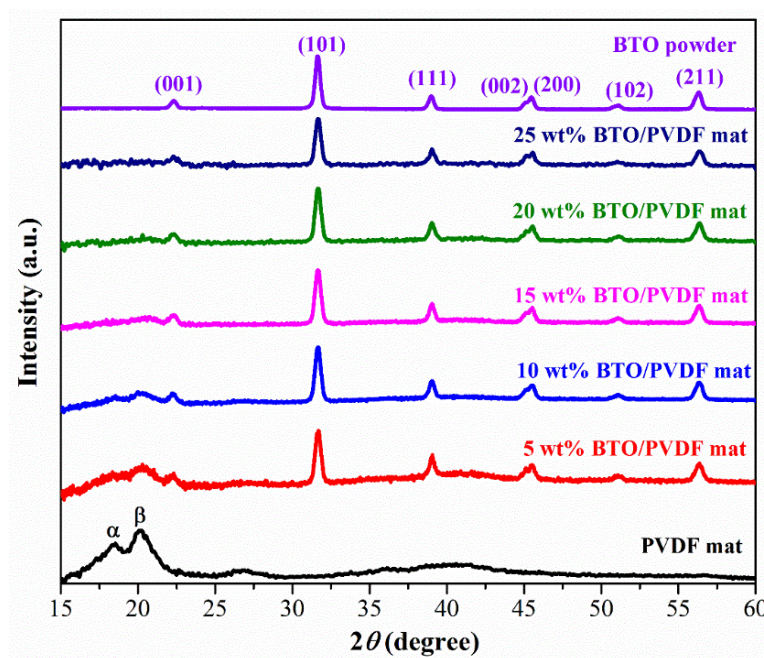


Figure 5.15: The XRD patterns of the PVDF mats featuring different BTO concentrations

For the nanocomposites, when the BTO concentration is lower than 15%, we can observe a weak peak at  $20.4^\circ$  (characteristic of the  $\beta$  phase in PVDF). However, when the BTO concentration is higher than 15%, the two peaks that are characteristic to scattering in amorphous PVDF (see the left hand side of the bottom panel in Supplementary Fig. 5.15) cannot be clearly observed, which is ascribed to the shielding effect due to high intensity diffraction peaks in BTO nanocrystals.



### Supplementary Note 2. Effective electric circuit of the planar piezoelectric generator

Analysis of the effective electric circuit presented in Fig. 5.4b, lead to the following differential equations that govern time dynamics of the individual capacitor discharges:

$$\begin{aligned} \frac{q_3}{C/4} + \frac{R_e}{2} \cdot \dot{q}_3 + \frac{R_e}{2} \cdot (\dot{q}_2 + \dot{q}_3) + R_L(\dot{q}_1 + \dot{q}_2 + \dot{q}_3) &= 0 \\ \frac{R_e}{2}(\dot{q}_1 + \dot{q}_2) + \frac{R_e}{2}\dot{q}_1 + \frac{q_1}{C/4} + R_L(\dot{q}_1 + \dot{q}_2 + \dot{q}_3) &= 0 \\ \frac{R_e}{2}(\dot{q}_1 + \dot{q}_2) + \frac{q_2}{C/2} + \frac{R_e}{2} \cdot (\dot{q}_2 + \dot{q}_3) + R_L(\dot{q}_1 + \dot{q}_2 + \dot{q}_3) &= 0 \end{aligned} \quad (1)$$

Solution of which has to also satisfy the initial conditions:

$$(q_1, q_2, q_3)_{t=0} = (-\Delta Q, 2\Delta Q, -\Delta Q) \quad (2)$$

Assuming solution of the system of linear differential equations (1) in the form  $\bar{q} = \bar{q}_\lambda e^{-\lambda t}$  ( $\lambda$  is a constant), one can find particularly simple solutions that satisfy both (1) and initial conditions (2) in the case of an open circuit  $R_L = \infty$ , and short circuit  $R_L = 0$ , which results in the following expressions for the open circuit voltage  $V^{oc}(t)$  and the short circuit currents  $I^{sc}(t)$ :

$$\begin{aligned} \text{Open-circuit voltage:} \quad V^{oc}(t) &= -\frac{4\Delta Q}{C} e^{-\frac{t}{\tau_0}} \\ V_{max}^{oc} &= V^{oc}(0) = -\frac{4\Delta Q}{C} \\ \Delta t^{oc} &\sim 2\tau_0 \\ \text{Short-circuit current:} \quad I^{sc}(t) &= \frac{\Delta Q}{\tau_0} (1.1707 e^{-\frac{1.3090}{\tau_0} t} - 0.1707 e^{-\frac{0.1910}{\tau_0} t}) \\ I_{max}^{sc} &= I^{sc}(0) = \frac{\Delta Q}{\tau_0} \\ \Delta t^{sc} &\sim 1.5279\tau_0 \end{aligned} \quad (3)$$

where the time constant is defined as:

$$\tau_0 = \frac{R_e C}{8} = \frac{\rho \epsilon_p \epsilon_0}{8} \frac{l^2}{d_p d_e} \quad (4)$$

From Eq. (3) one can then calculate the effective generator resistance  $V_{max}^{oc}/I_{max}^{sc} = \frac{R_e}{2}$ .



### Supplementary Note 3. Mechanical analysis of the laminated generators under bending

Here we discuss in more details evaluation of strain  $\varepsilon$  in the bent laminated generators. Consider, for example, the second region in Fig. 5.4a of length  $\frac{l}{2}$  and suppose that it has a fixed curvature  $1/r$ . Then, the strain can be calculated using a theoretical model [51]. In that model (see Supplementary Fig. 5.16), the strain neutral plain can be calculated by the Eq. (5):

$$Y_1 d_1 y_1 + Y_2 d_2 y_2 + Y_3 d_3 y_3 + Y_4 d_4 y_4 = 0 \quad (5)$$

Where  $Y$ 's and  $d$ 's are the Young's modulus and the thicknesses of various films in the generator structure, while the distances between the centers of the four layers (Kapton, PVDF mat, Kapton and PS substrate) and the neutral plane are  $y_1, y_2, y_3$  and  $y_4$  (counted from top down). Assuming that the substrate (PS) thickness dominates  $d_4 \gg d_{1,2,3}$ , while Young's modulus of the materials are comparable to each other then  $y_2 \sim d_{PS}/2$ .

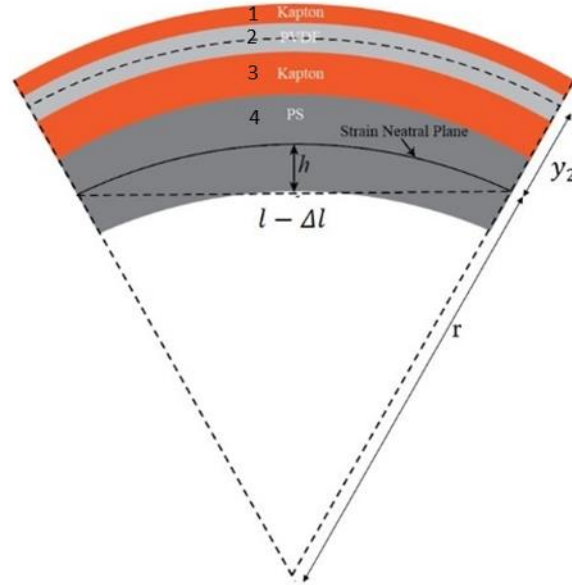


Figure 5.16: Strain calculation in the laminated piezoelectric generators under bending.

Using a model for the buckling of thin beams (see Supplementary Fig. 5.17), according to ref. [187] the beam generator shape and the corresponding curvature (at the point of maximum deflection) for relatively large beam displacements ( $l \gg \Delta l \gg d_{PS}^2/l$ ) are given by:

$$h(x) = \frac{A}{2} \left( 1 + \cos \left( \frac{2\pi x}{l - \Delta l} \right) \right); \quad A \approx \frac{2}{\pi} \sqrt{\Delta l \cdot l}$$



$$\frac{1}{r} = \frac{h''}{(1+(h')^2)^{3/2}} \Big|_{x=\frac{l-\Delta l}{2}} \approx 2\pi^2 \frac{A}{l^2} \approx 4\pi \frac{\sqrt{\Delta l}}{l^{3/2}} \quad (6)$$

While the strain in the PVDF mat can be determined from ref. [51] as:

$$\varepsilon = \frac{y_2}{r} \approx 2\pi \frac{d_{PS}\sqrt{\Delta l}}{l^{3/2}} \quad (7)$$

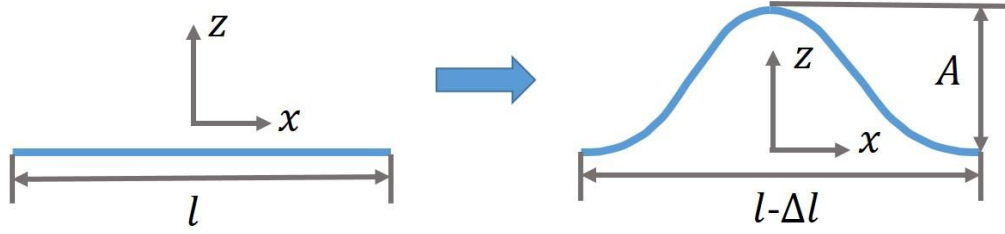


Figure 5.17: Schematic diagram of mechanics model for the planar piezoelectric generators under bending



## **CHAPTER 6      GENERAL DISCUSSION**

In this thesis, the micro- and nanostructured piezoelectric fibers were thermally drawn from a solid structured preform that was heated and deformed in its viscous state. The performance of the as-drawn piezoelectric fibers could be improved by widening the range of materials that are compatible with the thermal drawing process. Thus, in this chapter we first discuss the materials could be used in the drawings of piezoelectric fibers (not limited to the C-LDPE and PVDF-based nanocomposites mentioned before), then we study the effect of electrical poling, and finally we talk about the potential applications of the piezoelectric fiber inside blood vessels.

### **6.1 The material selection in the piezoelectric fibers**

#### **6.1.1 The piezoelectric material selection**

As discussed in Chapter 2, piezoelectric ceramics such as barium titanate ( $\text{BaTiO}_3$ ) and lead zirconate titanate (PZT) have high piezoelectric coefficients. However, these piezoceramics all have melting temperatures above  $1000\text{ }^\circ\text{C}$ , thus making them unsuitable for co-drawing with thermoplastics. On the other hand, piezoelectric polymers such as poly(vinylidene fluoride) (PVDF) have relatively low melting temperatures ( $150\text{ }^\circ\text{C}$  -  $250\text{ }^\circ\text{C}$ ), making them thermally compatible with a variety of thermoplastics. However, compared to the case of the piezoceramics, the piezoelectric coefficients of piezoelectric polymers are relatively low.

To overcome the limitations and obtain fibers with high piezoelectricity, in this thesis we use the PVDF-based nanocomposites by impregnating nanofillers including BTO, PZT and CNT into the PVDF polymer. In the thesis, the nanocomposites were fabricated using electrospinning as this process allows fine-tuning of the thermo-mechanical properties of nanocomposites by changing the polymer molecular weight, the fractions of the nanofillers and the processing conditions. Generally, a higher concentration of the nanofillers would lead to improved piezoelectric properties. However, when the concentration is too high (Fig. 6.1), the nanofillers in the melt will aggregate and form multiple macroscopic domains. While the preform diameter is being reduced, these low-viscosity domains will also experience a significant reduction in the transverse dimension, leading to a capillary break-up and mixing resulting from flow instabilities



as claimed in Ref [66, 67]. Thus, it is necessary to properly choose the concentration of the nanofillers.



Figure 6.1: Photos of the drawn fiber (when the BTO concertation is higher than 30%).

The PVDF-based copolymers can also be used in the fiber drawing process. Particularly, P(VDF-trifluoroethylene) [P(VDF-TrFE)] with VDF content of ~70% has attracted tremendous attention due to its higher piezoelectric constant and degree of crystallinity when compared with those of the PVDF [97]. Because of the steric hindrance by the bulky F atoms, P(VDF-TrFE) spontaneously crystallizes into the ferroelectric  $\beta$  phase from the polymer melt without the must of mechanical stretching [188]. Also, the crystallinity of P(VDF-TrFE) can be nearly 100%, while that of PVDF is typically limited to 50%, thus resulting into higher piezoelectric response. However, the price of P(VDF-TrFE) is extremely higher than that of PVDF. According to the company of PolyK Technologies, the price of P(VDF-TrFE) copolymer resin can be as high as 5000 USD/kg (larger order) and 10 USD/g (smaller order). The price of P(VDF-TrFE) film is even higher, which can be ~100 times higher than that of PVDF film. Thus, due to its low-cost, in this thesis we choose the PVDF as the piezoelectric material.

Apart from electrospinning, piezoelectric nanocomposites could also be fabricated using film-casting [189-193] or melt-extrusion [194-196]. When the functional repeating units of host polymers are highly compatible with the nanofillers, nanofiller-polymer composites can be obtained by film-casting. In film-casting process, polymers and the desired amount of nanofillers are firstly dissolved into organic solvents, and then the solution is poured into a substrate. Finally, the film is obtained after solvent evaporation. When the host polymer is totally non-polar and non-interacting with the nanofillers, phase-separation may be induced during film-casting process. In this case, nanofiller-polymer blends can be realized by means of melt-extrusion where the nanofiller dispersion is achieved by mechanical mixing. During the process, the phase morphology



is a result of the shearing forces overcoming the interfacial tension. When the process is stopped, the high viscosity of polymer matrix may prevent the nanofillers from aggregation.

To conclude, a variety of piezoelectric materials including piezoelectric ceramics and polymers can be adopted in the fiber drawing process. And a range of techniques including electrospinning, melt-extrusion and film-casting could be used to fabricate the piezoelectric nanocomposites. To enable a successful drawing, particular attention should be paid to the concentration of the nanofillers.

### **6.1.2 The conductive material selection**

There are two types of conductive polymers: intrinsically conductive polymers (ICPs) and conductive filled thermoplastics. ICPs are not thermoformable, and thus, unsuitable for use in fiber drawings. Conductive filled polymers can be re-melted or re-drawn while preserving their electrical conductivities. This key characteristic makes conductive filled thermoplastics promising candidates for thermal drawings.

One of the simplest methods used to fabricate conductive filled thermoplastics is to blend conductive fillers such as metal powders [197], carbon black [198], carbon nanofibers [199], or carbon nanotubes (CNT) [200] into melts of traditional thermoplastic polymers like nylon, polyethylene, polyamide, and polyester. In this thesis, we used carbon-loaded polyethylene (C-LDPE) as the electrode material. The C-LDPE films were purchased from Bystat International Inc. and had a volume resistivity of  $2.2 \Omega \cdot \text{m}$ . Other composites could also be explored for the viscous electrode material, for example, CNT or metallic particles loaded-polymer composites, which have higher conductivities than carbon-loaded polymers. In particular, the electrical percolation threshold of CNT-polymer composites can be as low as 0.0025 wt% [201]. Moreover, CNT would enhance the mechanical properties of polymer composites which is important for fiber fabrication.

The fiber drawing process can significantly change the bulk resistivity of the conductive composites (e.g. C-LDPE) due to re-distribution of the conductive fillers in the polymer matrix. In extreme cases, the conductive composite can even lose its electrical conductivity after drawing. Therefore, the drawing parameters should be carefully chosen. In our experiments, we observed that drawing at very low speeds (e.g.  $\sim 500 \text{ mm/min}$ ) results in conductive films of almost the same



conductivity as the original ones used in the preform. In this case, the conductive fillers have enough time to rearrange themselves in the polymer matrix to result in conductive films.

## **6.2 The relationship between fiber performance and structural parameters**

In Chapter 5, we proposed an electro-mechanical model for the planar generator, confirmed our predictions with experiments, and gave an estimated value of the piezoelectric coefficient. In that model, we also showed the relationships between the generated voltages and currents with the applied stage displacements, piezoelectric mat width, and thickness. Initially, one would think the behavior of the piezoelectric fibers would be similar to that of the planar generator described in Chapter 5, with the generated current being the most affected by the number of turns (more turns = more current). However, unlike the planar generator where we can simply cut the generator to smaller widths while keeping its length fixed, experimental verification of the effect that the number of turns (of a piezoelectric layer) has on fiber performance is problematic, and this is due to several technological complications.

Firstly, fibers with different number of turns have to be fabricated separately from different preforms. As a result, due to somewhat different final geometries, variable processing conditions and the lack of high degree of the process control during drawing and poling, the resultant fibers will exhibit not only different number of turns but also somewhat different geometrical and electrical parameters such as layer thickness and conductive layer resistivity, that will all have a significant impact on the fiber piezoelectric response. In fact, we have tried several drawings of fibers with smaller number of turns and clearly saw their inferior piezoelectric performance compared to the fibers with higher number of turns. This finding, however, is difficult to quantify in terms of a simple power law dependence as too many parameters are varied when changing turns between the fibers.

Moreover, we find that extending a simple electro-mechanical model developed in the case of planar generators to the case of a fiber is not trivial. In particular, finding stress distribution in the fiber is a far more complex problem than it is for the planar structures. Just to give you an idea, the hollow-core piezoelectric fiber has a diameter of  $\sim 1$  mm, which is similar to the thickness of the PS substrate (1 mm) to which the fiber is fixed. As piezoelectric layers in the fiber are circular,



they will be subjected to a strong position dependent strain which will be the largest at the fiber surface located the furthest from the PS substrate, while being practically zero at the point of contact with a PS layer.

Therefore, we have concluded that while the general trends in the piezoelectric fiber performance could be indeed inferred from the electro-mechanical model developed for the planar generators, at this point fitting the fiber electrical response to its structural parameters is still challenging due to variation in the material properties and geometries during drawing of the distinct fibers, as well as due to lack of a good electro-mechanical model for the fiber generators.

### 6.3 Electrical poling for the fiber performance

The electrical poling process (during and after drawings) is necessary if we want to improve the performance of the piezoelectric fiber. In this section, I will explain the effects of electrical poling in detail.

PVDF is the host piezoelectric material in the drawn fibers. Generally, PVDF in the polymer melts is in the form of non-polar  $\alpha$  phase, where the dipole moments have a random orientation and result in canceling each other out. Fig. 6.2 shows a typical process used to obtain piezoelectric PVDF films. First, an application of mechanical stress induces a transformation from the non-polar  $\alpha$  phase to the piezoelectric  $\beta$  phase. Second, the stretched PVDF film is poled to obtain macroscopic polarization.

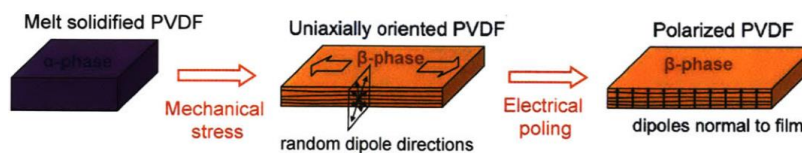


Figure 6.2: Processes commonly employed to obtain piezoelectric PVDF films.

Reprint from Ref [37].

The mechanical extension can be achieved by the fiber draw itself, as the polymer melts experience high stresses during the drawing process. Recent reports [189] have shown that, electrical poling during drawings may further promote phase transformation, as well as align the electric dipoles. Thus, we experimented with the application of high voltages to the preform electrodes during the fiber drawing process. As shown in Fig. 6.3b, the copper wires were glued to



the preform electrodes. After that, the preform was placed into the vertical furnace of the draw tower, and then connected to the high voltage supply using copper wires. During drawing, a voltage of up to 5 kV was applied to the electrodes of the preform.

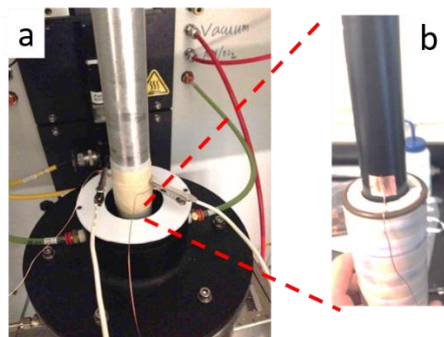


Figure 6.3 : (a), The fiber preform was placed into the furnace of the draw tower. (b), The preform electrode was connected to the copper wire.

However, the electrical measurements demonstrated that the output voltage values of the as-drawn fibers were in the range of the mV scale. This is because the electrical poling time (1-2 h) is insufficient to provide a significant effect. On the other hand, we found that the application of high voltage could effectively control the layer thickness in the drawn fibers, since the two conductive layers in the molten polymer were forced to pull together due to the strong electrical force. Using this technique, piezoelectric fibers with several tens of nm layer thicknesses could be obtained.

In order to further enhance their piezoelectric property, the fibers were poled in a silicone oil bath (80 °C) using a voltage of 1 kV for 12 hours. The poling voltage was then increased to 5 kV for 12 hours and finally 9 kV for 12 hours. We noted that the electrical poling process plays a major role in determining the piezoelectric response of the piezoelectric fibers. The fibers with poling exhibit an open-circuit voltage of  $\sim 1.5$  V, which is three orders of magnitude higher than that of their non-poled counterparts (Chapter 4, Fig. 4.4b, c).

Therefore, we have concluded that electrical poling during fiber drawings could effectively control the layer thicknesses, while poling after drawings could greatly improve the piezoelectric properties of the fiber.



## 6.4 Switching-polarity tests of the piezoelectric generators

To confirm that the output signal was generated by bending the piezoelectric generators, a widely used switching-polarity test [47, 51-53] was also conducted. As shown in Fig. 6.4a, when a measuring instrument was front connected to the planar generator, a positive voltage and current pulse was generated during the periodic bending of the planar generators. In the case of the reverse connection (corresponding to Fig. 6.4b), negative output signals were recorded.

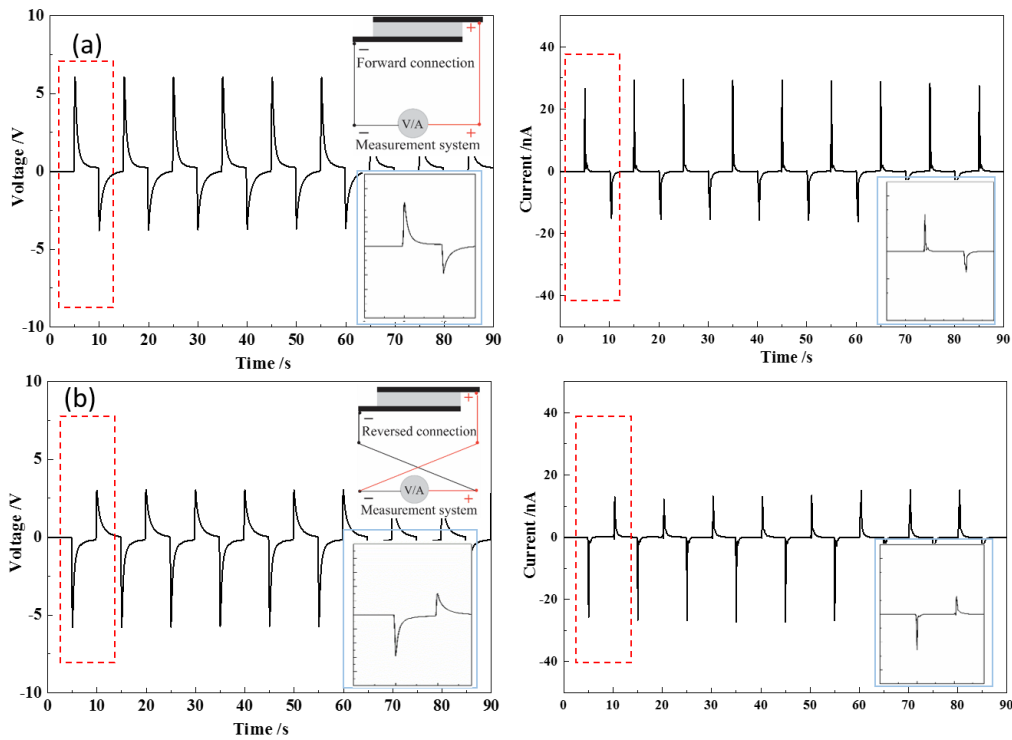


Figure 6.4 : (a), The measured output voltage and current signals of the planar device with 20 wt% BTO/PVDF in the forward connection during the periodic bending and unbending motions. (b), The output voltage and current signals generated in the reverse connection.

Similarly, we also conducted the switching-polarity test on the piezoelectric fiber generator. The results in Fig. 6.5 indicate that the measured outputs are the true signals generated from the bending motions of our piezoelectric fibers.



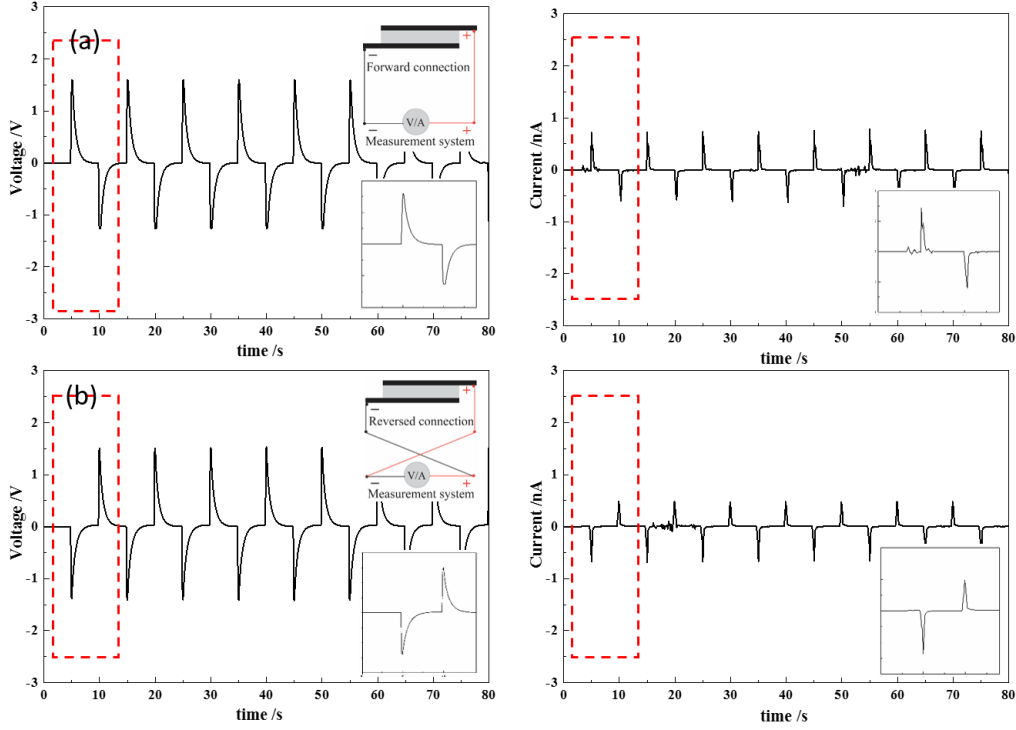


Figure 6.5 : (a), The measured output voltage and current signals of the piezoelectric fiber of 20 wt% BTO/PVDF in the forward connection during the periodic bending and unbending motions. (b), The output voltage and current signals generated in the reverse connection.

## 6.5 The piezoelectric stability of the fibers with respect to temperature

Our piezoelectric fibers are made of the carbon-filled low density polyethene (C-LDPE) and piezoelectric polymer nanocomposites (e.g. BTO-PVDF, PZT-PVDF and CNT-PVDF). The carbon-filled low density polyethene has a soften temperature of  $\sim 110$  °C. Therefore, the work temperature of piezoelectric fibers should be lower than  $\sim 110$  °C.

During the operation of the piezoelectric fibers, we also need to consider the Curie temperature of the piezoelectric materials. When the applied temperature is higher than the Curie temperature, the permanent polarization in the piezoelectric materials will disappear, and thus the piezoelectric fibers will lose the piezoelectric properties. Table 6.1 summarizes the Curie temperature of the piezoelectric materials.



In conclusion, the piezoelectric properties of our fibers will be stable when the temperature is lower than 110°C, which is appropriate for most of the applications in our daily life

Table 6.1. The Curie temperature of the piezoelectric materials

Piezoelectric materials	Curie temperature	Ref
BTO	~130°C	[202]
PZT	~500°C	[203]
PVDF	~195°C	[204]

## 6.6 The potential applications of the piezoelectric fiber inside the blood vessels

The diameter of our piezoelectric fibers are in the range of microscale, which enables their potential applications inside the blood vessels. Firstly, the piezoelectric fibers can be used as the microactuator for the biological cell manipulation. When the electrical field is applied to the electrodes, it will induce a bending displacement of the piezoelectric fiber. And the displacements can be adjusted by changing the applied voltages. This is called as “the converse piezoelectric effect” [205]. Using this effect, Tajitsu *et al.* [206] reported the electrically controlled tweezers made of a pair of piezoelectric fibers. In their publication, they inserted the tweezer into a blood vessel, and then, grasped and removed the thrombosis. Also, the piezoelectric fibers can be used as the ultrasound transducers, for the purpose of *in vivo* intravascular ultrasound imaging. Wang *et al.* [207] demonstrated a piezoelectric transducer, and also performed its imaging for the blood vessels of chicken embryo chorioallantoic membrane. They also claimed that the piezoelectric transducer had the potential to monitor the neovascularization in tumor angiogenesis. In their experiment, the blood vessels with diameters ranged from 0.1 mm to 0.6 mm was imaged, while microvessels were not visible. The resolution and sensitivity of the piezoelectric transducers could be improved by using piezoelectric fiber arrays [66]. Additionally, the piezoelectric fibers can measure the flow rate and accurate pressure inside the blood vessels [66].



## CHAPTER 7 CONCLUSION AND PERSPECTIVES

### 7.1 Summary of accomplishments

In this thesis we have proposed and experimentally demonstrated piezoelectric planar generators, piezoelectric fibers and textiles for sensing and energy generation applications including the real-time monitoring of human movements, micro-power-generation in automotive industries and stand-off sound detecting. We have also present several examples of the practical applications of the proposed piezoelectric fibers and textiles: for distributed stand-off sound detector using CNT-PVDF fibers, and for energy harvesting using textile-based piezoelectric generators that incorporate BTO-PVDF fibers and PZT-PVDF fibers.

Firstly, we have demonstrated the fabrication and applications of the piezoelectric planar generators, which were assembled first in order to study energy harvesting properties of the piezoelectric electrospun nanocomposites. We have studied the charge separation mechanism and effective electric model of the piezoelectric planar generators in the bent state. From both theoretical analysis and experimental verification, we concluded that the voltages and currents generated from the piezoelectric planar generators are indeed proportional to the thickness of the piezoelectric electrospun mat, and also depend in a non-linear manner with the generator bending displacements. From the cyclic bend-release measurements, we have found that such planar generators can generate open-circuit voltages of up to 8 V and short-circuit voltage of up to 40 nA with an active area of several tens of  $\text{cm}^2$ . Finally, we have demonstrated that the piezoelectric planar generators have excellent durability as their output voltages and currents did not change after three days' continuous bend-release measurements.

Then, we have fabricated all-polymer piezoelectric micro- and nanostructured fibers using fiber drawing technique. The as-fabricated fibers feature a hollow PC core surrounded by a multilayer cladding consisting of the alternating piezoelectric and conductive polymer layers. We have also performed comparative study of three material combinations. A BTO/PVDF microstructured fiber (10 cm long; BTO concentration: 20 wt%) could generate an open-circuit voltage of 1.4 V and a short-circuit current of 0.8 nA, when the moving end of the generator was displaced transversely by 10 mm. The corresponding voltage and current were  $\sim 6$  V and  $\sim 4$  nA for a PZT-PVDF (20 wt% PZT) fiber generator, and  $\sim 3$  V and  $\sim 1.2$  nA for a CNT-PVDF (0.4 wt%



CNT) fiber generator. Perovskite ceramics (such as BTO and PZT) could improve the fiber performance owing to their high piezoelectric coefficient. On the other hand, CNT could induce the crystallization of polar phase in PVDF layers, thus leading to remarkable improvements in piezoelectric performance. Also we note in passing that the CNT/PVDF microstructured fibers are easier to draw to smaller diameters and they appear to have better mechanical flexibility. The resultant fibers exhibit excellent durability with high piezoelectric voltages (of up to 6 V) in a cyclic bend-release test (greater than 26000 cycles).

Finally, we have fabricated the piezoelectric textiles by integrating the piezoelectric fibers into the cotton textiles using a traditional loom. Then, we demonstrated the potential applications of the piezoelectric fibers and textiles for powering personal electronics and wearable sensing in the smart garments, automotive and aerospace industries.

## 7.2 Future work

Here I will discuss the areas of research that should be further explored, based on the results presented in this thesis. One interesting direction could take is to further investigate the use of composite materials. The properties of the piezoelectric fibers described in the thesis could be improved by widening the range of materials that are compatible with the thermal drawing process. Here, the piezoelectric fibers used carbon-loaded polyethylene (C-LDPE) as the electrodes. However, because of the high resistivities of the fiber electrodes, the output currents of the as-fabricated piezoelectric fibers were in the range of nA. To increase the output currents, it would be necessary to explore other conductive composites with higher conductivities, for example composites combining a polymer matrix with metallic particles, or CNT. Moreover, other piezoelectric nanocomposites should be explored to increase the generated voltages of the fibers. For instance, piezoceramics with higher piezoelectric coefficients could be embedded into the polymer matrices using a range of fabrication techniques such as electrospinning, melt-extrusion, and film-casting.

Another interesting direction is to study the “converse piezoelectric effect” [37] in the piezoelectric fibers. When an electric field is applied to the fiber electrodes, the fibers experience a deformation. Such fibers may pave the way for the realization of fiber electromechanical systems (FEMS) [206-208]. Potential applications include micro-positioning actuator for single-cell



manipulation [209, 210], scanning tunneling microscopes (STM), atomic force microscopes (AFM), and laser mirror alignment; electrically controllable microfluidic pumps [28], and many more.

The use of piezoelectric nanocomposites in fibers also presents us with new opportunities to answer questions grounded in fundamental science. In particular, it would be beneficial to study the crystalline phase and the molecular structure of the nanocomposites during and after drawing. Also, a much deeper understanding of the polarization uniformity and depolarization in piezoelectric fibers needs to be established. X-ray diffraction (XRD) can be used for the phase identification of the materials and can provide information on unit cell dimensions; Piezoresponse force microscopy (PFM) [211] allows imaging and switching of ferroelectric domains on a sub-micrometer scale. However, at this moment, it is still challenging to accomplish these goals as the typical fiber is a small diameter object where multiple materials are fused together and it is difficult to separate the conductive layers from the piezoelectric layers and a passive core.

Finally, interesting applications can also be imagined by taking advantage of the unique characteristics of the piezoelectric fibers. Owing to the thermal fiber drawing process, the dimensions of piezoelectric fibers can be as small as hundreds of microns, which could enable accurate pressure and flow measurements in very small tubes (e.g. blood vessels); the length of piezoelectric fibers can be as long as hundreds of meters, which makes them ideal for harvesting electricity from ocean waves or ocean tides, as well as studying the large-area distribution of pressure and velocity in the oceanic current.

### **7.3 Conclusion**

In this thesis, we demonstrated the fabrication of piezoelectric planar generators using electrospun piezoelectric nanocomposites as the active materials. Then, we studied the fabrication and applications of piezoelectric fibers and textiles. Our multimaterial preform-to-fiber process enables the rapid fabrication of kilometer-long piezoelectric fiber with precise dimensional tolerances and cost-effectiveness. The piezoelectric fiber generators were characterized using electrical, optical, and acoustic techniques. The potential applications of the proposed piezoelectric fibers and textiles include micro-power-generation and remote sensing in the wearable, military, automotive and aerospace industries.



Compared with the piezoelectric planar generators, the piezoelectric fibers and textiles have the more advantages such as higher output power, better flexibility, three-dimensionally deformable, lightweight and comfortable. The all-polymer fibers have the ability to retain their structural integrity towards a number of washing and wear cycles. The properties of the piezoelectric fibers can be stable when the temperature is lower than 110 °C, which is appropriate for most of the applications in our daily life. Thus, the commercialization of the piezoelectric fibers and textiles could be imagined in the near future. However, it is still necessary to conduct systematic fundamental studies on the hierarchy structures and electronic properties of the fibers and textiles [208]. Based on much improved fundamental understandings, the powerful design tools will be established to guide the selection and design of the fiber and textile architectures for the wearable energy generators and systems. Also, it is essential to study the packaging and connection of the electronic fibers together with other textiles and electronic devices. To meet the requirements of the practical applications, these connections and packages has to be soft and flexible, as well as stand the long-time deformation and friction [209]. Additionally, it is important to study the strength and failure modes of the fibers in order to improve the durability of the fibers. Finally, we believe the studies on the flexible piezoelectric fibers and textiles will pave the way of future generation of self-powered wearable systems and smart personalized health-monitoring clothing systems.



## BIBLIOGRAPHY

- [1] Q. Bao and K. P. Loh, "Graphene Photonics, Plasmonics, and Broadband Optoelectronic Devices," *Acs Nano*, vol. 6, pp. 3677-3694, May 2012.
- [2] D. Astruc, E. Boisselier, and C. Ornelas, "Dendrimers Designed for Functions: From Physical, Photophysical, and Supramolecular Properties to Applications in Sensing, Catalysis, Molecular Electronics, Photonics, and Nanomedicine," *Chemical Reviews*, vol. 110, pp. 1857-1959, Apr 2010.
- [3] H. Gharavi, "Smart Grid (Wireless Communications): IEEE Wireless Communications," *IEEE wireless communications*, vol. 24, pp. 2-3, Apr 2017.
- [4] I. F. Akyildiz, J. M. Jornet, and C. Han, "TeraNets: ultra-broadband communication networks in the terahertz band," *IEEE Wireless Communications*, vol. 21, pp. 130-135, 2014.
- [5] P. Hatto and S. MacLachlan, "Standardising nanotechnologies," *Materials World*, vol. 18, pp. 15, Dec 2010.
- [6] B. Halford, "Nanotechnology," *Chemical & Engineering News*, vol. 87, pp. 8-8, May 2009.
- [7] N. Miki, G. S. Prihandana, H. Ito, R. Jun, Y. Nishinaka, and Ieee, "Innovative biomedical devices enabled by micro/nano fabrication technologies," in *6th IEEE International Conference on Nano/Molecular Medicine and Engineering*, ed, 2012.
- [8] T. Qian and Y. Wang, "Micro/nano-fabrication technologies for cell biology," *Medical & Biological Engineering & Computing*, vol. 48, pp. 1023-1032, Oct 2010.
- [9] A. Lasagni, A. Manzoni, and F. Muecklich, "Micro/nano fabrication of periodic hierarchical structures by multi-pulsed laser interference structuring," *Advanced Engineering Materials*, vol. 9, pp. 872-875, Oct 2007.
- [10] S. Kawata, H.-B. Sun, and S. Nakanishi, "Recent advances in two-photon photopolymeric micro-nano fabrication," *Abstracts of Papers of the American Chemical Society*, vol. 231, Mar 2006.
- [11] X. Tao, "1 - Introduction," in *Wearable Electronics and Photonics*, ed: Woodhead Publishing, 2005, pp. 1-12.
- [12] G. Tieri, G. Morone, S. Paolucci, and M. Iosa, "Virtual reality in cognitive and motor rehabilitation: facts, fiction and fallacies," *Expert Review of Medical Devices*, vol. 15, pp. 107-117, 2018.
- [13] J. Ahn, Y. Y. Kim, and R. Y. Kim, "Virtual Reality-Wireless Local Area Network: Wireless Connection-Oriented Virtual Reality Architecture for Next-Generation Virtual Reality Devices," *Applied Sciences-Basel*, vol. 8, Jan 2018.
- [14] B. H. Kim, Y. J. An, G. H. Yun, and J. G. Yook, "RF interferometric wearable wrist pulse detection system," *Iet Microwaves Antennas & Propagation*, vol. 12, pp. 167-172, Feb 2018.



- [15] T. Nguyen Gia, V. K. Sarker, I. Tcareno, A. M. Rahmani, T. Westerlund, P. Liljeberg, *et al.*, "Energy efficient wearable sensor node for IoT-based fall detection systems," *Microprocessors and Microsystems*, vol. 56, pp. 34-46, 2018.
- [16] M. Amjadi, S. Sheykhansari, B. J. Nelson, and M. Sitti, "Recent Advances in Wearable Transdermal Delivery Systems," *Advanced Materials*, vol. 30, Feb 2018.
- [17] R. Zhang and O. Amft, "Monitoring Chewing and Eating in Free-Living Using Smart Eyeglasses," *Ieee Journal of Biomedical and Health Informatics*, vol. 22, pp. 23-32, Jan 2018.
- [18] M. S. Mahmud, H. G. Wang, A. M. Esfar-E-Alam, and H. Fang, "A Wireless Health Monitoring System Using Mobile Phone Accessories," *IEEE Internet of Things Journal*, vol. 4, pp. 2009-2018, Dec 2017.
- [19] W. C. Huang, X. Y. Li, Y. Xiong, P. L. Yang, Y. Q. Hu, X. F. Mao, *et al.*, "Stride-in-the-Loop Relative Positioning Between Users and Dummy Acoustic Speakers," *Ieee Journal on Selected Areas in Communications*, vol. 35, pp. 1104-1117, May 2017.
- [20] Y. Zhang, Y. Zhao, J. Ren, W. Weng, and H. Peng, "Advances in Wearable Fiber-Shaped Lithium-Ion Batteries," *Advanced Materials*, vol. 28, pp. 4524-4531, 2016.
- [21] T. Yuan, Z. Tan, C. Ma, J. Yang, Z.-F. Ma, and S. Zheng, "Challenges of Spinel  $\text{Li}_4\text{Ti}_5\text{O}_{12}$  for Lithium-Ion Battery Industrial Applications," *Advanced Energy Materials*, vol. 7, p. 1601625, 2017.
- [22] H. Wang, A. Jasim, and X. D. Chen, "Energy harvesting technologies in roadway and bridge for different applications - A comprehensive review," *Applied Energy*, vol. 212, pp. 1083-1094, Feb 2018.
- [23] Y. Xin, X. Li, H. Tian, C. Guo, C. Qian, S. Wang, *et al.*, "Shoes-equipped piezoelectric transducer for energy harvesting: A brief review," *Ferroelectrics*, vol. 493, pp. 12-24, 2016.
- [24] Y.-M. Choi, M. Lee, and Y. Jeon, "Wearable Biomechanical Energy Harvesting Technologies," *Energies*, vol. 10, p. 1483, 2017.
- [25] M. F. Daqaq, R. Masana, A. Erturk, and D. D. Quinn, "On the Role of Nonlinearities in Vibratory Energy Harvesting: A Critical Review and Discussion," *Applied Mechanics Reviews*, vol. 66, Jul 2014.
- [26] Y. Yang, L. Tang, and H. Li, "Vibration energy harvesting using macro-fiber composites," *Smart Materials & Structures*, vol. 18, Nov 2009.
- [27] X. B. Shan, J. Deng, R. J. Song, and T. Xie, "A Piezoelectric Energy Harvester with Bending-Torsion Vibration in Low-Speed Water," *Applied Sciences-Basel*, vol. 7, Feb 2017.
- [28] N. Gallah, N. Habbachi, and K. Besbes, "Design and modelling of droplet based microfluidic system enabled by electroosmotic micropump," *Microsystem Technologies-Micro-and Nanosystems-Information Storage and Processing Systems*, vol. 23, pp. 5781-5787, Dec 2017.
- [29] L. Chaofeng, W. Shuang, L. Bingwei, Z. Yangyang, D. Yangkun, and F. Xue, "Ultrathin flexible piezoelectric sensors for monitoring eye fatigue," *Journal of Micromechanics and Microengineering*, vol. 28, p. 025010, 2018.



- [30] B. Wang, C. Liu, Y. J. Xiao, J. W. Zhong, W. B. Li, Y. L. Cheng, *et al.*, "Ultrasensitive cellular fluorocarbon piezoelectret pressure sensor for self-powered human physiological monitoring," *Nano Energy*, vol. 32, pp. 42-49, Feb 2017.
- [31] M. A. P. Mahmud, N. Huda, S. H. Farjana, M. Asadnia, and C. Lang, "Recent Advances in Nanogenerator-Driven Self-Powered Implantable Biomedical Devices," *Advanced Energy Materials*, vol. 8, Jan 2018.
- [32] W. F. Liu and X. B. Ren, "Large Piezoelectric Effect in Pb-Free Ceramics," *Physical Review Letters*, vol. 103, Dec 2009.
- [33] H. X. Fu and R. E. Cohen, "Polarization rotation mechanism for ultrahigh electromechanical response in single-crystal piezoelectrics," *Nature*, vol. 403, pp. 281-283, Jan 2000.
- [34] D. Damjanovic, "Ferroelectric, dielectric and piezoelectric properties of ferroelectric thin films and ceramics," *Reports on Progress in Physics*, vol. 61, pp. 1267-1324, Sep 1998.
- [35] C. Tzong-Jih, C. Hsein-Chang, and L. Tsun-Mei, "A piezoelectric quartz crystal sensor for the determination of coagulation time in plasma and whole blood," *Biosensors and Bioelectronics*, vol. 13, pp. 147-156, 1998.
- [36] T. Nomura and F. Tanaka, "Crystal mass sensor using frequency difference between two piezoelectric quartz crystals," *Bunseki kagaku*, vol. 38, pp. 343-346, 1989.
- [37] A. J. Lovinger, "Ferroelectric Polymers," *Science*, vol. 220, pp. 1115-1121, 1983.
- [38] M. Acosta, N. Novak, V. Rojas, S. Patel, R. Vaish, J. Koruza, *et al.*, "BaTiO<sub>3</sub>-based piezoelectrics: Fundamentals, current status, and perspectives," *Applied Physics Reviews*, vol. 4, Dec 2017.
- [39] N. W. Hagood and A. von Flotow, "Damping of structural vibrations with piezoelectric materials and passive electrical networks," *Journal of Sound and Vibration*, vol. 146, pp. 243-268, 1991.
- [40] F. R. Fan, W. Tang, and Z. L. Wang, "Flexible Nanogenerators for Energy Harvesting and Self-Powered Electronics," *Advanced Materials*, vol. 28, pp. 4283-4305, Jun 2016.
- [41] S. Xu, B. J. Hansen, and Z. L. Wang, "Piezoelectric-nanowire-enabled power source for driving wireless microelectronics," *Nature Communications*, vol. 1, Oct 2010.
- [42] M. C. Tellers, J. S. Pulskamp, S. S. Bedair, R. Q. Rudy, I. M. Kierzewski, R. G. Polcawich, *et al.*, "Characterization of a piezoelectric MEMS actuator surface toward motion-enabled reconfigurable RF circuits," *Journal of Micromechanics and Microengineering*, vol. 28, p. 035001, 2018.
- [43] Y. Fujimura, T. Tsukamoto, and S. Tanaka, "Piezoelectric Moonie-type Resonant Microactuator," *Electronics and Communications in Japan*, vol. 101, pp. 3-10, Mar 2018.
- [44] S. Tadigadapa, "Piezoelectric microelectromechanical systems — challenges and opportunities," *Procedia Engineering*, vol. 5, pp. 468-471, 2010.
- [45] Y. K. Fuh, S. C. Li, C. Y. Chen, and C. Y. Tsai, "A fully packaged self-powered sensor based on near-field electrospun arrays of poly(vinylidene fluoride) nano/micro fibers," *Express Polymer Letters*, vol. 12, pp. 136-145, Feb 2018.



- [46] X. Chen, Y. Song, Z. Su, H. Chen, X. Cheng, J. Zhang, *et al.*, "Flexible fiber-based hybrid nanogenerator for biomechanical energy harvesting and physiological monitoring," *Nano Energy*, vol. 38, pp. 43-50, Aug 2017.
- [47] M. H. Malakooti, B. A. Patterson, H.-S. Hwang, and H. A. Sodano, "ZnO nanowire interfaces for high strength multifunctional composites with embedded energy harvesting," *Energy & Environmental Science*, vol. 9, pp. 634-643, 2016.
- [48] F. Yiin-Kuen, H. Hsi-Chun, W. Bo-Sheng, and L. Shan-Chien, "All-fiber transparent piezoelectric harvester with a cooperatively enhanced structure," *Nanotechnology*, vol. 27, p. 435403, 2016.
- [49] S. Anand, N. Soin, T. H. Shah, and E. Siores, "Energy harvesting "3-D knitted spacer" based piezoelectric textiles," *IOP Conference Series: Materials Science and Engineering*, vol. 141, p. 012001, 2016.
- [50] C. Pan, Z. Li, W. Guo, J. Zhu, and Z. L. Wang, "Fiber-Based Hybrid Nanogenerators for/as Self-Powered Systems in Biological Liquid," *Angewandte Chemie-International Edition*, vol. 50, pp. 11192-11196, 2011.
- [51] M. Lee, C.-Y. Chen, S. Wang, S. N. Cha, Y. J. Park, J. M. Kim, *et al.*, "A Hybrid Piezoelectric Structure for Wearable Nanogenerators," *Advanced Materials*, vol. 24, pp. 1759-1764, Apr 2012.
- [52] Y. Qin, X. Wang, and Z. L. Wang, "Microfibre-nanowire hybrid structure for energy scavenging," *Nature*, vol. 451, pp. 809-U5, Feb 2008.
- [53] C. K. Jeong, J. Lee, S. Han, J. Ryu, G. T. Hwang, D. Y. Park, *et al.*, "A Hyper-Stretchable Elastic-Composite Energy Harvester," *Advanced Materials*, vol. 27, pp. 2866, May 2015.
- [54] H. Jiang, M. E. Kiziroglou, D. C. Yates, and E. M. Yeatman, "A Motion-Powered Piezoelectric Pulse Generator for Wireless Sensing via FM Transmission," *IEEE Internet of Things Journal*, vol. 2, pp. 5-13, Feb 2015.
- [55] Q. Zheng, B. J. Shi, Z. Li, and Z. L. Wang, "Recent Progress on Piezoelectric and Triboelectric Energy Harvesters in Biomedical Systems," *Advanced Science*, vol. 4, Jul 2017.
- [56] U. Aridogan, I. Basdogan, and A. Erturk, "Analytical modeling and experimental validation of a structurally integrated piezoelectric energy harvester on a thin plate," *Smart Materials and Structures*, vol. 23, p. 045039, 2014.
- [57] Z. L. Wang, "Towards Self-Powered Nanosystems: From Nanogenerators to Nanopiezotronics," *Advanced Functional Materials*, vol. 18, pp. 3553-3567, Nov 24 2008.
- [58] L. Persano, C. Dagdeviren, Y. Su, Y. Zhang, S. Girardo, D. Pisignano, *et al.*, "High performance piezoelectric devices based on aligned arrays of nanofibers of poly(vinylidene fluoride-co-trifluoroethylene)," *Nature Communications*, vol. 4, Mar 2013.
- [59] Z. Hasan, H. Hammoudeh, G. Atmeh, and Asme, *DESIGN AND ANALYSIS OF A SMART COMPOSITE WING*, 2012.
- [60] S. R. Anton and D. J. Inman, "Performance modeling of unmanned aerial vehicles with on-board energy harvesting," in *Active and Passive Smart Structures and Integrated Systems 2011*. vol. 7977, M. N. GhasemiNejhad, Ed., ed, 2011.



- [61] W. Zeng, L. Shu, Q. Li, S. Chen, F. Wang, and X.-M. Tao, "Fiber-Based Wearable Electronics: A Review of Materials, Fabrication, Devices, and Applications," *Advanced Materials*, vol. 26, pp. 5310-5336, 2014.
- [62] R. S. Martins, R. Goncalves, T. Azevedo, J. G. Rocha, J. M. Nobrega, H. Carvalho, *et al.*, "Piezoelectric Coaxial Filaments Produced by Coextrusion of Poly(vinylidene fluoride) and Electrically Conductive Inner and Outer Layers," *Journal of Applied Polymer Science*, vol. 131, Sep 2014.
- [63] A. Lund and B. Hagstrom, "Melt Spinning of beta-Phase Poly(vinylidene fluoride) Yarns With and Without a Conductive Core," *Journal of Applied Polymer Science*, vol. 120, pp. 1080-1089, Apr 2011.
- [64] W. T. Liu, R. Chen, X. D. Ruan, and X. Fu, "Polymeric piezoelectric fiber with metal core produced by electrowetting-aided dry spinning method," *Journal of Applied Polymer Science*, vol. 133, Oct 2016.
- [65] A. Lund, C. Jonasson, C. Johansson, D. Haagenzen, and B. Hagstrom, "Piezoelectric polymeric bicomponent fibers produced by melt spinning," *Journal of Applied Polymer Science*, vol. 126, pp. 490-500, Oct 2012.
- [66] S. Egusa, Z. Wang, N. Chocat, Z. M. Ruff, A. M. Stolyarov, D. Shemuly, *et al.*, "Multimaterial piezoelectric fibres," *Nature Materials*, vol. 9, pp. 643-648, Aug 2010.
- [67] A. F. Abouraddy, M. Bayindir, G. Benoit, S. D. Hart, K. Kuriki, N. Orf, *et al.*, "Towards multimaterial multifunctional fibres that see, hear, sense and communicate," *Nature Materials*, vol. 6, pp. 336-347, May 2007.
- [68] M. Bayindir, F. Sorin, A. F. Abouraddy, J. Viens, S. D. Hart, J. D. Joannopoulos, *et al.*, "Metal-insulator-semiconductor optoelectronic fibres," *Nature*, vol. 431, pp. 826-829, Oct 2004.
- [69] I. Katsouras, K. Asadi, M. Li, T. B. van Driel, K. S. Kjaer, D. Zhao, *et al.*, "The negative piezoelectric effect of the ferroelectric polymer poly(vinylidene fluoride)," *Nat Mater*, vol. 15, pp. 78-84, 2016.
- [70] Y. L. Zhao, Q. L. Liao, G. J. Zhang, Z. Zhang, Q. J. Liang, X. Q. Liao, *et al.*, "High output piezoelectric nanocomposite generators composed of oriented BaTiO<sub>3</sub> NPs@PVDF," *Nano Energy*, vol. 11, pp. 719-727, Jan 2015.
- [71] L. Carballeira, A. J. Pereiras, and M. A. Rios, "CONFORMATIONAL PROPERTIES OF POLY(VINYLLIDENE BROMIDE) AND POLY(VINYLLIDENE FLUORIDE)," *Macromolecules*, vol. 23, pp. 1309-1312, Mar 1990.
- [72] J. Kymissis, C. Kendall, J. Paradiso, and N. Gershenfeld, "Parasitic power harvesting in shoes," in *Digest of Papers. Second International Symposium on Wearable Computers (Cat. No.98EX215)*, 1998, pp. 132-139.
- [73] Y. Ahn, J. Y. Im, Y. Seo, and S. M. Hong, "Enhanced piezoelectric properties of electrospun poly(vinylidene fluoride)/multiwalled carbon nanotube composites," in *Adaptive, Active and Multifunctional Smart Materials Systems*. vol. 77, P. Vincenzini, Y. B. Hahn, S. Iannotta, A. Lendlein, V. Palermo, S. Paul, *et al.*, Eds., ed, 2013, pp. 82-+.



- [74] A. Baji, Y.-W. Mai, Q. Li, and Y. Liu, "Electrospinning induced ferroelectricity in poly(vinylidene fluoride) fibers," *Nanoscale*, vol. 3, pp. 3068-3071, 2011.
- [75] W. Zeng, X.-M. Tao, S. Chen, S. Shang, H. L. W. Chan, and S. H. Choy, "Highly durable all-fiber nanogenerator for mechanical energy harvesting," *Energy & Environmental Science*, vol. 6, pp. 2631-2638, Sep 2013.
- [76] Y. Qi and M. C. McAlpine, "Nanotechnology-enabled flexible and biocompatible energy harvesting," *Energy & Environmental Science*, vol. 3, pp. 1275-1285, Sep 2010.
- [77] C.-T. Pan, C.-K. Yen, S.-Y. Wang, Y.-C. Lai, L. Lin, J. C. Huang, *et al.*, "Near-field electrospinning enhances the energy harvesting of hollow PVDF piezoelectric fibers," *RSC Advances*, vol. 5, pp. 85073-85081, 2015.
- [78] W. Y. Si, H. D. Zhang, Y. J. Liu, A. J. Zhao, Z. G. Zhang, M. G. Gong, *et al.*, "Fabrication and Pressure Sensing Analysis of ZnO/PVDF Composite Microfiber Arrays by Low-voltage Near-field Electrospinning," *Chemical Journal of Chinese Universities-Chinese*, vol. 38, pp. 997-1001, Jun 2017.
- [79] C. T. Pan, K. C. Tsai, S. Y. Wang, C. K. Yen, and Y. L. Lin, "Large-Area Piezoelectric PVDF Fibers Fabricated by Near-Field Electrospinning with Multi-Spinneret Structures," *Micromachines*, vol. 8, Apr 2017.
- [80] N. B. Bu, Y. A. Huang, Y. J. Ding, and Z. P. Yin, "An Energy-Harvesting Device Based on Mechano-Electrospun Aligned Poly(vinylidene fluoride) Fiber Arrays," *Sensors and Materials*, vol. 28, pp. 757-762, 2016.
- [81] Z. H. Liu, C. T. Pan, L. W. Lin, J. C. Huang, and Z. Y. Ou, "Direct-write PVDF nonwoven fiber fabric energy harvesters via the hollow cylindrical near-field electrospinning process," *Smart Materials and Structures*, vol. 23, Feb 2014.
- [82] C. E. Chang, V. H. Tran, J. B. Wang, Y. K. Fuh, and L. W. Lin, "Direct-Write Piezoelectric Polymeric Nanogenerator with High Energy Conversion Efficiency," *Nano Letters*, vol. 10, pp. 726-731, Feb 2010.
- [83] Y.-K. Fuh, J.-C. Ye, P.-C. Chen, H.-C. Ho, and Z.-M. Huang, "Hybrid Energy Harvester Consisting of Piezoelectric Fibers with Largely Enhanced 20 V for Wearable and Muscle-Driven Applications," *Acs Applied Materials & Interfaces*, vol. 7, pp. 16923-16931, Aug 2015.
- [84] Y. K. Fuh and B. S. Wang, "Near field sequentially electrospun three-dimensional piezoelectric fibers arrays for self-powered sensors of human gesture recognition," *Nano Energy*, vol. 30, pp. 677-683, Dec 2016.
- [85] K. Jeong, D. H. Kim, Y. S. Chung, S. K. Hwang, H. Y. Hwang, and S. S. Kim, "Effect of processing parameters of the continuous wet spinning system on the crystal phase of PVDF fibers," *Journal of Applied Polymer Science*, vol. 135, Jan 2018.
- [86] D. Matsouka, S. Vassiliadis, K. Prekas, D. V. Bayramol, N. Soin, and E. Siores, "On the Measurement of the Electrical Power Produced by Melt Spun Piezoelectric Textile Fibres," *Journal of Electronic Materials*, vol. 45, pp. 5112-5126, Oct 2016.



- [87] E. Nilsson, A. Lund, C. Jonasson, C. Johansson, and B. Hagstrom, "Poling and characterization of piezoelectric polymer fibers for use in textile sensors," *Sensors and Actuators a-Physical*, vol. 201, pp. 477-486, Oct 2013.
- [88] A. Lund, C. Gustafsson, H. Bertilsson, and R. W. Rychwalski, "Enhancement of beta phase crystals formation with the use of nanofillers in PVDF films and fibres," *Composites Science and Technology*, vol. 71, pp. 222-229, Jan 2011.
- [89] A. Lund and B. Hagstrom, "Melt Spinning of Poly(vinylidene fluoride) Fibers and the Influence of Spinning Parameters on beta-Phase Crystallinity," *Journal of Applied Polymer Science*, vol. 116, pp. 2685-2693, Jun 2010.
- [90] B. Glauß, W. Steinmann, S. Walter, M. Beckers, G. Seide, T. Gries, *et al.*, "Spinnability and Characteristics of Polyvinylidene Fluoride (PVDF)-based Bicomponent Fibers with a Carbon Nanotube (CNT) Modified Polypropylene Core for Piezoelectric Applications," *Materials*, vol. 6, p. 2642, 2013.
- [91] X. Lu, H. Qu, and M. Skorobogatiy, "Piezoelectric Micro- and Nanostructured Fibers Fabricated from Thermoplastic Nanocomposites Using a Fiber Drawing Technique: Comparative Study and Potential Applications," *ACS Nano*, vol. 11, pp. 2103-2114, 2017.
- [92] V. V. Ginzburg, "Kinetic model of fibre drawing," *Polymer*, vol. 34, pp. 5123-5127, 1993.
- [93] M. Kanik, O. Aktas, H. S. Sen, E. Durgun, and M. Bayindir, "Spontaneous High Piezoelectricity in Poly(vinylidene fluoride) Nanoribbons Produced by Iterative Thermal Size Reduction Technique," *ACS Nano*, vol. 8, pp. 9311-9323, Sep 2014.
- [94] X. Y. Li, X. S. Qian, H. M. Gu, X. Z. Chen, S. G. Lu, M. R. Lin, *et al.*, "Giant electrocaloric effect in ferroelectric poly(vinylidenefluoride-trifluoroethylene) copolymers near a first-order ferroelectric transition," *Applied Physics Letters*, vol. 101, Sep 2012.
- [95] D. S. Zhang, B. Shen, X. Yao, X. G. Chen, W. H. Yi, and L. Y. Zhang, "Abnormal ferroelectric relaxation in electron-irradiated copolymers of vinylidenefluoride and trifluoroethylene," *Ferroelectrics*, vol. 261, pp. 717-722, 2001.
- [96] J. Glatzreichenbach, F. Epple, and K. Dransfeld, "THE FERROELECTRIC SWITCHING TIME IN THIN VDF-TRFE COPOLYMER FILMS," *Ferroelectrics*, vol. 127, pp. 13-18, 1992.
- [97] L. Persano, C. Dagdeviren, C. Maruccio, L. De Lorenzis, and D. Pisignano, "Cooperativity in the Enhanced Piezoelectric Response of Polymer Nanowires," *Advanced Materials*, vol. 26, pp. 7574-7580, Dec 2014.
- [98] H. J. Sim, C. Choi, C. J. Lee, Y. T. Kim, G. M. Spinks, M. D. Lima, *et al.*, "Flexible, Stretchable and Weavable Piezoelectric Fiber," *Advanced Engineering Materials*, vol. 17, pp. 1270-1275, Sep 2015.
- [99] I. Kim and D. Y. Khang, "Facile patterning and transfer printing of ferroelectric P (VDF-TrFE) microstructures by topographic dewetting and Rayleigh-Plateau instability," *Journal of Applied Polymer Science*, vol. 134, Jul 2017.
- [100] S. Bodkhe, C. Noonan, F. P. Gosselin, and D. Therriault, "Coextrusion of Multifunctional Smart Sensors," *Advanced Engineering Materials*, vol. 0, pp. 1800206, 2018.



- [101] M. Zhang, T. Gao, J. Wang, J. Liao, Y. Qiu, H. Xue, *et al.*, "Single BaTiO<sub>3</sub> nanowires-polymer fiber based nanogenerator," *Nano Energy*, vol. 11, pp. 510-517, Jan 2015.
- [102] M. S. Woo, J. H. Ahn, J. H. Eom, W. S. Hwang, J. H. Kim, C. H. Yang, *et al.*, "Study on increasing output current of piezoelectric energy harvester by fabrication of multilayer thick film," *Sensors and Actuators A-Physical*, vol. 269, pp. 524-534, Jan 2018.
- [103] M. T. Todaro, F. Guido, V. Mastronardi, D. Desmaele, G. Epifani, L. Algieri, *et al.*, "Piezoelectric MEMS vibrational energy harvesters: Advances and outlook," *Microelectronic Engineering*, vol. 183, pp. 23-36, Nov 2017.
- [104] H. B. Xu, T. G. Lee, S. J. Park, B. Y. Kim, and S. Nahm, "Sodium-potassium niobate nanorods with various crystal structures and their application to nanogenerator," *Journal of the American Ceramic Society*, vol. 100, pp. 1673-1681, Apr 2017.
- [105] C. K. Jeong, K. I. Park, J. Ryu, G. T. Hwang, and K. J. Lee, "Large-Area and Flexible Lead-Free Nanocomposite Generator Using Alkaline Niobate Particles and Metal Nanorod Filler," *Advanced Functional Materials*, vol. 24, pp. 2620-2629, May 2014.
- [106] Y. K. Jin, S. Sarker, K. S. Lee, H. W. Seo, D. M. Kim, and Ieee, *PIEZOELECTRIC MATERIALS FOR HIGH PERFORMANCE ENERGY HARVESTING DEVICES*, 2016.
- [107] P. Rajagopalan, V. Singh, and I. A. Palani, "Enhancement of ZnO-based flexible nano generators via a sol-gel technique for sensing and energy harvesting applications," *Nanotechnology*, vol. 29, Mar 2018.
- [108] E. S. Nour, O. Nur, and M. Willander, "Zinc oxide piezoelectric nano-generators for low frequency applications," *Semiconductor Science and Technology*, vol. 32, Jun 2017.
- [109] A. Sultana, M. M. Alam, S. Garain, T. K. Sinha, T. R. Middya, and D. Mandal, "An Effective Electrical Throughput from PANI Supplement ZnS Nanorods and PDMS-Based Flexible Piezoelectric Nanogenerator for Power up Portable Electronic Devices: An Alternative of MWCNT Filler," *Acs Applied Materials & Interfaces*, vol. 7, pp. 19091-19097, Sep 2015.
- [110] M. A. Johar, J. H. Kang, J. S. Ha, J. K. Lee, and S. W. Ryu, "Controlled conductivity of p-type Cu<sub>x</sub>O/GaN piezoelectric generator to harvest very high piezoelectric potential," *Journal of Alloys and Compounds*, vol. 726, pp. 765-771, Dec 2017.
- [111] D. K. Jeong, J. H. Kang, J. S. Ha, and S. W. Ryu, "Enhanced piezoelectric operation of NiO/GaN heterojunction generator by suppressed internal carrier screening," *Journal of Physics D-Applied Physics*, vol. 50, Oct 2017.
- [112] M. Moret, S. Ruffenach, O. Briot, B. Gil, and M. Pauthe, "The epitaxial growth of indium nitride using berlinite (AlPO<sub>4</sub>) and other piezoelectric crystals of the quartz family as substrates," *Applied Physics Letters*, vol. 95, Jul 2009.
- [113] L. Gu, N. Cui, L. Cheng, Q. Xu, S. Bai, M. Yuan, *et al.*, "Flexible Fiber Nanogenerator with 209 V Output Voltage Directly Powers a Light-Emitting Diode," *Nano Letters*, vol. 13, pp. 91-94, Jan 2013.
- [114] G. Zhang, Q. Liao, Z. Zhang, Q. Liang, Y. Zhao, X. Zheng, *et al.*, "Novel Piezoelectric Paper-Based Flexible Nanogenerators Composed of BaTiO<sub>3</sub> Nanoparticles and Bacterial Cellulose," *Advanced Science*, vol. 3, Feb 2016.



- [115] C. Bowland, Z. Zhou, and H. A. Sodano, "Multifunctional Barium Titanate Coated Carbon Fibers," *Advanced Functional Materials*, vol. 24, pp. 6303-6308, Oct 2014.
- [116] S. Bai, L. Zhang, Q. Xu, Y. Zheng, Y. Qin, and Z. L. Wang, "Two dimensional woven nanogenerator," *Nano Energy*, vol. 2, pp. 749-753, Sep 2013.
- [117] Y. Su and G. J. Weng, "A self-consistent polycrystal model for the spontaneous polarization of ferroelectric ceramics," *Proceedings of the Royal Society A: Mathematical, Physical and Engineering Science*, vol. 462, pp. 1763-1789, 2006.
- [118] S. H. Shin, Y. H. Kim, M. H. Lee, J. Y. Jung, and J. Nah, "Hemispherically Aggregated BaTiO<sub>3</sub> Nanoparticle Composite Thin Film for High-Performance Flexible Piezoelectric Nanogenerator," *Acs Nano*, vol. 8, pp. 2766-2773, Mar 2014.
- [119] T. Gao, J. J. Liao, J. S. Wang, Y. Q. Qiu, Q. Yang, M. Zhang, *et al.*, "Highly oriented BaTiO<sub>3</sub> film self-assembled using an interfacial strategy and its application as a flexible piezoelectric generator for wind energy harvesting," *Journal of Materials Chemistry A*, vol. 3, pp. 9965-9971, 2015.
- [120] K. I. Park, M. Lee, Y. Liu, S. Moon, G. T. Hwang, G. Zhu, *et al.*, "Flexible Nanocomposite Generator Made of BaTiO<sub>3</sub> Nanoparticles and Graphitic Carbons," *Advanced Materials*, vol. 24, pp. 2999-3004, Jun 2012.
- [121] X. L. Chen, X. M. Li, J. Y. Shao, N. L. An, H. M. Tian, C. Wang, *et al.*, "High-Performance Piezoelectric Nanogenerators with Imprinted P(VDF-TrFE)/BaTiO<sub>3</sub> Nanocomposite Micropillars for Self-Powered Flexible Sensors," *Small*, vol. 13, Jun 2017.
- [122] P. Pulpan, L. Rusin, and J. Erhart, "Influence of Poling Conditions on Material Properties of Lead Zirconate-Lead Titanate Ceramics," *Japanese Journal of Applied Physics*, vol. 47, pp. 7953-7958, Oct 2008.
- [123] S. F. Huang, D. Y. Xu, X. Cheng, and M. H. Jiang, "Dielectric and Piezoelectric Properties of 2-2 Cement Based Piezoelectric Composite," *Journal of Composite Materials*, vol. 42, pp. 2437-2443, Dec 2008.
- [124] H. Thomann, "PIEZOELECTRIC CERAMICS," *Advanced Materials*, vol. 2, pp. 458-463, Oct 1990.
- [125] G. Gaillardgroleas, M. Lagier, and D. Sornette, "CRITICAL-BEHAVIOR IN PIEZOELECTRIC CERAMICS," *Physical Review Letters*, vol. 64, pp. 1577-1580, Mar 1990.
- [126] J. Kwon, W. Seung, B. K. Sharma, S.-W. Kim, and J.-H. Ahn, "A high performance PZT ribbon-based nanogenerator using graphene transparent electrodes," *Energy & Environmental Science*, vol. 5, pp. 8970-8975, 2012.
- [127] X. Chen, S. Y. Xu, N. Yao, W. H. Xu, and Y. Shi, "Potential measurement from a single lead zirconate titanate nanofiber using a nanomanipulator," *Applied Physics Letters*, vol. 94, Jun 2009.
- [128] X. Chen, S. Y. Xu, N. Yao, and Y. Shi, "1.6 V Nanogenerator for Mechanical Energy Harvesting Using PZT Nanofibers," *Nano Letters*, vol. 10, pp. 2133-2137, Jun 2010.



- [129] W. W. Wu, S. Bai, M. M. Yuan, Y. Qin, Z. L. Wang, and T. Jing, "Lead Zirconate Titanate Nanowire Textile Nanogenerator for Wearable Energy-Harvesting and Self-Powered Devices," *ACS Nano*, vol. 6, pp. 6231-6235, Jul 2012.
- [130] Y. Qi, N. T. Jafferis, K. Lyons, C. M. Lee, H. Ahmad, and M. C. McAlpine, "Piezoelectric Ribbons Printed onto Rubber for Flexible Energy Conversion," *Nano Letters*, vol. 10, pp. 524-528, Feb 2010.
- [131] J. H. Zhan, Y. Bando, J. Q. Hu, D. Golberg, and K. Kurashima, "Fabrication of ZnO nanoplate-nanorod junctions," *Small*, vol. 2, pp. 62-65, Jan 2006.
- [132] P. X. Gao and Z. L. Wang, "High-yield synthesis of single-crystal nanosprings of ZnO," *Small*, vol. 1, pp. 945-949, Sep 2005.
- [133] Z. L. Wang, "Zinc oxide nanostructures: growth, properties and applications," *Journal of Physics-Condensed Matter*, vol. 16, pp. R829-R858, Jun 2004.
- [134] Z. L. Wang and J. H. Song, "Piezoelectric nanogenerators based on zinc oxide nanowire arrays," *Science*, vol. 312, pp. 242-246, Apr 2006.
- [135] B. Yin, Y. Qiu, H. Q. Zhang, J. Y. Ji, and L. Z. Hu, "Low-frequency flexible piezoelectric nanogenerators based on ZnO nanorods grown on Cu wires," *Crystengcomm*, vol. 16, pp. 6831-6835, 2014.
- [136] L. Zhang, S. Bai, C. Su, Y. Zheng, Y. Qin, C. Xu, *et al.*, "A High-Reliability Kevlar Fiber-ZnO Nanowires Hybrid Nanogenerator and its Application on Self-Powered UV Detection," *Advanced Functional Materials*, vol. 25, pp. 5794-5798, Sep 23 2015.
- [137] P. Ke, X.-N. Jiao, X.-H. Ge, W.-M. Xiao, and B. Yu, "From macro to micro: structural biomimetic materials by electrospinning," *RSC Advances*, vol. 4, pp. 39704-39724, 2014.
- [138] J. Wu, N. Wang, Y. Zhao, and L. Jiang, "Electrospinning of multilevel structured functional micro-/nanofibers and their applications," *Journal of Materials Chemistry A*, vol. 1, pp. 7290-7305, 2013.
- [139] N. Masaji, N. Yoichiro, and M. Hidenori, "Single-crystalline poly(vinylidene fluoride–trifluoroethylene) nanofiber webs fabricated by electrospinning," *Japanese Journal of Applied Physics*, vol. 54, p. 021601, 2015.
- [140] H. Shao, J. Fang, H. X. Wang, and T. Lin, "Effect of electrospinning parameters and polymer concentrations on mechanical-to-electrical energy conversion of randomly-oriented electrospun poly(vinylidene fluoride) nanofiber mats," *RSC Advances*, vol. 5, pp. 14345-14350, 2015.
- [141] S. N. Cha, J. S. Seo, S. M. Kim, H. J. Kim, Y. J. Park, S. W. Kim, *et al.*, "Sound-Driven Piezoelectric Nanowire-Based Nanogenerators," *Advanced Materials*, vol. 22, pp. 4726-+, Nov 2010.
- [142] R. Calì, U. Rongala, D. Camboni, M. Milazzo, C. Stefanini, G. de Petris, *et al.*, "Piezoelectric Energy Harvesting Solutions," *Sensors*, vol. 14, p. 4755, 2014.
- [143] A. M. Siddique, S. Mahmud, and B. Van Heyst, "A comprehensive review on vibration based micro power generators using electromagnetic and piezoelectric transducer mechanisms," *Energy Conversion and Management*, vol. 106, pp. 728-747, Dec 2015.



- [144] A. R. H. Henni, C. Bacon, and B. Hosten, "Acoustic generation in piezoelectric materials by microwave excitation," *Journal of the Acoustical Society of America*, vol. 118, pp. 2281-2288, Oct 2005.
- [145] K. S. Ramadan, D. Sameoto, and S. Evoy, "A review of piezoelectric polymers as functional materials for electromechanical transducers," *Smart Materials and Structures*, vol. 23, Mar 2014.
- [146] S. Anand, N. Soin, T. H. Shah, and E. Siores, "Energy harvesting "3-D knitted spacer" based piezoelectric textiles," in *48th Conference of the International Federation of Knitting Technologists*. vol. 141, S. Aumann, A. Ehrmann, and M. O. Weber, Eds., ed, 2016.
- [147] M. H. M. Ramli, M. H. M. Yunus, C. Y. Low, and A. Jaffar, "Scavenging energy from human activities using piezoelectric material," in *2nd International Conference on System-Integrated Intelligence: Challenges for Product and Production Engineering*. vol. 15, K. D. Thoben, M. Busse, B. Denkena, and J. Gausemeier, Eds., ed, 2014, pp. 827-831.
- [148] G. M'Boungui, K. Adendorff, R. Naidoo, A. A. Jimoh, and D. E. Okojie, "A hybrid piezoelectric micro-power generator for use in low power applications," *Renewable & Sustainable Energy Reviews*, vol. 49, pp. 1136-1144, Sep 2015.
- [149] R. Hinchet and S. W. Kim, "Wearable and Implantable Mechanical Energy Harvesters for Self-Powered Biomedical Systems," *Acs Nano*, vol. 9, pp. 7742-7745, Aug 2015.
- [150] J. Lee and B. Choi, "Development of a piezoelectric energy harvesting system for implementing wireless sensors on the tires," *Energy Conversion and Management*, vol. 78, pp. 32-38, Feb 2014.
- [151] A. Mouapi, N. Hakem, G. Y. Delisle, and N. Kandil, "A novel piezoelectric micro-generator to power Wireless Sensors Networks in vehicles," in *2015 IEEE 15th International Conference on Environment and Electrical Engineering (EEEIC)*, 2015, pp. 1089-1092.
- [152] J. H. Qiu, J. Tani, N. Yamada, and H. Takahashi, "Fabrication of piezoelectric fibers with metal core," in *Smart Structures and Materials 2003: Active Materials: Behavior and Mechanics*. vol. 5053, D. C. Lagoudas, Ed., ed, 2003, pp. 475-483.
- [153] N. Soin, T. H. Shah, S. C. Anand, J. F. Geng, W. Pornwannachai, P. Mandal, *et al.*, "Novel "3-D spacer" all fibre piezoelectric textiles for energy harvesting applications," *Energy & Environmental Science*, vol. 7, pp. 1670-1679, May 2014.
- [154] A. K. Yetisen, H. Qu, A. Manbachi, H. Butt, M. R. Dokmeci, J. P. Hinestroza, *et al.*, "Nanotechnology in Textiles," *ACS Nano*, vol. 10, pp. 3042-3068, Mar 2016.
- [155] S. Park and S. Jayaraman, "Smart textiles: Wearable electronic systems," *Mrs Bulletin*, vol. 28, pp. 585-591, Aug 2003.
- [156] Y. N. Hao, X. H. Wang, S. O'Brien, J. Lombardi, and L. T. Li, "Flexible BaTiO<sub>3</sub>/PVDF gradated multilayer nanocomposite film with enhanced dielectric strength and high energy density," *Journal of Materials Chemistry C*, vol. 3, pp. 9740-9747, 2015.
- [157] D. Vatansever, R. L. Hadimani, T. Shah, and E. Siores, "An investigation of energy harvesting from renewable sources with PVDF and PZT," *Smart Materials & Structures*, vol. 20, May 2011.



- [158] Y. Ahn, J. Y. Lim, S. M. Hong, J. Lee, J. Ha, H. J. Choi, *et al.*, "Enhanced Piezoelectric Properties of Electrospun Poly(vinylidene fluoride)/Multiwalled Carbon Nanotube Composites Due to High beta-Phase Formation in Poly(vinylidene fluoride)," *Journal of Physical Chemistry C*, vol. 117, pp. 11791-11799, Jun 2013.
- [159] S. Huang, W. A. Yee, W. C. Tjiu, Y. Liu, M. Kotaki, Y. C. F. Boey, *et al.*, "Electrospinning of Polyvinylidene Difluoride with Carbon Nanotubes: Synergistic Effects of Extensional Force and Interfacial Interaction on Crystalline Structures," *Langmuir*, vol. 24, pp. 13621-13626, Dec 2008.
- [160] S. K. Rath, S. Dubey, G. S. Kumar, S. Kumar, A. K. Patra, J. Bahadur, *et al.*, "Multi-walled CNT-induced phase behaviour of poly(vinylidene fluoride) and its electro-mechanical properties," *Journal of Materials Science*, vol. 49, pp. 103-113, Jan 2014.
- [161] G. Mago, F. T. Fisher, and D. M. Kalyon, "Deformation-Induced Crystallization and Associated Morphology Development of Carbon Nanotube-PVDF Nanocomposites," *Journal of Nanoscience and Nanotechnology*, vol. 9, pp. 3330-3340, May 2009.
- [162] C. M. Wu and M. H. Chou, "Polymorphism, piezoelectricity and sound absorption of electrospun PVDF membranes with and without carbon nanotubes," *Composites Science and Technology*, vol. 127, pp. 127-133, Apr 2016.
- [163] W. A. Yee, J. H. Kong, C. Zhang, T. X. Liu, M. Kotaki, and X. H. Lu, "Polymorphism of electrospun polyvinylidene difluoride/carbon nanotube (CNT) nanocomposites: Synergistic effects of CNT surface chemistry, extensional force and supercritical carbon dioxide treatment," *Polymer*, vol. 53, pp. 5097-5102, Oct 2012.
- [164] I. Katsouras, K. Asadi, M. Y. Li, T. B. van Driel, K. S. Kjaer, D. Zhao, *et al.*, "The negative piezoelectric effect of the ferroelectric polymer poly(vinylidene fluoride)," *Nature Materials*, vol. 15, pp. 78-+, Jan 2016.
- [165] G. D. Zhu, Z. G. Zeng, L. Zhang, and X. J. Yan, "Piezoelectricity in beta-phase PVDF crystals: A molecular simulation study," *Computational Materials Science*, vol. 44, pp. 224-229, Dec 2008.
- [166] J. F. Gu, S. Gorgutsa, and M. Skorobogatiy, "Soft capacitor fibers using conductive polymers for electronic textiles," *Smart Materials & Structures*, vol. 19, Nov 2010.
- [167] J. A. F. Gu, S. Gorgutsa, and M. Skorobogatiy, "Soft capacitor fibers for electronic textiles," *Applied Physics Letters*, vol. 97, Sep 2010.
- [168] Q. F. Zhou, K. H. Lam, H. R. Zheng, W. B. Qiu, and K. K. Shung, "Piezoelectric single crystal ultrasonic transducers for biomedical applications," *Progress in Materials Science*, vol. 66, pp. 87-111, Oct 2014.
- [169] R. G. M. Kolkman, E. Hondebrink, W. Steenbergen, and F. F. M. de Mul, "In vivo photoacoustic imaging of blood vessels using an extreme-narrow aperture sensor," *Ieee Journal of Selected Topics in Quantum Electronics*, vol. 9, pp. 343-346, Mar-Apr 2003.
- [170] X. Lu, H. Qu, and M. Skorobogatiy, "Piezoelectric Microstructured Fibers via Drawing of Multimaterial Preforms," *Scientific Reports*, vol. 7, Jun 2017.



- [171] W. Honda, S. Harada, T. Arie, S. Akita, and K. Takei, "Wearable, Human-Interactive, Health-Monitoring, Wireless Devices Fabricated by Macroscale Printing Techniques," *Advanced Functional Materials*, vol. 24, pp. 3299-3304, Jun 2014.
- [172] Z. T. Li and Z. L. Wang, "Air/Liquid-Pressure and Heartbeat-Driven Flexible Fiber Nanogenerators as a Micro/Nano-Power Source or Diagnostic Sensor," *Advanced Materials*, vol. 23, pp. 84-89, Jan 2011.
- [173] T. Huang, C. Wang, H. Yu, H. Z. Wang, Q. H. Zhang, and M. F. Zhu, "Human walking-driven wearable all-fiber triboelectric nanogenerator containing electrospun polyvinylidene fluoride piezoelectric nanofibers," *Nano Energy*, vol. 14, pp. 226-235, May 2015.
- [174] Y. T. Wang, L. Wang, T. H. Cheng, Z. Y. Song, and F. Qin, "Sealed piezoelectric energy harvester driven by hyperbaric air load," *Applied Physics Letters*, vol. 108, Jan 2016.
- [175] C. A. K. Kwiimy, G. Litak, M. Borowiec, and C. Nataraj, "Performance of a piezoelectric energy harvester driven by air flow," *Applied Physics Letters*, vol. 100, Jan 2012.
- [176] J. Zhong, Y. Zhang, Q. Zhong, Q. Hu, B. Hu, Z. L. Wang, *et al.*, "Fiber-Based Generator for Wearable Electronics and Mobile Medication," *ACS Nano*, vol. 8, pp. 6273-6280, Jun 2014.
- [177] X. Li, Z.-H. Lin, G. Cheng, X. Wen, Y. Liu, S. Niu, *et al.*, "3D Fiber-Based Hybrid Nanogenerator for Energy Harvesting and as a Self-Powered Pressure Sensor," *ACS Nano*, vol. 8, pp. 10674-10681, Oct 2014.
- [178] M. Q. Le, J. F. Capsal, M. Lallart, Y. Hebrard, A. Van Der Ham, N. Reffe, *et al.*, "Review on energy harvesting for structural health monitoring in aeronautical applications," *Progress in Aerospace Sciences*, vol. 79, pp. 147-157, Nov 2015.
- [179] X. L. Zhao, T. Qian, G. Mei, C. Kwan, R. Zane, C. Walsh, *et al.*, "Active health monitoring of an aircraft wing with an embedded piezoelectric sensor/actuator network: II. Wireless approaches," *Smart Materials & Structures*, vol. 16, pp. 1218-1225, Aug 2007.
- [180] X. L. Zhao, H. D. Gao, G. F. Zhang, B. Ayhan, F. Yan, C. Kwan, *et al.*, "Active health monitoring of an aircraft wing with embedded piezoelectric sensor/actuator network: I. Defect detection, localization and growth monitoring," *Smart Materials & Structures*, vol. 16, pp. 1208-1217, Aug 2007.
- [181] D. Brei and B. J. Cannon, "Piezoceramic hollow fiber active composites," *Composites Science and Technology*, vol. 64, pp. 245-261, Feb 2004.
- [182] Y. Wu, X. Zeng, C. Hou, J. Bai, and G. Yang, "A tunable all-fiber filter based on microfiber loop resonator," *Applied Physics Letters*, vol. 92, May 2008.
- [183] S. S. Yu, W. T. Zheng, W. X. Yu, Y. J. Zhang, Q. Jiang, and Z. D. Zhao, "Formation Mechanism of beta-Phase in PVDF/CNT Composite Prepared by the Sonication Method," *Macromolecules*, vol. 42, pp. 8870-8874, Nov 2009.
- [184] S. M. Damaraju, S. L. Wu, M. Jaffe, and T. L. Arinze, "Structural changes in PVDF fibers due to electrospinning and its effect on biological function," *Biomedical Materials*, vol. 8, Jun 2013.



- [185] S. K. Karan, D. Mandal, and B. B. Khatua, "Self-powered flexible Fe-doped RGO/PVDF nanocomposite: an excellent material for a piezoelectric energy harvester," *Nanoscale*, vol. 7, pp. 10655-10666, 2015.
- [186] H. W. Lee, S. Moon, C. H. Choi, and D. K. Kim, "Synthesis and Size Control of Tetragonal Barium Titanate Nanopowders by Facile Solvothermal Method," *Journal of the American Ceramic Society*, vol. 95, pp. 2429-2434, Aug 2012.
- [187] J. Song, Y. Huang, J. Xiao, S. Wang, K. C. Hwang, H. C. Ko, *et al.*, "Mechanics of noncoplanar mesh design for stretchable electronic circuits," *Journal of Applied Physics*, vol. 105, Jun 2009.
- [188] Q. M. Zhang, V. Bharti, and X. Zhao, "Giant electrostriction and relaxor ferroelectric behavior in electron-irradiated poly(vinylidene fluoride-trifluoroethylene) copolymer," *Science*, vol. 280, pp. 2101-2104, Jun 1998.
- [189] J. G. Lee, S. H. Kim, H. C. Kang, and S. H. Park, "Effect of TiO<sub>2</sub> on PVDF/PMMA Composite Films Prepared by Thermal Casting," *Macromolecular Research*, vol. 21, pp. 349-355, Apr 2013.
- [190] J. G. Lee and S. H. Kim, "Structure development of PVDF/PMMA/TiO<sub>2</sub> composite film with casting conditions," *Macromolecular Research*, vol. 19, pp. 72-78, Jan 2011.
- [191] A. Salimi and A. A. Yousefi, "Conformational changes and phase transformation mechanisms in PVDF solution-cast films," *Journal of Polymer Science Part B-Polymer Physics*, vol. 42, pp. 3487-3495, Sep 2004.
- [192] N. P. Chen and L. Hong, "Surface phase morphology and composition of the casting films of PVDF-PVP blend," *Polymer*, vol. 43, pp. 1429-1436, Feb 2002.
- [193] K. J. Shon and H. J. Kang, "Effects of isothermal crystallization on the crystal transformation of solution casting poly(vinylidene fluoride) films," *Polymer-Korea*, vol. 20, pp. 572-581, Jul 1996.
- [194] F. Z. Benabid, L. X. Rong, D. Benachour, M. E. Cagiao, M. Poncot, F. Zouai, *et al.*, "Nanostructural characterization of poly (vinylidene fluoride)-clay nanocomposites prepared by a one-step reactive extrusion process," *Journal of Polymer Engineering*, vol. 35, pp. 181-190, Mar 2015.
- [195] F. Sadeghi and A. Ajji, "Study of Crystal Structure of (Polyvinylidene fluoride/Clay) Nanocomposite Films: Effect of Process Conditions and Clay Type," *Polymer Engineering and Science*, vol. 49, pp. 200-207, Jan 2009.
- [196] W. H. Tang, T. G. Zhu, P. P. Zhou, W. Zhao, Q. Wang, G. Feng, *et al.*, "Poly(vinylidene fluoride)/poly(methyl methacrylate)/TiO<sub>2</sub> blown films: preparation and surface study," *Journal of Materials Science*, vol. 46, pp. 6656-6663, Oct 2011.
- [197] A. R. Kakroodi, Y. Kazemi, and D. Rodrigue, "Effect of conductive particles on the mechanical, electrical, and thermal properties of maleated polyethylene," *Polymers for Advanced Technologies*, vol. 26, pp. 362-368, Apr 2015.
- [198] K. Dai, X.-B. Xu, and Z.-M. Li, "Electrically conductive carbon black (CB) filled in situ microfibrillar poly(ethylene terephthalate) (PET)/polyethylene (PE) composite with a selective CB distribution," *Polymer*, vol. 48, pp. 849-859, 2007.



- [199] B. Wang and M. Sain, "Dispersion of soybean stock-based nanofiber in a plastic matrix," *Polymer International*, vol. 56, pp. 538-546, 2007.
- [200] P. Pötschke, A. R. Bhattacharyya, and A. Janke, "Morphology and electrical resistivity of melt mixed blends of polyethylene and carbon nanotube filled polycarbonate," *Polymer*, vol. 44, pp. 8061-8069, 2003/12/01/ 2003.
- [201] J. K. W. Sandler, J. E. Kirk, I. A. Kinloch, M. S. P. Shaffer, and A. H. Windle, "Ultra-low electrical percolation threshold in carbon-nanotube-epoxy composites," *Polymer*, vol. 44, pp. 5893-5899, 2003/09/01/ 2003.
- [202] K. Sakayori, Y. Matsui, H. Abe, E. Nakamura, M. Kenmoku, T. Hara, *et al.*, "CURIE-TEMPERATURE OF BATIO<sub>3</sub>," *Japanese Journal of Applied Physics Part 1-Regular Papers Short Notes & Review Papers*, vol. 34, pp. 5443-5445, Sep 1995.
- [203] C. K. Kwok and S. B. Desu, "A Novel Method for Determining the Curie Temperature of Ferroelectric Films," *MRS Proceedings*, vol. 310, p. 429, 2011.
- [204] A. J. Lovinger, D. D. Davis, R. E. Cais, and J. M. Kometani, "On the Curie temperature of poly(vinylidene fluoride)," *Macromolecules*, vol. 19, pp. 1491-1494, 1986.
- [205] Y. Hu, Y. Gao, S. Singamaneni, V. V. Tsukruk, and Z. L. Wang, "Converse Piezoelectric Effect Induced Transverse Deflection of a Free-Standing ZnO Microbelt," *Nano Letters*, vol. 9, pp. 2661-2665, 2009.
- [206] Y. Tajitsu, M. Kanesaki, M. Tsukiji, K. Imoto, M. Date, and E. Fukada, "Novel tweezers for biological cells using piezoelectric polyactic acid fibers," *Ferroelectrics*, vol. 320, pp. 601-607, 2005.
- [207] W. Hui, X. Da, and X. Liangzhong, "Photoacoustic imaging using an ultrasonic Fresnel zone plate transducer," *Journal of Physics D: Applied Physics*, vol. 41, p. 095111, 2008.
- [208] W. Zeng, L. Shu, Q. Li, S. Chen, F. Wang, and X. M. Tao, "Fiber-Based Wearable Electronics: A Review of Materials, Fabrication, Devices, and Applications," *Advanced Materials*, vol. 26, pp. 5310-5336, Aug 2014.
- [209] D. Zou, Z. Lv, X. Cai, and S. Hou, "Macro/microfiber-shaped electronic devices," *Nano Energy*, vol. 1, pp. 273-281, 2012.